UNIVERSIDAD DE CHILE
FACULTAD DE CIENCIAS FÍSICAS Y MATEMÁTICAS
DEPARTAMENTO DE INGENIERÍA MATEMÁTICA

SOURCE TIME REVERSAL METHODS FOR ACOUSTIC AND ELASTIC WAVES

TESIS PARA OPTAR AL GRADO DE DOCTOR EN CIENCIAS DE LA INGENIERÍA,
MENCIÓN MODELACIÓN MATEMÁTICA

RODRIGO IGNACIO BREVIS VERGARA

PROFESOR GUÍA:
JAIME H. ORTEGA PALMA

MIEMBROS DE LA COMISIÓN:
JOAQUÍN FONTBONA TORRES
ALEJANDRO JOFRÉ CÁCERES
GINO MONTECINOS GUZMÁN
DAVID PARDO ZUBIAUR

Este trabajo ha sido parcialmente financiado por CONICYT, CMM-Conicyt PIA AFB170001 y el proyecto GEAGAM

SANTIAGO DE CHILE
2018

RESUMEN DE LA MEMORIA PARA OPTAR
AL GRADO DE DOCTOR EN CIENCIAS DE LA
INGENIERÍA, MENCIÓN MODELACIÓN MATEMÁTICA
POR: RODRIGO IGNACIO BREVIS VERGARA
FECHA: 2018
PROF. GUÍA: JAIME H. ORTEGA PALMA

SOURCE TIME REVERSAL METHODS FOR ACOUSTIC AND ELASTIC WAVES

Esta tesis estudia la detección y reconstrucción del término espacial de una fuente de variables separables en problemas de onda acústica y elástica. Para esto, estudiamos el método time-reversal mirror, el cual explota una invariancia intrínseca de la física a nivel microscópico que se observa también a nivel macroscópico en las ecuaciones de ondas. Esto significa que es posible recuperar la condición inicial de una ecuación de ondas homogénea revirtiendo la onda a través del tiempo. Para localizar y reconstruir el término espacial de la fuente, desarrollamos un método llamado *source time reversal*.

La aplicación subyacente aquí es la detección de fuentes sísmicas en la minería. Es sabido que la actividad minera induce temblores dentro de las minas [50]. Esto se vuelve bastante peligroso si no se toman las precauciones adecuadas. Conocer sobre el origen de las actividades sísmicas puede ser utilizado para reducir el peligro de derrumbes y mejorar la seguridad dentro de las minas.

Este trabajo se divide en tres capítulos; cada uno de ellos constituye un documento autocontenido para ser presentado como artículo. El primer capítulo aborda el problema de reconstrucción de fuente para ondas acústicas. Para esto introducimos el método *source time reversal*, la cual reconstruye el término espacial de una fuente de la forma $f(\boldsymbol{x})g(t)$, donde $f(\boldsymbol{x})$ entrega la forma y $g(t)$ representa la distribución en tiempo de la fuente. Además, presentamos una estimación del error de la reconstrucción para el caso cuando f es una función de cuadrado integrable. Aquí, proponemos un método de regularización para implementar la reconstrucción de la fuente numéricamente. Adicionalmente, analizamos las principales características y limitaciones del método propuesto cuando se aplica a ondas acústicas.

El capítulo dos estudia el problema de reconstrucción de fuente para ondas elásticas. Extendemos el método source time reversal para problemas elásticos. Además, introducimos un nuevo método de regularización para implementar la reconstrucción del término espacial de la fuente numéricamente para grandes volúmenes de datos. El nuevo método de regularización elimina las altas frecuencias presentes en la señal procesada, lo que permite utilizar mallas numéricas más gruesas y reduce el costo computacional. Finalmente, este capítulo presenta diversos experimentos numéricos para probar que el método es válido en el caso elástico.

El último capítulo analiza un problema de reconstrucción de fuente diferente. Aquí consideramos una fuente compuesta por una suma finita de funciones de variable separable, donde cada término temporal de la fuente es una función delta de Dirac actuando a un tiempo diferente. Basado en una propiedad de tiempo reverso, la fuente puede ser localizada observando el desplazamiento y la velocidad de desplazamiento en el problema reverso [31]. Nosotros extendemos esta idea a sistemas de ondas elásticas. Adicionalmente, proponemos un algoritmo para la implementación numérica.

RESUMEN DE LA MEMORIA PARA OPTAR
AL GRADO DE DOCTOR EN CIENCIAS DE LA
INGENIERÍA, MENCIÓN MODELACIÓN MATEMÁTICA
POR: RODRIGO IGNACIO BREVIS VERGARA
FECHA: 2018
PROF. GUÍA: JAIME H. ORTEGA PALMA

SOURCE TIME REVERSAL METHODS FOR ACOUSTIC AND ELASTIC WAVES

This dissertation studies the detection and reconstruction of the space term for a variable separable source in acoustic and elastic wave problems. To do this, we study the *time-reversal mirror* method, which exploits an intrinsic invariance of physics at microscopic level that is also observed at macroscopic level for wave equations. This means that it is possible to recover the initial condition of a homogeneous wave equation by reversing the wave through time. To locate and reconstruct the space term of the source, we develop a method called *source time reversal*.

The underlying application here is the seismic source detection in mining. It is known that mining activity induces tremors inside mines [50]. This become very dangerous if the adequate precautions are not considered. Knowing the origin of the seismic activities could be used to reduce the collapse hazard and improve the safety inside mines.

This work is divided into three chapters; each of them constitutes a self-contained document to be presented as an article. The first chapter deals with the problem of source reconstruction for acoustic waves. To do this, we introduce the source time reversal method, which reconstructs the space term of a source of the form $f(\boldsymbol{x})g(t)$, where $f(\boldsymbol{x})$ gives the shape and $g(t)$ represents the time distribution of the source. We also present an error estimate for the reconstruction for the case when f is a square-integrable function. Here, we propose a regularization method to implement the source reconstruction numerically. Additionally, we analyze numerically the main features and limitations of the proposed method when applied to acoustic waves.

Chapter two studies the problem of source reconstruction for elastic waves. We thus extend the source time reversal method to elastic problems. We also introduce a new regularization method to implement the space-source term reconstruction numerically for a large datasets. The new regularization method eliminates the high frequencies present in the processed signals, which allows coarser numerical meshes and reduces the computational cost. Finally, this chapter presents several numerical experiments to prove that the method is valid in the elastic case.

The last chapter analyzes different source reconstruction problem. Here we consider a source composed by a finite sum of variable separable functions, where each time-source term is a Dirac delta function acting at a different time. Based on a time reversal property, the source can be located by observing the displacement and the displacement velocity of the reversed problem [31]. We extend this idea to systems of elastic waves. Additionally, we propose an algorithm for its numerical implementation.

I dedicate this dissertation to my parents, Luis Brevis *and* Patricia Vergara.

Acknowledgements

First, I would like to thank Jaime H. Ortega not only for taking me as a student and guiding me during all this learning process, but also for the different academic opportunities along the way. Thanks to David Pardo for offering me the internship at the Universidad del País Vasco, and also for being an essential part of my learning process. Both of you helped me a lot to grow as a student. Thanks to you for the goodwill and all the advice, in the personal and academic fields.

Many thanks to Ángel Rodríguez and Gino Montecinos for collaborating in the papers generated as part of this dissertation. To Juan Carlos López and Alejandro Lavado for helping me on more than one occasion with the redaction and revision of the manuscripts. To Mauricio Cerda for trusting on me to be part of his project before this dissertation ended.

I would like to thank the Comisión Nacional de Investigación Científica y Tecnológica (CONICYT) for funding my Ph.D. studies at Universidad de Chile and the internship at the Universidad del País Vasco (UPV/EHU) under the grant No 21120646. To the projects PFB03-CMM, Fondecyt 1111012, and the European Union's Horizon 2020 research and innovation programme under the Marie Sklodowska-Curie grant agreement No 644602 GEAGAM for funding part of this work. To Universidad de Chile and the Departamento de Ingeniería Matemática (DIM) for accepting me in the Ph.D. program, and allowing me to continue with the study in mathematics field. To the Universidad de Santiago de Chile (USACH) for giving me the initial formation in mathematics and engineering.

Also, thanks to Marilyn Gatica for being part of my life during all these years. Concerning this work, thanks to you for supporting me, joining me, and encouraging me to continue with my studies. Kanela, for everything we have shared together and all we will share in the future, thank you. ☺

To my parents Luis Brevis and Patricia Vergara, to my brother Patricio Brevis, and all my extended family for the life lessons and always supporting the decisions I have made. Also thanks to Marilyn's family, which I feel as mine after all these years.

Finally, thanks to the people I met at DIM during all these years: Alexis, Bao, Cristhian, Erwin, Eterin, Giorgina, Juan Carlos, Karen, Sebastián, Silvia, and Víctor. To my friends from my beloved USACH: César, Coca, Daniela, Guille, Lidia, Marcelo, Marite, Pauly, Sole, Thamara, Víctor, and Vivi. Last but not least, to my childhood friends: Bitman, Diego, Gary, Orlando, and Seba. And to all of you I did not list here but you know are or have been my friend.

Contents

List of Tables

List of Figures

Introduction

In Chile (and in several others countries) mining activity is significant for the country development. Unfortunately, this activity is not risk-free. Mining activity produces seismic movements due to all the work inside mines (e.g., underground explosions and fluid injections) that pre-stresses the rocks. Eventually, this stress concentration is released as seismic activity [72]. The overall stability of a mine depends on several factors as the composition and nature of the orebody and the surrounding host rock, the in situ stresses and the geometry and excavation sequence of the stopes [58]. The seismic activity inside an unstable mine could be hazardous for the miners. Usually, the lack of safety ends in accidents ranging from minor injuries to death of miners. Big disasters can be avoided by developing methods to know the place where a seism began. A dynamic map of the mine with major seismic areas helps with the planning of the tunnels reinforcement (e.g., rockbolts [16, 80]) and the design of new tunnels inside the mine. Tunnel reinforcement is a key element for improving and conserving the overall rock mass properties from within the rock mass, and it has been widely used to stabilize underground excavations [39]. Then, the study of this kind of seismic activity helps to prevent mining accidents by improving the knowledge about the zones inside mines with highest seismic hazard.

Here, we are interested in the identification and shape reconstruction of the origin of tremors in mining, mathematically characterized by an external source in a hyperbolic equation. To do this, we consider a variable separable function as the external source that generates the tremor. Then, this dissertation will be focused on the reconstruction of the space-source term for acoustic and elastic wave systems. Specifically, we focus on the study of source detection for seismicity induced by mining problems. The primary tools considered in this work are the *time-reversal mirror* and the *Duhamel's principle*. The physic problem of the seismic event is modeled by a non-homogeneous second-order hyperbolic equation. Here, we consider the acoustic and elastic equations. Broadly speaking, we use this principle to relate the solution to the partial differential equation with source and null initial condition (physic problems) with the solution to a partial differential equation without source and non-null initial conditions (auxiliary problem). Then, using the time-reversal process, which is based on the reversibility on time of the wave equations, we reverse the waves to its initial position. This method allows us to recover the space-source term. We named this process as *Source Time Reversal* (STR), and it works for acoustic and elastic system of waves. We also consider a different type of source that simulates several seismic events occurring close in space and time. To do this, we consider a discrete-in-time source composed of a sum of variable separable functions, where the time-source terms are Dirac delta functions. The problem of source reconstruction is classified as an inverse problem.

In [52], V. B. Glasko introduces an inverse problem as an object inaccessible to direct study and where its properties must be estimated indirectly, for example, the bowels of the Earth. Here, we will consider the direct (or forward) problem as the solution to a system where the model input parameters are known. The inverse (or backward) problem consists of the inference of one (or more) input parameter, given by some measurement of the solution to the system [107]. An example of a direct problem in wave propagation theory is to compute the wavefront from a given initial condition or source. Then an inverse problem is given by the determination of the initial condition or source from measurements of the wavefront in a determined subset of the domain. For a more detailed description of inverse problems, see [11, 15, 65, 68, 71].

A pioneer contribution that enabled several mathematical developments in inverse problems was the work of A. Calderón in 1980 [21]. This work entitled "On an inverse boundary value problem" (and its reprint in 2006 [22]) studies the problem of *Electrical Impedance Tomography*. Let $\Omega \subset \mathbb{R}^n$ be a bounded domain with smooth boundary. Under the assumption of no sources or sinks of current in Ω, a voltage potential f at the boundary induces a voltage potential u. This problem is modeled by the Dirichlet problem

$$\begin{cases} \nabla \cdot (\gamma \nabla u) = 0, & \text{in } \Omega, \\ u = f, & \text{on } \partial\Omega, \end{cases}$$

where γ is a bounded positive function that represents the conductivity. Let us note that since γ is positive, then there is a unique weak solution $u \in H^1(\Omega)$ for any $f \in H^{1/2}(\partial\Omega)$ [97]. The inverse problem is given by determining the conductivity of a body by measuring current and voltage on the boundary of the body. The current is giving by

$$\Lambda_\gamma(f) := \left(\gamma \frac{\partial u}{\partial \nu}\right)\Big|_{\partial\Omega}.$$

Mathematically, the inverse problem is to determine γ by knowing Λ_γ. In other words, we want to study the properties of the map $\gamma \to \Lambda_\gamma$. Let us note that $\Lambda_\gamma : H^{1/2}(\partial\Omega) \to H^{-1/2}(\partial\Omega)$ is bounded [109]. This problem can be divided into four parts.

- If $\Lambda_{\gamma_1} = \Lambda_{\gamma_2}$, prove that $\gamma_1 = \gamma_2$ (uniqueness).
- If Λ_{γ_1} and Λ_{γ_2} are close, prove that γ_1 and γ_2 are close in some sense (stability).
- Find a theoretical formula to recover γ from Λ_γ. (reconstruction)
- Given some boundary measurements Λ_γ, find an numerical algorithm to reconstruct γ (numerical reconstruction).

For more detailed explanation about the Calderón problem and its main results see: for a general survey [97, 110], for uniqueness results [106, 86, 67, 55], for uniqueness with partial data [70, 62], for a stability result [3], for reconstruction [85], and for reconstruction with partial data [87].

We recall that J. Hadamard postulated three requirements for problems in mathematical physics: the existence of a solution, the uniqueness of the solution, and the continuous dependence on the data (stability). A problem accomplishing the three previous requirements is called *well-posed problem*, whereas if it does not satisfy any of the requirements, it is called

ill-posed problem [28]. Inverse problems typically lead to ill-posed mathematical models. A common problems is that their solution is unstable under data perturbations. Numerical methods that deal with this kind of problems are called *regularization methods*. Let us consider the following example form [36]: let $f \in C^1[0,1]$ be any function, $n \geq 2$ be an integer, $\delta \ll 1$ be a positive real, and

$$f_{\delta,n}(x) := f(x) + \delta \sin\left(\frac{nx}{\delta}\right).$$

If, we compute the derivative of the functions and their difference in the uniform norm, we obtain

$$f'_{\delta,n}(x) := f'(x) + n\cos\left(\frac{nx}{\delta}\right),$$

and

$$\|f - f_{\delta,n}\| = \delta, \quad \|f' - f'_{\delta,n}\| = n.$$

Considering f as the exact data and $f_{\delta,n}$ as the perturbed one, we obtain that for an arbitrarily small error δ, the error in the result can be as large as n. Then, the derivative does not depend continuously on the data with respect to the uniform norm.

Now, let us consider the following problem

$$(Kh)(x) := \int_0^x h(s)\,ds = f(x) - f(0),$$

which it has solution in $C[0,1]$ for $f \in C^1[0,1]$. The direct problem would be to find f from h, which is a stable process for continuous functions. The inverse problem would be to compute h from f, where small error can create large oscillations in the solution. In this dissertation, we deal with a stability problem present in an first kind integral equation for the reconstruction of the source term.

Several techniques employed in this dissertation come from thermoacoustic tomography (TAT), which is a medical imaging technique where the object of interest is exposed to an electromagnetic pulse [108]. The underlying inverse problem is to reconstruct the object of interest. Based on wave propagation, this technique detects cancerous masses due to its different behavior with respect to healthy tissue as response to radio frequency pulses. The standard mathematical model for TAT is given by

$$\begin{cases} \partial_t^2 p(\boldsymbol{x},t) - c^2\Delta p(\boldsymbol{x},t) = 0, & \text{in } \mathbb{R}^3 \times (0,\infty), \\ p(\boldsymbol{x},0) = \varphi(\boldsymbol{x}), \\ \partial_t p(\boldsymbol{x},0) = 0, \end{cases}$$

where $p(\boldsymbol{x},t)$ is the value of the pressure in $\boldsymbol{x}$ at the time t and $c(\boldsymbol{x})$ is the speed of the ultrasound propagation in the position $\boldsymbol{x}$ of the tissue [61] (TAT can be also considered in elastic media [108]). Let $\Omega \subset \mathbb{R}^3$ contains the object of interest. Then, the inverse problem can be formulated as follow: given $c(\boldsymbol{x})$ and $\{m(\boldsymbol{y},t) := p(\boldsymbol{y},t) : (\boldsymbol{y},t) \in \partial\Omega \times (0,T)\}$ find $\varphi(\boldsymbol{x})$. From a mathematical point of view, there exist three methods commonly used in TAT to recover $\varphi(\boldsymbol{x})$: the filtered backprojection [88], the eigenfunctions expansion method [73], and the time-reversal method [14]. In [61, 108], we encounter two surveys about these methods where they discuss their advantages and limitations. For a more complete mathematical

description about TAT and its results, see [1, 20, 60, 115, 114]. From the methods mentioned above, the time reversal is the less restrictive and can be easily implemented. Several of the TAT techniques have also been applied to seismicity. As we mentioned above, we employ the time reversal method known as Time-Reversal Mirror (TRM) for this work. We refer to Section 1.3 and 3.2 for a better explanation of TRM from a mathematical point of view.

The idea of going back in time has been present in humans for many years. Although it is still impossible to travel in time, there exist some systems where it is feasible to reverse the time. This concept has been exploited in waves for years. In the 60's, A. Parvulescu developed the Matched Equivalent-Space Signal (M.E.S.S.) technique, in which a complicate signal is designed such it is recombined by the medium into a pulse in the receiver device [93]. During the 70's, the Phase Conjugate Optics (PCO) [118] was developed, which allows reversing in time quasi-monochromatic electromagnetic waves [9]. In 1989, M. Fink et al. developed the first TRM working in a pulse-echo mode that overcomes the monochromatic restriction [46]. Here, they focused an acoustic wave through a heterogeneous medium. The experiment was designed by using a large array of transducers, devices that work as receiver and emitters at the same time, to record and re-emit a signal and backpropagate it to its initial state. The transducers act as special mirrors sending back first the last recorded signal and at the end the first recorded one. This process is known under the acronym LIFO *last in, first out* [47].

The foundations of the TRM lie on the time reversal symmetry. Until the 20th century, symmetries played a small role in theoretical physics. In 1905, Einstein recognized the symmetry implicit in Maxwell's equations, which puts the symmetry principle as the primary feature of nature that constrains the allowable dynamical laws [54]. In physics, many fundamental symmetries have been discovered during the history. For example, geometric symmetries, space-time symmetries, gauge symmetries, dynamical symmetries, permutation symmetries, and duality symmetries [105]. The time reversal symmetry consists of an invariance under the transformation $t \to -t$. This symmetry valid at the microscopic level (either in the quantum or classical description) does not hold at macroscopic level due to the arrow of time described by the second law of thermodynamics [57]. M. Fink shows this symmetry holds for acoustic and elastic wave equations in non-dissipative heterogeneous media [44]. TRM has been studied for many years. The first time-reversal experiment was performed by M. Fink with ultrasonic waves in 1989 [46]. After that, it was generalized to acoustic [40, 43], elastic [33], electromagnetic [79], and water waves [25, 94]. Also, TRM has been employed for applications in medicine, underwater acoustics, geophysics, and non-destructive testing among others. Here, we are interested in TRM for acoustic and elastic waves.

This dissertation is divided into three chapters, followed by the main achievements and conclusions. In Chapter 1, we offer an extended version of the published work entitled "A source time reversal method for seismicity induced by mining" [17] published on *Inverse Problems and Imaging*. Here, we present the source time reversal method to reconstruct the space term of a source with the form $f(\boldsymbol{x})g(t)$ for acoustic wave problems. That is

$$\begin{cases} \partial_t^2 u(\boldsymbol{x},t) - c^2(\boldsymbol{x})\Delta u(\boldsymbol{x},t) = f(\boldsymbol{x})g(t), & \text{in } \mathbb{R}^n \times (0,T), \\ u(\boldsymbol{x},0) = 0, \\ \partial_t u(\boldsymbol{x},0) = 0, \end{cases}$$

where $n \in \{2, 3\}$. Here, we propose a regularization method to obtain a stable reconstruction of the space-source term $f(\boldsymbol{x})$ via adding a regularization constant denoted by c_0 into a deconvolution expression. We also present a detailed proof of an estimate to bound the error in the reconstruction. Additionally, we include section with several numerical results to test the methodology with mathematical meaning examples and with seismicity induced by mining examples. In the numerical simulations, we study the influence of the smoothness of space- and time-terms on the reconstruction. We analyze the reconstruction behavior when we $g(t)$ is unknown. We also study the influence of the regularization constant c_0. And we perform numerical simulations with parameters and configurations employed in seismicity.

Chapter 2 shows the work submitted for publication entitled "Source time reversal (STR) method for linear elasticity" [18]. This chapter consists of an extension of the STR methodology to linear elasticity

$$\begin{cases} \rho\partial_t^2 \boldsymbol{u}(\boldsymbol{x}, t) - L_{\mu,\lambda}\boldsymbol{u}(\boldsymbol{x}, t) = \boldsymbol{f}(\boldsymbol{x})g(t), \quad \text{in } \mathbb{R}^n \times (0, T), \\ \boldsymbol{u}(\boldsymbol{x}, 0) = \boldsymbol{0}, \\ \partial_t \boldsymbol{u}(\boldsymbol{x}, 0) = \boldsymbol{0}, \end{cases}$$

where $L_{\mu,\lambda}\boldsymbol{u} = \mu\Delta\boldsymbol{u} + (\mu + \lambda)\nabla(\nabla \cdot \boldsymbol{u})$ and $n \in \{2, 3\}$. The aim is to reconstruct the space term of a variable separable source with the form $\boldsymbol{f}(\boldsymbol{x})g(t)$. Here, we present a proof of a local decay result needed to implement STR methodology for elastic systems. We also propose an alternative regularization method with a low computational cost. Finally, we dedicate two sections for presenting the numerical results. Here, we show 2D and 3D numerical experiments. We present numerical experiments to validate and compare the STR method. We perform source reconstructions with partial boundary data. We study the decay of relative error numerically. We compare the traditional and the alternative regularization methods. And we present numerical experiments with parameters and configuration of seismic events.

Chapter 3 introduces my current work on source reconstruction for linear elasticity

$$\begin{cases} \rho\partial_t^2 \boldsymbol{u}(\boldsymbol{x}, t) - L_{\mu,\lambda}\boldsymbol{u}(\boldsymbol{x}, t) = \displaystyle\sum_{j=i}^{J} \boldsymbol{f}_j(\boldsymbol{x})\delta(t - t_j), \quad \text{in } \mathbb{R}^n \times (0, \infty), \\ \boldsymbol{u}(\boldsymbol{x}, 0) = \boldsymbol{0}, \\ \partial_t \boldsymbol{u}(\boldsymbol{x}, 0) = \boldsymbol{0}. \end{cases}$$

In here, we consider sources $\sum_{j=1}^{J} \boldsymbol{f}(\boldsymbol{x})\delta(t - t_j)$ composed of a sum of variable separable functions, where each component on time of the functions is Dirac delta function. This type of source simulates a sequence of seismic events striking close in time and space. Here, we present a reconstruction algorithm which identifies the times of occurrence and reconstructs the shape of the sources in the seismic sequence. We also include a section with numerical experiments for the 2D acoustic case, the 2D elastic case, and the 3D elastic case. Here, we show the time identification and the shape reconstruction under different configurations.

Chapter 1

A source time reversal method for seismicity induced by mining

In this chapter, we present a modified time-reversal mirror method, called *source time reversal*, to find the spatial distribution of a seismic source induced by mining activity. This methodology is based on a known full description of the temporal dependence of the source, the Duhamel's principle, and the time-reverse property of the wave equation. We also provide an error estimate of the reconstruction when the measurements are acquired over the entire boundary, and we show experimentally the influence of measuring on a subdomain of the boundary. Numerical results indicate that the proposed method recovers continuous and discontinuous sources, and it remains stable for partial boundary measurements.

1.1 Introduction

As mining is a very important activity around the world and also one of the principal economic activities in several countries such as Chile, Peru, South Africa, and China, and it is expected to continue for a long time. In this dangerous labor, many precautions are considered in order to prevent mining accidents. In several cases, the lack of safety ends on accidents ranging from minor injuries to death of miners. For example, India had, in the 90's, around 1.100 serious accidents and 230 fatal accidents per year [82]; in Spain 70.000 fatal and non-fatal accidents occurred between 2003 and 2012 [98]; and 28.868 accidents with 47.875 deaths took place on coal mines in China between 2001 and 2011 [26]. Also, numerous studies have been performed to measure and try to prevent accidents, e.g. [66, 26, 29, 113]. Rock failures (or rockbursts) are the principal cause of those accidents in mines [50].

Mining is a labor that for its nature induces seismic activity. Due to the work inside mines, the rocks are stressed, often producing tremors or microseisms (in reference to its magnitude), a process that is known as block caving. This type of seismic activity is named *induced seismicity*. Knowing the sources of induced microseisms and studying the hazard in those zones is useful to improve the miners' safety inside mines. In this work, we focus on the characterization of sources in induced seismicity.

There are no systematic differences between seismicity and induced seismicity [50]. Thus, it is possible to use the same mathematical model for describing a seism and an induced seism. As models for seismicity and induced seismicity are the same, it is natural to apply seismicity source location techniques also to the case of induced seismicity.

A widely employed technique to determine source locations in traditional seismic methods is a time-reversal method introduced by M. Fink [46]. This method takes advantage of the time symmetries of waves, and it was introduced in 2006 for source location at the global scale with the work of C. Larmat et al. [77]. In this work, they reversed seismogram measurements of the Sumatra Earthquake on time, refocusing the seismic wave energy on the earthquake source location.

On the other hand, the problem of locating the tremor source in induced seismicity is often studied in a simplified form as: to find simultaneously the time when the tremor began (origin time t_0) and the position where it started (hypocenter $\boldsymbol{x}_0$, where it is also often assumed that $\boldsymbol{f}(\boldsymbol{x}) = \boldsymbol{\delta}(\boldsymbol{x} - \boldsymbol{x}_0)$). To do that, we look for an estimate of the wave travel time at each measurement station (travel time). More precisely, we only know the time at which the wave arrives at a measurement station (arrival time). Then, we have the following identity for the i-th station:

$$\text{arrival time}_i = \text{origin time} + \text{travel time}_i.$$

In 1912, L. Geiger [49] developed one of the most classical methods for locating sources in mining, based on an accurate propagation velocity map of the mine's structure and a least-square technique. This method is able to estimate the hypocenter location using the arrival time to measurement stations. Depending on the geometric distribution of the stations, this method could present problems of accuracy or unicity. Later, in the 80s, W. Spence [102] modified Geiger's least-square method to consider the P-wave arrival time difference data, which allowed to eliminate anomalies produced by velocity heterogeneities. In 1984, M. Matsu'ura [84] proposed a method for locating the space-dependence of the source with a Bayesian approach using prior spatial information. In addition, the origin time is eliminated of the problem via integration on a density function over the whole origin time range. In another work, F. Du et al. [34] considered the wave propagation velocity as a random variable into the minimization method for undersea mining microseismicity. Additionally, these authors divided the space of the mine into three areas based on the tremor occurrence probability to predict possible future hazard. As we can see, the methods for finding the source in seismicity induced by mining are more focused on finding the origin time by estimating the travel times and then obtaining the spatial position.

The main difference between seismicity and induced seismicity for mining is the scale. In the former, scales are in the order of tens or hundreds of kilometers, while in the latter, scales are of one hundred meters or below. Related to the scale and the tremor duration, in seismicity, the source could be considered as a Dirac delta source, while in induced seismicity it is convenient to include the source duration effect in the mathematical model. More precisely, in mathematical terms, in seismicity is often assumed that the source $\boldsymbol{s}(\boldsymbol{x}, t)$ is of the form $\boldsymbol{s}(\boldsymbol{x}, t) = \boldsymbol{f}(\boldsymbol{x})\delta(t - t_0)$, where t_0 is the time when the seismic movement starts. In induced seismicity, the form of the time-dependence of the source may significantly affect the models. For this reason, in here we only assume that source $\boldsymbol{s}(\boldsymbol{x}, t)$ can be described using separation of variables as $\boldsymbol{s}(\boldsymbol{x}, t) = \boldsymbol{f}(\boldsymbol{x})g(t)$, but we do not make any further assumption

on $g(t)$. We note that this assumption of considering the source as $\boldsymbol{f}(\boldsymbol{x})g(t)$ has been used in hyperbolic problems (e.g., [116]) and parabolic problems (e.g., [48]) to obtain stability conditions and to reconstruct the spatial dependence of the source. This approach has also been used for medical imaging, see e.g., chapter 12 of [7], where authors summarize time-reversal methods applied to tomography techniques by considering Dirac delta functions as a source.

In contrast to previous approaches, we are going to assume that the time-dependence form of the source $g(t)$ is known, and it is not necessarily given by a Dirac delta function of the form $\delta(t-t_0)$. Works as [95] attempt to find an accurate representation of the amplitude of a seismic wave using Ricker wavelet, and if we include any method to estimate the origin time t_0 as [49, 102], it is possible to obtain a complete characterization of the temporal source term $g(t)$. Based on a full description of $g(t)$, in this work we look for a more accurate representation of $\boldsymbol{f}(\boldsymbol{x})$ than that obtained when assuming that $g(t) = \delta(t - t_0)$, and this allows us to produce a more realistic mathematical model and a better reconstruction of $\boldsymbol{f}(\boldsymbol{x})$. In this work, for simplicity of the analysis of our proposed method, we restrict to acoustic equations instead of the more complex elastic equations. The former equations are known to provide adequate estimates of compressional velocities, and they are widely used as first approximations of the true compressional and shear velocities dictated by the elastic equations (see e.g., [2]).

The main contribution of this work is to enhance the accuracy of the spatial source term reconstruction in induced seismicity. To do that, we adapt a time-reversal method in order to find an approximation of the spatial term using the temporal source information and the geophones measurements. We denote this novel method as *Source Time Reversal*. Besides, we study numerically the properties of such source reconstruction technique. In particular, we show numerically that continuous sources are easier to reconstruct than discontinuous ones. While classical time-reversal methods allow to accurately recover initial conditions or sources acting for an instant of time (i.e., $\boldsymbol{f}(\boldsymbol{x})\delta(t - t_0)$), the method developed in this work is able to recover the spatial characteristics for a more general class of sources $\boldsymbol{f}(\boldsymbol{x})g(t)$ where $g(t)$ is assumed to be known.

This chapter is divided into five sections. In section 1.2, we present some previous results for acoustic waves. In Section 1.3, we state the problem and introduce a modified Time-Reversal Mirror from M. Fink point of view, and we provide a three-dimensional example of how the time-reversal mirror method works in an exact case. In Section 1.4, we present the Source Time Reversal (STR) methodology and also show an error estimate for our problem following the ideas of [60]. Section 1.5 introduces four different numerical experiments to study the characteristics of the method, including a synthetic microseismic experiment, where we compare the proposed method with the standard time-reversal mirror method.

1.2 Previous results

Let v be solution of the following problem

$$\begin{cases} \partial_t^2 v - c^2 \Delta v = 0, & \text{in } \mathbb{R}^n \times (0,\infty), \\ v = \varphi, & \text{in } \mathbb{R}^n \times \{t=0\}, \\ \partial_t v = \psi, & \text{in } \mathbb{R}^n \times \{t=0\}, \end{cases} \tag{1.1}$$

where $c(\boldsymbol{x}) > c_1 > 0$ for all $\boldsymbol{x} \in \mathbb{R}^n$. Let us assume all the inhomogeneities of the medium and the initial perturbations are confined to a bounded subset of $\mathbb{R}^n$. We mathematically represent these conditions by considering $(1-c)$, φ, and ψ having compact support [35].

Let Ω be a bounded subset of $\mathbb{R}^n$. Then, we define the *local energy* in Ω as

$$\mathcal{E}(t) = \frac{1}{2}\int_\Omega |\nabla v(\boldsymbol{x},t)|^2 + c^{-2}(\boldsymbol{x})|\partial_t v(\boldsymbol{x},t)|^2 \, d\boldsymbol{x}.$$

A classical result of B. R. Vainberg [111] establishes a decay rate of the local energy under certain conditions for the speed of propagation over the medium. The condition to obtain this decay rate is called *non-trapping condition.*

Definition 1.1 (non-trapping condition [35]) *Let $c : \mathbb{R}^n \to \mathbb{R}$ be a $C^\infty(\mathbb{R}^n)$ function. We define the Hamiltonian $H(\boldsymbol{x},\boldsymbol{\xi}) = \frac{1}{2}c^2(\boldsymbol{x})|\boldsymbol{\xi}|^2$ and the following system*

$$\begin{cases} \boldsymbol{x}_t' = \frac{\partial H}{\partial \boldsymbol{\xi}} = \boldsymbol{\xi} c^2(\boldsymbol{x}), \\ \boldsymbol{\xi}_t' = -\frac{\partial H}{\partial \boldsymbol{x}} = -\frac{1}{2}|\boldsymbol{\xi}|^2 \nabla(c^2(\boldsymbol{x})), \\ \boldsymbol{x}|_{t=0} = \boldsymbol{x}_0, \\ \boldsymbol{\xi}|_{t=0} = \boldsymbol{\xi}_0, \\ H(\boldsymbol{x}_0,\boldsymbol{\xi}_0) = H_0. \end{cases} \tag{1.2}$$

The solutions of (1.2) are called bicharacteristics, and the projection of the $\boldsymbol{x}$-components into $\mathbb{R}^n$ of a bicharacteristic is called ray. We define the non-trapping condition *as: all the rays go to infinity as $t \to \infty$, that is*

$$\lim_{t\to\infty} \|\boldsymbol{x}(t)\| = +\infty.$$

Then, if the wave speed c in the problem (1.1) accomplishes the above condition, this ensures that all wavefronts leave the domain after a specific time. The following theorem summarizes this property.

Theorem 1.2 (Decay of the local energy [35]) *Let assume $c \in C^\infty(\mathbb{R}^n)$ in problem (1.1) accomplishes the non-trapping condition. Let consider a bounded set $\Omega \subset \mathbb{R}^n$ such that $\varphi, \psi \in L^2(\mathbb{R}^n)$ and $\operatorname{supp}(\varphi) \cup \operatorname{supp}(\psi) \subset \Omega$. Then, there exists $T_0 > 0$, such that the solution of problem (1.1) verifies $v \in C^\infty(\Omega \times (T_0,\infty))$ and*

$$\left| \frac{\partial^{|\alpha|} v(\boldsymbol{x},t)}{\partial t^{\alpha_0} \partial x_1^{\alpha_1} \cdots \partial x_n^{\alpha_n}} \right| \leq C\eta_{\alpha_0}(t) \left(\|\varphi\|_{L^2(\Omega)} + \|\psi\|_{L^2(\Omega)} \right),$$

for all $\boldsymbol{x} \in \Omega$, *for all* $t \geq T_0$, *and for all* $\alpha = (\alpha_0, \alpha_1, \ldots, \alpha_n) \in \mathbb{N}^{n+1}$, *where* $C := C(\Omega, \alpha)$. *Here*

$$\eta_k(t) = \begin{cases} t^{1-n-k} & \text{for even } n \\ e^{-\delta t} & \text{for odd } n, \end{cases}$$

where δ *is a constant depending on* $c(\boldsymbol{x})$.

Another interesting classical result about the regularity of solutions is needed to obtain an error decay estimate. This result is also valid for more general second-order partial differential hyperbolic operators. We first associate with u a mapping $u^* : [0, T] \to H_0^1(\Omega)$ defined by $[u^*(t)](\boldsymbol{x}) := u(\boldsymbol{x}, t)$ for $\boldsymbol{x} \in \Omega$ and $t \in [0, T]$ ([38]). To simplify the notation, we denote u and u^* indistinctly by u.

Theorem 1.3 (Infinity differentiability [38]) *Let* Ω *be an open bounded set. Let us consider the following boundary value problem*

$$\begin{cases} \partial_t^2 u + Lu = f_e, & \text{in } \Omega \times (0, T), \\ u = g, & \text{in } \Omega \times \{t = 0\}, \\ \partial_t u = h, & \text{in } \Omega \times \{t = 0\}, \\ u = 0, & \text{on } \partial\Omega \times (0, T), \end{cases} \tag{1.3}$$

where L *denotes a second-order partial differential operator such that* $\partial_t^2 + L$ *is a hyperbolic operator. Assume* $g, h \in C^\infty(\overline{\Omega})$ *and* $f_e \in C^\infty(\overline{\Omega \times (0, T)})$. *If the following compatibility conditions hold for all* $l \in \mathbb{N}$

$$\begin{cases} g_0 := g & \in H_0^1(\Omega), \\ h_1 := h & \in H_0^1(\Omega), \\ g_{2l} := \dfrac{d^{2l-2}}{dt^{2l-2}} f_e(\cdot, 0) - L g_{2l-2} & \in H_0^1(\Omega), \\ h_{2l+1} := \dfrac{d^{2l-1}}{dt^{2l-1}} f_e(\cdot, 0) - L h_{2l-1} & \in H_0^1(\Omega), \end{cases}$$

then, problem (1.3) has a unique solution $u \in C^\infty(\overline{\Omega \times (0, T)})$ *and*

$$\max_{0 \leq t \leq T} \left(\|u(t)\|_{H^1(\Omega)} + \|\partial_t u(t)\|_{L^2(\Omega)} \right) \leq C \left(\|f_e\|_{L^2(0,T;L^2(\Omega))} + \|g\|_{H_0^1(\Omega)} + \|h\|_{L^2(\Omega)} \right),$$

where C *is a constant depending on* Ω, *the coefficients of* L *and* T.

To simplify the above notation, from here we denote by $\|\cdot\|_{\mathcal{H}(\Omega)}$ the sum of the following norms

$$\|u(t)\|_{\mathcal{H}(\Omega)} := \|u(t)\|_{H^1(\Omega)} + \|\partial_t u(t)\|_{L^2(\Omega)}.$$

Theorem 1.4 (Gronwall's inequality [38]) *Let* η *be a non-negative, absolute continuous function on* $[t_0, t_1]$, *which satisfies for a.e.* t *the differential inequality*

$$\eta'(t) \leq \phi(t)\eta(t) + \psi(t),$$

where ϕ and ψ are non-negative, summable functions on $[t_0, t_1]$. Then

$$\eta(t) \leq e^{\int_{t_0}^{t} \phi(s)\, ds} \left[\eta(t_0) + \int_{t_0}^{t} \psi(s)\, ds \right],$$

for all $t_0 \leq t \leq t_1$.

By considering the above Gronwall's inequality, it is possible to extend Theorem 1.3 to a more general time interval (t_0, T).

Remark 1.5 *If the domain in problem 1.3 is $\Omega \times (t_0, T)$, then Theorem 1.3 still holds and the corresponding estimate is given by*

$$\max_{t_0 \leq t \leq T} \left(\|u(t)\|_{\mathcal{H}(\Omega)} \right) \leq e^{C_1(T-t_0)} \left(C_2 \|f_e\|_{L^2(t_0,T;L^2(\Omega))} + C_3 \left(\|g\|_{H_0^1(\Omega)} + \|h\|_{L^2(\Omega)} \right) \right),$$

where C_1, C_2, and C_3 are constants depending on Ω and $c(\boldsymbol{x})$.

1.3 Model assumptions and the time-reversal method

In what follows, we assume our seismic events are governed by the wave equation in an isotropic media. The source can be expressed using separation of variables as $f(\boldsymbol{x})g(t)$, where $f \in L^2(\mathbb{R}^n)$ is compactly supported in a bounded set $\Omega \subset \mathbb{R}^n$. Thus, our original problem is given by

$$\begin{cases} \partial_t^2 u(\boldsymbol{x}, t) - c^2(\boldsymbol{x}) \Delta u(\boldsymbol{x}, t) = f(\boldsymbol{x}) g(t), \quad \text{in } \mathbb{R}^n \times (0, T), \\ u(\boldsymbol{x}, 0) = 0, \\ \partial_t u(\boldsymbol{x}, 0) = 0, \end{cases} \qquad \text{(ORIGINAL PR.)}$$

where $c \in C^\infty(\mathbb{R}^n)$, $c(\boldsymbol{x}) > c_1 > 0$ for all $\boldsymbol{x} \in \mathbb{R}^n$ is a known propagation velocity map with $(1 - c(\boldsymbol{x}))$ having compact support, and $c(\boldsymbol{x})$ verifies the non-trapping condition (see Definition 1.1). Also, the temporal source distribution $g \in W^{1,\infty}(0, T)$ is assumed to be known.

Let us consider a set of measurements obtained by using geophones. The information recorded by the geophones is the velocity of the displacements. Then, we define the boundary of the set Ω as the place where we measure the velocity of displacement, given by $\partial_t u(\boldsymbol{y}, t)$ for all $\boldsymbol{y} \in \partial\Omega$ and for all $t \in [0, T]$. To develop the methodology, we start assuming the geophones are located on the entire boundary of Ω. The objective is to reconstruct the spatial source contribution $f(\boldsymbol{x})$. To mathematically express these measurements, we introduce the following operator

$$\Lambda(f, g) := \partial_t u|_{\partial\Omega \times (0,T)}.$$

Then, the measurement of the velocity recorder at the geophones will be given by $m_u(\boldsymbol{y}, t) = \Lambda(f, g)(\boldsymbol{y}, t)$ for all $\boldsymbol{y} \in \partial\Omega$ and all $t \in (0, T)$. Now, we can define our inverse problem: find $f(\boldsymbol{x})$ given $\{m_u(\boldsymbol{y}, t) := \partial_t u(\boldsymbol{y}, t) : (\boldsymbol{y}, t) \in \partial\Omega \times (0, T)\}$ and $\{g(t) : t \in (0, T)\}$ such that u solves (ORIGINAL PR.).

To study the inverse problem defined above, we first introduce the Time-Reversal Mirror (TRM). The TRM was first introduced for acoustic waves by M. Fink. This method has been applied in several areas of physics and engineering, including optics [24, 119, 117], underwater acoustic [101, 74], ultrasound [40, 112], and wireless communications [89, 75]. TRM is based on the invariance of the wave equation on time. This method allows to recover the initial perturbation or *initial wave*[1] through measurements performed by transducers located at some fixed points inside the domain where the waves propagate. Each transducer records a signal and acts as a special mirror by sending back the recorded signal (reflecting first the last measurement and last the first measurement). The reflected signal moves back towards the initial wave due to the time invariance of the wave equation. For a more detailed explanation on the TRM, see [42].

To detail the TRM process, let us consider an acoustic problem in a heterogeneous medium with initial conditions: an initial position $\varphi \in L^2(\mathbb{R}^n)$ and a null initial velocity. Here, the initial position propagates into $\mathbb{R}^n$ as an acoustic wave modeled by (1.4), where $c(\boldsymbol{x})$ represents the speed of the wave at the point $\boldsymbol{x}$ and contains the information of the heterogeneities in the medium. We consider the initial position $\varphi := \varphi(\boldsymbol{x})$ as a function with compact support contained in a bounded set $\Omega \subset \mathbb{R}^n$.

Then, the idea is to find $\varphi(\boldsymbol{x})$ given $\{m(\boldsymbol{y},t) := v(\boldsymbol{y},t) : (\boldsymbol{y},t) \in \partial\Omega \times (0,T)\}$ such that

$$\begin{cases} \partial_t^2 v(\boldsymbol{x},t) - c^2(\boldsymbol{x})\Delta v(\boldsymbol{x},t) = 0, & \text{in } \mathbb{R}^n \times (0,T), \\ v(\boldsymbol{x},0) = \varphi(\boldsymbol{x}), \\ \partial_t v(\boldsymbol{x},0) = 0, \end{cases} \tag{1.4}$$

where $c \in C^\infty(\mathbb{R}^n)$, $c(\boldsymbol{x}) > c_1 > 0$, $(1-c)$ has compact support, and $c(\boldsymbol{x})$ verifies the non-trapping condition.

It is well known that the direct problem has a unique strong solution. Moreover, if we consider the above conditions, we have a unique $v \in C(0,T;H^2(\mathbb{R}^n)) \cap C^1(0,T;H^1(\mathbb{R}^n)) \cap C^2(0,T;L^2(\mathbb{R}^n))$, see for instance [19].

The goal of the TRM method is to recover the initial condition $\varphi(\boldsymbol{x})$ by recording and reversing $v(\boldsymbol{y},t)$ on the boundary. To do this, we define the following operator to model the measurement

$$\widetilde{\Lambda}\varphi := v|_{\partial\Omega\times[0,T]}.$$

Then, after recording the measurements $m(\boldsymbol{y},t) = \widetilde{\Lambda}\varphi(\boldsymbol{y},t)$ on the entire boundary $\partial\Omega$ for a period of time $(0,T)$, we define the *exact reverse problem* inside Ω with final conditions

$$\begin{cases} \partial_t^2 w(\boldsymbol{x},t) - c^2(\boldsymbol{x})\Delta w(\boldsymbol{x},t) = 0, & \text{in } \Omega \times (0,T), \\ w(\boldsymbol{x},T) = v(\boldsymbol{x},T), \\ \partial_t w(\boldsymbol{x},T) = \partial_t v(\boldsymbol{x},T), \\ w(\boldsymbol{y},t) = m(\boldsymbol{y},t), & \text{on } \partial\Omega \times (0,T). \end{cases} \tag{1.5}$$

[1] Some authors use the term *source*, we reserve this word to refer an external force. Usually, the right-hand side of the equation.

Notice that solution to problem (1.5) is exactly the solution to problem (1.4) inside $\Omega\times(0,T)$. Then, $w(\boldsymbol{x},t)$ at time $t=0$ recovers exactly the initial condition in problem (1.4), i.e.,

$$w(\boldsymbol{x},0)=\varphi(\boldsymbol{x}),$$

for all $x\in\Omega$.

In practical applications, often we only have access to measure information on the boundary of Ω. Thus, it is impossible to obtain the values of $v(\boldsymbol{x},T)$ and $\partial_t v(\boldsymbol{x},T)$ inside the domain Ω. We overcome this problem by considering Theorem 1.2, where we can approximate the final conditions $v(\boldsymbol{x},T)$ and $\partial_t v(\boldsymbol{x},T)$ by zeros in (1.5) if the final time T is large enough, i.e., $T>T_0$.

Based on the previous argument, we define the *approximate reverse problem* inside Ω with final conditions equal to zero,

$$\begin{cases}\partial_t^2\widetilde{w}(\boldsymbol{x},t)-c^2(\boldsymbol{x})\Delta\widetilde{w}(\boldsymbol{x},t)=0, & \text{in } \Omega\times(0,T),\\ \widetilde{w}(\boldsymbol{x},T)=0,\\ \partial_t\widetilde{w}(\boldsymbol{x},T)=0,\\ \widetilde{w}(\boldsymbol{y},t)=m(\boldsymbol{y},t)\phi_\varepsilon(t), & \text{on } \partial\Omega\times(0,T),\end{cases}\tag{1.6}$$

where $\phi_\varepsilon\in C^\infty(0,\infty)$, for a given small $\varepsilon>0$, is a smooth function such that $\phi_\varepsilon(t)=1$ for $t\in(0,T-\varepsilon)$ and $\phi_\varepsilon(t)=0$ for $t\geq T$. This function ϕ_ε facilitates the matching of the boundary condition with the conditions at time $t=T$ by introducing a smooth transition. Then, the solution of (1.6) at time $t=0$ is an approximation of $\varphi(\boldsymbol{x})$ when $m(\boldsymbol{y},t)$ is given by $\widetilde{\Lambda}\varphi(\boldsymbol{y},t)$, i.e.,

$$\widetilde{w}(\boldsymbol{x},0)\approx\varphi(\boldsymbol{x}).$$

It is posible to solve problem (1.6), with final data equal to zero and boundary condition $m(\boldsymbol{y},t)=\Lambda\varphi(\boldsymbol{y},t)$, and recover exactly $\psi(\boldsymbol{x})$ when $T\to\infty$. In the case when $T<\infty$, we can recover exactly $\psi(\boldsymbol{x})$ only for odd dimensions and constant wave speed (Huygens' principle, see e.g. [78]). For even dimensions or variable wave speed (i.e. heterogeneous media), it is only possible to approximate $\varphi(\boldsymbol{x})$ by assuming the final data equal to zero. Y. Hristova estimates the error of approximating the initial data $\varphi(\boldsymbol{x})$ in problem (1.4) with $\widetilde{w}(\boldsymbol{x},0)$ in the following theorem

Theorem 1.6 (Error estimate [60]) *Let w and $\widetilde{w}$ solve problems (1.5) and (1.6), respectively. Then, there exists T_0 such that for any $T>T_0>1$ and $\varepsilon>0$ satisfying $T-\varepsilon>T_0$, we obtain*

$$\max_{0\leq t\leq T}\left(\|w(t)-\widetilde{w}(t)\|_{H^1(\Omega)}+\|\partial_t w(t)-\partial_t\widetilde{w}(t)\|_{L^2(\Omega)}\right)\leq C(\varepsilon)\eta(T-\varepsilon)\|\varphi\|_{L^2(\Omega)},$$

and in particular

$$\|\varphi-\widetilde{w}(0)\|_{H^1(\Omega)}\leq C(\varepsilon)\eta(T-\varepsilon)\|\varphi\|_{L^2(\Omega)},$$

where $C(\varepsilon)=C/\min\{\varepsilon^2,1\}$, for some constant C depending on Ω and $c(x)$, and

$$\eta(t)=\begin{cases}t^{1-n} & \text{for even dimensions } n\\ e^{-\delta t} & \text{for odd dimensions } n.\end{cases}$$

1.3.1 Example of an exact reconstruction

We present a brief example, based on the Huygens' principle, of an exact reconstruction of the initial condition by using TRM.

Let us consider the following problem in $\mathbb{R}^3$ given by

$$\begin{cases} \partial_t^2 v(\boldsymbol{x},t) - \Delta v(\boldsymbol{x},t) = 0, & \text{in } \mathbb{R}^3 \times (0,T), \\ v(\boldsymbol{x},0) = \varphi(\boldsymbol{x}), \\ \partial_t v(\boldsymbol{x},0) = 0. \end{cases}$$

We want to recover the initial condition $\varphi(\boldsymbol{x})$ of the previous problem with constant propagation velocity $c(\boldsymbol{x}) \equiv 1$. Then, we measure $m(\boldsymbol{x},t) = u(\boldsymbol{x},t)|_{\partial\Omega\times[0,T]}$ over a bounded domain Ω, such that we register the signal everywhere on $\partial\Omega$. In this case, $v(\boldsymbol{x},T) = \partial_t v(\boldsymbol{x},T) = 0$, since all waves leave Ω (due to Huygens' principle) after certain time T_0. Also, when we consider $T > T_0$, the use of ϕ_ε is unnecessary. Then, we backpropagate the measurements in the homogeneous media by considering the problem (1.6) as follows

$$\begin{cases} \partial_t^2 \widetilde{w}(\boldsymbol{x},t) - \Delta \widetilde{w}(\boldsymbol{x},t) = 0, & \text{in } \Omega \times (0,T), \\ \widetilde{w}(\boldsymbol{x},0) = 0, \\ \partial_t \widetilde{w}(\boldsymbol{x},0) = 0, \\ \widetilde{w}(\boldsymbol{y},t) = m(\boldsymbol{y},T-t), & \text{on } \partial\Omega \times (0,T). \end{cases} \tag{1.7}$$

Thus, if we solve (1.7) at time T, we obtain $\widetilde{w}(\boldsymbol{x},T) = \psi(\boldsymbol{x})$ for all $\boldsymbol{x} \in \Omega$. For this case, we consider a problem with initial conditions (at time $t = 0$) instead of one with conditions at final time $t = T$. To make this change consistent, we reverse the measurements. For a simple proof based on Huygens' principle of how TRM works in this exact case example, see [14]. For further information about another approaches on time-reversal methods, we refer to [14, 103, 6].

1.4 Source time reversal (STR) method

In this section, we extend the time-reversal idea to a nonhomogeneous wave equation, as that considered in our model problem (ORIGINAL PR.). In this extension, we introduce a new approach of a time-reversal method called Source Time Reversal (STR). This method employs the information of the temporal source dependence to improve the reconstruction of the spatial source term. We also provide an error estimate.

Based on the Duhamel's principle idea [38], we consider an auxiliary problem, where the unknown term of the source $f(\boldsymbol{x})$ of (ORIGINAL PR.) now appears as part of the initial condition. Then, it is easy to see that we can write the solution of system (ORIGINAL PR.) as a convolution of a function v with the time-term of the source

$$u(x,t) = \int_0^t v(\boldsymbol{x}, t-\tau) g(\tau)\, d\tau, \tag{1.8}$$

where v solves the auxiliary problem

$$\begin{cases} \partial_t^2 v - c(\boldsymbol{x})^2 \Delta v = 0, & \text{in } \mathbb{R}^n \times (0,\infty), \\ v(\boldsymbol{x},0) = 0, \\ \partial_t v(\boldsymbol{x},0) = f(\boldsymbol{x}). \end{cases} \qquad \text{(FORWARD PR.)}$$

This convolution allows relating a nonhomogeneous problem with a homogeneous initial-value problem. Also, it gives us a relation between the boundary information in the problem (FORWARD PR.) and the measurements obtained in (ORIGINAL PR.). Thus we have the following result.

Proposition 1.7 *Let v be solution to problem (FORWARD PR.) and u be as in (1.8). Then, u is solution to problem (ORIGINAL PR.).*

Proof. The proof of this proposition is direct from the definition of $\boldsymbol{u}$ in (1.8). We compute the first and second derivatives of $\boldsymbol{u}$ with respect to t

$$\partial_t u(\boldsymbol{x},t) = v(\boldsymbol{x},0)g(t) + \int_0^t \partial_t v(\boldsymbol{x},t-\tau)g(\tau)\,d\tau, \tag{1.9}$$

and

$$\partial_t^2 u(\boldsymbol{x},t) = f(\boldsymbol{x})g(t) + \int_0^t \partial_t^2 v(\boldsymbol{x},t-\tau)g(\tau)\,d\tau. \tag{1.10}$$

Let us define $Lu(\boldsymbol{x},t) := c^2(\boldsymbol{x})\Delta u(\boldsymbol{x},t)$ Then, we apply operator L in both sides of the identity (1.8) and obtain

$$Lu(\boldsymbol{x},t) = \int_0^t Lv(x,t-\tau)g(\tau)\,d\tau. \tag{1.11}$$

Then, using the above identities, we obtain $\partial_t^2 u(\boldsymbol{x},t) - Lu(\boldsymbol{x},t) = f(\boldsymbol{x})g(t)$ by replacing (1.10) and (1.11). We obtain $u(\boldsymbol{x},0) = 0$ and $\partial_t u(\boldsymbol{x},0) = 0$ by evaluating (1.8) and (1.9) at $t = 0$, which completes the proof. □

The classical TRM method objective is to recover the initial position $\varphi(\boldsymbol{x})$ (see problem (1.4)) by recording $v(\boldsymbol{x},t)$ on the boundary. In our case, the goal is to recover the initial velocity $f(\boldsymbol{x})$ in problem (FORWARD PR.) (also the space-term of the source in (ORIGINAL PR.)) by recording the velocity of the displacement $\partial_t v(\boldsymbol{x},t)$ on the entire $\partial\Omega$. Then, to recover the initial condition $f(\boldsymbol{x})$ from (FORWARD PR.), we define the following operator to model the measurements

$$\Lambda_0 f := \partial_t v|_{\partial\Omega\times(0,T)}.$$

This operator records the displacement velocity over the boundary. The measurements are given by $m_{\boldsymbol{v}}(\boldsymbol{y},t) = \Lambda_0 f(\boldsymbol{y},t)$ for all $\boldsymbol{y} \in \partial\Omega$ and for all $t \in (0,T)$. Then, we define the following boundary value problem

$$\begin{cases} \partial_t^2 w - c(\boldsymbol{x})^2 \Delta \widetilde{w} = 0, & \text{in } \Omega \times (0,\infty), \\ w(\boldsymbol{x},T) = \partial_t v(\boldsymbol{x},T), & \\ \partial_t w(\boldsymbol{x},T) = \partial_t^2 v(\boldsymbol{x},T), & \\ w(\boldsymbol{y},t) = m_v(\boldsymbol{y},t), & \text{on } \partial\Omega \times (0,T). \end{cases} \tag{1.12}$$

Using the same procedure as in problem 1.5, we realize that the solution of problem (1.12) is $w(\boldsymbol{x},t) = \partial_t v(\boldsymbol{x},t)$ in $\Omega \times (0,T)$ and in order to recover exactly $f(\boldsymbol{x})$, we need to know the values of $\partial_t v(\boldsymbol{x},T)$ and $\partial_t^2 v(\boldsymbol{x},T)$ inside Ω. Then, for practical applications it is possible to obtain an approximation of $f(\boldsymbol{x})$ by defining

$$\begin{cases} \partial_t^2 \widetilde{w} - c(\boldsymbol{x})^2 \Delta \widetilde{w} = 0, & \text{in } \Omega \times (0,\infty), \\ \widetilde{w}(\boldsymbol{x},T) = 0, & \\ \partial_t \widetilde{w}(\boldsymbol{x},T) = 0, & \\ \widetilde{w}(\boldsymbol{y},t) = m_v(\boldsymbol{y},t)\phi_\varepsilon(t), & \text{on } \partial\Omega \times (0,T), \end{cases} \tag{BACKWARD PR.}$$

where ϕ_ε is a cut-off function as in (1.6). By solving (BACKWARD PR.) with boundary condition $m_v = \Lambda_0 f$ at time $t = 0$, we obtain an approximation of $f(\boldsymbol{x})$, where the error committed by approximating $f(\boldsymbol{x})$ with $\widetilde{f}(\boldsymbol{x}) := \widetilde{w}(\boldsymbol{x},0)$ is given by the following result.

Theorem 1.8 *Let w and $\widetilde{w}$ be solutions to problems (1.12) and (BACKWARD PR.), respectively. We assume $f \in L^2(\mathbb{R}^n)$ and its support is contained in $\Omega \subset \mathbb{R}^n$ a bounded set. We also assume $c \in C^\infty(\Omega)$, with $c(\boldsymbol{x}) > c_1 > 0$, $(1 - c(\boldsymbol{x}))$ has compact support in Ω, and $c(\boldsymbol{x})$ satisfies the non-trapping condition. Then, we have the following estimate*

$$\|w(t) - \widetilde{w}(t)\|_{\mathcal{H}(\Omega)} \leq \frac{C}{\varepsilon^2} \eta_k(T-\varepsilon) \|f\|_{L^2(\Omega)}, \tag{1.13}$$

for all $t \in (0,T)$, where

$$\eta_k(t) = \begin{cases} t^{1-n-k} & \text{for even } n \\ e^{-\delta t} & \text{for odd } n, \end{cases}$$

the constant C depends on Ω and $c(\boldsymbol{x})$ and δ depends on $c(\boldsymbol{x})$ ($k = 3$ for $t \in (0,1)$, and $k = 1$ for $t > 1$).

Before proving Theorem 1.8, we make a remark about the solution of the acoustic equation.

Remark 1.9 *Let u be a smooth function solution of the problem $\partial_t^2 u(\boldsymbol{x},t) - c^2(\boldsymbol{x})\Delta u(\boldsymbol{x},t) = 0$, then u is also solution of $\partial_t^{2n} u(\boldsymbol{x},t) - (c^2(\boldsymbol{x})\Delta)^n u(\boldsymbol{x},t) = 0$.*

Proof of Theorem 1.8. We follow the proof performed in [60]. To do that, we define the error function $e_T(\boldsymbol{x},t) = w(\boldsymbol{x},t) - \widetilde{w}(\boldsymbol{x},t)$, where $w(\boldsymbol{x},t)$ and $\widetilde{w}(\boldsymbol{x},t)$ are solutions of (1.12) and (BACKWARD PR.), respectively. We take $\varepsilon > 0$ fixed and $\phi_\varepsilon \in C^\infty(0,T)$ such that $\max_{0\leq t\leq T} |\phi_\varepsilon'(t)| \leq \widetilde{C}_1/\varepsilon$ and $\max_{0\leq t\leq T} |\phi_\varepsilon''(t)| \leq \widetilde{C}_2/\varepsilon^2$, where $\widetilde{C}_1$ and $\widetilde{C}_2$ are constants.

Then, the error function solves the following problem

$$\begin{cases} \partial_t^2 e_T - c^2 \Delta e_T = 0, & \text{in } \Omega \times (0,T), \\ e_T = \partial_t v, & \text{in } \Omega \times \{t = T\}, \\ \partial_t e_T = \partial_t^2 v, & \text{in } \Omega \times \{t = T\}, \\ e_T = m_{v,\varepsilon}, & \text{on } \partial\Omega \times (0,T), \end{cases}$$

where $m_{v,\varepsilon}(\boldsymbol{y},t) = (1-\phi_\varepsilon(t))m_v(\boldsymbol{y},t)$ for all $\boldsymbol{y} \in \partial\Omega$ and $t \in (0,T)$.

Let us consider the harmonic extension operator $E : H^{1/2}(\partial\Omega) \to H^1(\Omega)$, such that for $\gamma \in H^{1/2}(\partial\Omega)$ there is a unique $\theta := E\gamma$ solution of the problem

$$\begin{cases} \Delta\theta = 0, & \text{in } \Omega, \\ \theta = \gamma, & \text{on } \partial\Omega. \end{cases}$$

Then, we define the function $z := e_T - Em_{v,\varepsilon}$, which solves the problem

$$\begin{cases} \partial_t^2 z - c^2 \Delta z = -E(\partial_t^2 m_{v,\varepsilon}) & \text{in } \Omega \times (0,T) \\ z = \partial_t v - Em_v & \text{in } \Omega \times \{t = T\} \\ \partial_t z = \partial_t^2 v - E(\partial_t m_v) & \text{in } \Omega \times \{t = T\} \\ z = 0 & \text{on } \partial\Omega \times (0,T). \end{cases} \tag{1.14}$$

We are going to prove the infinite differentiability of z in problem (1.14). To do this, first let us consider the following energy in Ω

$$\mathcal{E}(t) = \frac{1}{2}\int_\Omega |\nabla z|^2 + c^{-2}|\partial_t z|^2 \, dx,$$

where $\mathcal{E}$ stays constant in $[0, T-\varepsilon]$. Indeed

$$\begin{aligned} \mathcal{E}'(t) &= \int_\Omega \nabla z \cdot \nabla(\partial_t z) + c^{-2}\partial_t z \partial_t^2 z \, dx \\ &= -\int_\Omega \Delta z \cdot (\partial_t z)\, dx + \int_{\partial\Omega} \partial_t z \nabla z \cdot \hat{n}\, dS + \int_\Omega c^{-2}\partial_t z \partial_t^2 z \, dx \\ &= -\int_\Omega \Delta z \cdot (\partial_t z)\, dx + \int_{\partial\Omega} \partial_t (e_T - m_{v,\varepsilon}) \nabla z \cdot \hat{n}\, dS + \int_\Omega c^{-2}\partial_t z (c^2 \Delta z - E(\partial_t^2 m_{v,\varepsilon}))\, dx \\ &= \int_{\partial\Omega} \partial_t (m_{v,\varepsilon} - m_{v,\varepsilon}) \nabla z \cdot \hat{n}\, dS - \int_\Omega c^{-2} E(\partial_t^2 m_{v,\varepsilon}) \partial_t z \, dx \\ &= -\int_\Omega c^{-2} E(\partial_t^2 m_{v,\varepsilon}) \partial_t z \, dx \\ &= 0, \end{aligned}$$

in $[0, T-\varepsilon]$. Then, it is enough to consider one point in $[0, T-\varepsilon]$ to find the maximum of the energy in the whole $[0,T]$, i.e.,

$$\max_{0 \le t \le T} \mathcal{E}(t) = \max_{T-\varepsilon \le t \le T} \mathcal{E}(t).$$

Second, from Theorem 1.2, we see that $v \in C^\infty(\Omega \times (T, \infty))$ for all $T > T_0$. Then, we select T such that $T - \varepsilon > T_0$ ($\partial_t v(x,T)$ and $\partial_t^2 v(x,T)$ are also infinitely smooth in Ω). Let us notice that ϕ_ε is infinitely smooth in $(0,T)$, and v is infinitely smooth in $\Omega \times (T-\varepsilon, \infty)$. Then $Em_{v,\varepsilon} := E((1-\phi_\varepsilon)m_v)$ is infinitely smooth in $\Omega \times (0,T)$. We also know that $(\partial_t v - Em_v)(T)$ and $(\partial_t^2 v - E(\partial_t m_v))(T)$ are in $C^\infty(\Omega)$, and $E(\partial_t^2 m_{v,\varepsilon}) \in C^\infty(\Omega \times (T-\varepsilon, T))$. It remains to prove the compatibility condition at time $t = T$ to accomplish the conditions in Theorem 1.3.

We have $g_0 = \partial_t v(T) - Em_v(T)$, $h_1 = \partial_t^2 v(T) - E(\partial_t m_v)(T)$, and $f_e = -E(\partial_t^2 m_{v,\varepsilon})$. As $\partial_t v - Em_v$ and $\partial_t^2 v - E(\partial_t m_v)$ are $C^\infty(\Omega)$ for $t = T$, and these functions vanish on $\partial\Omega$, we have $g_0, h_1 \in H_0^1(\Omega)$.

For $l = 1$ we have: $g_2 = f_e(\cdot, T) + c^2 \Delta g_0 \in H_0^1(\Omega)$ and $h_3 = \frac{d}{dt} f_e(\cdot, T) + c^2 \Delta h_1 \in H_0^1(\Omega)$ since $f_e(\cdot, T) = -E(\partial_t^2 m_\varepsilon)(T) \in C^\infty(\Omega)$, $c \in C^\infty(\Omega)$, $g_0, h_1 \in C^\infty(\Omega)$, and

$$
\begin{aligned}
g_2|_{\partial\Omega} &= \left(f_e(\cdot, T) + c^2 \Delta g_0\right)\big|_{\partial\Omega} \\
&= \left(-E(\partial_t^2 m_{v,\varepsilon})(T) + c^2 \Delta \partial_t v(T)\right)\big|_{\partial\Omega} \\
&= \left(-\partial_t^2 m_v(T) + c^2 \Delta \partial_t v(T)\right)\big|_{\partial\Omega} \\
&= \left(-\partial_t^2 z + c^2 \Delta z\right) \partial_t v(T)\big|_{\partial\Omega} \\
&= 0.
\end{aligned}
$$

$$
\begin{aligned}
h_3|_{\partial\Omega} &= \left(\frac{d}{dt} f_e(\cdot, T) + c^2 \Delta h_1\right)\Big|_{\partial\Omega} \\
&= \left(-\frac{d}{dt} E(\partial_t^2 m_{v,\varepsilon})(T) + c^2 \Delta \partial_t^2 v(T)\right)\Big|_{\partial\Omega} \\
&= \left(-\frac{d}{dt} \partial_t^2 m_v(T) + c^2 \Delta \partial_t^2 v(T)\right)\Big|_{\partial\Omega} \\
&= \left(-\partial_t^2 + c^2 \Delta\right) \partial_t^2 v(T)\big|_{\partial\Omega} \\
&= 0.
\end{aligned}
$$

For the general case $l = n$, we obtain

$$\begin{aligned}
g_{2n}|_{\partial\Omega} &= \left(-\frac{d^{2n-2}}{dt^{2n-2}}E(\partial_t^2 m_{v,\varepsilon})(T) + c^2\Delta g_{2n-2}\right)\Big|_{\partial\Omega} \\
&= \left(-\frac{d^{2n-2}}{dt^{2n-2}}\partial_t^2 m_v(T) + c^2\Delta\left(-\frac{d^{2n-4}}{dt^{2n-4}}E(\partial_t^2 m_{v,\varepsilon})(T) + c^2\Delta g_{2n-4}\right)\right)\Big|_{\partial\Omega} \\
&= \left(-\frac{d^{2n-2}}{dt^{2n-2}}\partial_t^2 m_v(T) + (c^2\Delta)^2 g_{2n-4}\right)\Big|_{\partial\Omega} \\
&= \left(-\frac{d^{2n-2}}{dt^{2n-2}}\partial_t^2 m_v(T) + (c^2\Delta)^2\left(-\frac{d^{2n-6}}{dt^{2n-6}}E(\partial_t^2 m_{v,\varepsilon})(T) + c^2\Delta g_{2n-6}\right)\right)\Big|_{\partial\Omega} \\
&= \left(-\frac{d^{2n-2}}{dt^{2n-2}}\partial_t^2 m_v(T) + (c^2\Delta)^3 g_{2n-6}\right)\Big|_{\partial\Omega} \\
&\vdots \\
&= \left(-\partial_t^{2n} m_v(T) + (c^2\Delta)^n g_0\right)\big|_{\partial\Omega} \\
&= \left(-\partial_t^{2n} + (c^2\Delta)^n\right)\partial_t v(T)\big|_{\partial\Omega} \\
&= 0,
\end{aligned}$$

and

$$\begin{aligned}
h_{2n+1}|_{\partial\Omega} &= \left(-\frac{d^{2n-1}}{dt^{2n-1}}E(\partial_t^2 m_{v,\varepsilon})(T) + c^2\Delta h_{2n-1}\right)\Big|_{\partial\Omega} \\
&= \left(-\frac{d^{2n-1}}{dt^{2n-1}}\partial_t^2 m_v(T) + c^2\Delta\left(-\frac{d^{2n-3}}{dt^{2n-3}}E(\partial_t^2 m_{v,\varepsilon})(T) + c^2\Delta h_{2n-3}\right)\right)\Big|_{\partial\Omega} \\
&= \left(-\frac{d^{2n-1}}{dt^{2n-1}}\partial_t^2 m_v(T) + (c^2\Delta)^2\left(h_{2n-3}\right)\right)\Big|_{\partial\Omega} \\
&\vdots \\
&= \left(-\partial_t^{2n}\partial_t m_v(T) + (c^2\Delta)^n h_1\right)\big|_{\partial\Omega} \\
&= \left(-\partial_t^{2n} + (c^2\Delta)^n\right)\partial_t^2 v(T)\big|_{\partial\Omega} \\
&= 0.
\end{aligned}$$

Here we have used Remark 1.9 and the fact that the Laplacian of the operator of harmonic extension is zero. Then g_{2n} and h_{2n+1} are in $H_0^1(\Omega)$ for all $n \in \mathbb{N}$.

Third, let us notice that there exist constants c_0 and C_0 that depend only on Ω and $c(\boldsymbol{x})$ such that

$$c_0\left(\|z(t)\|_{H^1(\Omega)}^2 + \|\partial_t z(t)\|_{L^2(\Omega)}^2\right) \leq \mathcal{E}(t) \leq C_0\left(\|z(t)\|_{H^1(\Omega)}^2 + \|\partial_t z(t)\|_{L^2(\Omega)}^2\right).$$

By using that $c(\boldsymbol{x})$ is a smooth bounded function, we obtain

$$\begin{aligned}
\mathcal{E}(t) &\leq \frac{1}{2}\max\left\{1, \sup_{\boldsymbol{x}\in\Omega} c^{-2}(\boldsymbol{x})\right\}\left(\|\nabla z(t)\|_{L^2(\Omega)}^2 + \|\partial_t z(t)\|_{L^2(\Omega)}^2\right) \\
&\leq C_0\left(\|z(t)\|_{H^1(\Omega)}^2 + \|\partial_t z(t)\|_{L^2(\Omega)}^2\right),
\end{aligned}$$

and

$$\begin{aligned}\mathcal{E}(t) &\geq \frac{1}{2}\min\left\{1, \inf_{\boldsymbol{x}\in\Omega} c^{-2}(\boldsymbol{x})\right\}\left(\|\nabla z(t)\|^2_{L^2(\Omega)} + \|\partial_t z(t)\|^2_{L^2(\Omega)}\right)\\ &\geq c_0\left(\|z(t)\|^2_{H^1(\Omega)} + \|\partial_t z(t)\|^2_{L^2(\Omega)}\right).\end{aligned}$$

Here we have used Poincaré's inequality.

By using Cauchy's inequality, we obtain the following estimate

$$\|e_T(t) - Em_{v,\varepsilon}(t)\|_{\mathcal{H}(\Omega)} \leq \sqrt{\frac{2}{c_0}}\sqrt{\mathcal{E}(t)}. \tag{1.15}$$

Now, we are in conditions to apply Remark 1.5 to (1.14), and obtain the following estimate

$$\max_{T-\varepsilon\leq t\leq T}\|z(t)\|_{\mathcal{H}(\Omega)} \leq e^{C_1\varepsilon}\left(C_2\|E(\partial_t^2 m_{v,\varepsilon})\|_{L^2(0,T;L^2(\Omega))} + C_3\|\partial_t v(T) - Em_v(T)\|_{\mathcal{H}(\Omega)}\right), \tag{1.16}$$

where C_1, C_2, and C_3 depend on Ω and $c(\boldsymbol{x})$. In the following, we denote with C to a generic constant that depends upon Ω and $c(\boldsymbol{x})$ but not upon ε or T.

Taking the maximum in both sides of inequality (1.15), we obtain

$$\begin{aligned}\max_{0\leq t\leq T}\|e_T(t)\|_{\mathcal{H}(\Omega)} &\leq C\left\{\max_{0\leq t\leq T}\sqrt{\mathcal{E}(t)} + \max_{0\leq t\leq T}\|Em_{v,\varepsilon}(t)\|_{\mathcal{H}(\Omega)}\right\}\\ &= C\left\{\max_{T-\varepsilon\leq t\leq T}\sqrt{\mathcal{E}(t)} + \max_{T-\varepsilon\leq t\leq T}\|Em_{v,\varepsilon}(t)\|_{\mathcal{H}(\Omega)}\right\}\\ &\leq C\max_{T-\varepsilon\leq t\leq T}\left\{\|z(t)\|_{\mathcal{H}(\Omega)} + \|Em_{v,\varepsilon}(t)\|_{\mathcal{H}(\Omega)}\right\}.\end{aligned}$$

In the above equality we have used that $(1-\phi_\varepsilon(t)) = 0$ between $[0, T-\varepsilon]$, which means that the maximum of $Em_{v,\varepsilon}$ and $E(\partial_t m_{v,\varepsilon})$ are the same in $[0,T]$ and $[t-\varepsilon, T]$. Then, by using (1.16) we obtain

$$\begin{aligned}\max_{0\leq t\leq T}\|e_T(t)\|_{\mathcal{H}(\Omega)} \leq C\Bigg\{&\max_{T-\varepsilon\leq t\leq T}\|Em_{v,\varepsilon}(t)\|_{\mathcal{H}(\Omega)} + \|E(\partial_t^2 m_{v,\varepsilon})\|_{L^2(T-\varepsilon,T;L^2(\Omega))}\\ &+\|\partial_t v(T) - Em_v(T)\|_{\mathcal{H}(\Omega)}\Bigg\}.\end{aligned} \tag{1.17}$$

We can estimate the right-hand side of the above identity by using the extension operator, the trace operator $\mathcal{T}: H^1(\Omega)\to H^{1/2}(\partial\Omega)$ (see [38]), and the bounds for the cut-off function ϕ_ε and its derivatives,

$$\begin{aligned}\|Em_{v,\varepsilon}(t)\|_{H^1(\Omega)} &\leq C\|m_{v,\varepsilon}(t)\|_{H^{1/2}(\partial\Omega)}\\ &= C\|(1-\phi_\varepsilon(t))\mathcal{T}(\partial_t v)(t)\|_{H^{1/2}(\partial\Omega)}\\ &\leq C\|(1-\phi_\varepsilon(t))\partial_t v(t)\|_{H^1(\Omega)}\\ &\leq C\|\partial_t v(t)\|_{H^1(\Omega)},\end{aligned} \tag{1.18}$$

$$
\begin{aligned}
\|E(\partial_t m_{v,\varepsilon})(t)\|_{L^2(\Omega)} &\le \|E(\partial_t m_{v,\varepsilon})(t)\|_{H^1(\Omega)} \\
&\le C\|\partial_t m_{v,\varepsilon}(t)\|_{H^{1/2}(\partial\Omega)} \\
&= C\|\partial_t((1-\phi_\varepsilon)\partial_t v)(t)\|_{H^1(\Omega)} \\
&\le C\|-\phi_\varepsilon'(t)\partial_t v(t) + (1-\phi_\varepsilon(t))\partial_t^2 v(t)\|_{H^1(\Omega)} \\
&\le \frac{C}{\varepsilon}\left[\|\partial_t v(t)\|_{H^1(\Omega)} + \|\partial_t^2 v(t)\|_{H^1(\Omega)}\right],
\end{aligned} \tag{1.19}
$$

$$
\begin{aligned}
\|E(\partial_t^2 m_{v,\varepsilon})(t)\|_{L^2(\Omega)} &\le \|E(\partial_t^2 m_{v,\varepsilon})(t)\|_{H^1(\Omega)} \\
&\le C\|\partial_t^2 m_{v,\varepsilon}(t)\|_{H^{1/2}(\partial\Omega)} \\
&= C\|\partial_t^2((1-\phi_\varepsilon)\partial_t v)(t)\|_{H^1(\Omega)} \\
&\le C\|-\phi_\varepsilon''(t)\partial_t v(t) - 2\phi_\varepsilon'(t) + (1-\phi_\varepsilon(t))\partial_t^3 v(t)\|_{H^1(\Omega)} \\
&\le \frac{C}{\varepsilon^2}\left[\|\partial_t v(t)\|_{H^1(\Omega)} + \|\partial_t^2 v(t)\|_{H^1(\Omega)} + \|\partial_t^3 v(t)\|_{H^1(\Omega)}\right],
\end{aligned} \tag{1.20}
$$

$$
\begin{aligned}
\|Em_v(T)\|_{H^1(\Omega)} &\le C\|m_v(T)\|_{H^{1/2}(\partial\Omega)} \\
&= C\|\mathcal{T}(\partial_t v)(T)\|_{H^{1/2}(\partial\Omega)} \\
&\le C\|\partial_t v(T)\|_{H^1(\Omega)},
\end{aligned} \tag{1.21}
$$

$$
\begin{aligned}
\|E(\partial_t m_v)(T)\|_{L^2(\Omega)} &\le \|E(\partial_t m_v)(T)\|_{H^1(\Omega)} \\
&\le C\|\partial_t m_v(T)\|_{H^{1/2}(\partial\Omega)} \\
&= C\|\partial_t^2 v(T)\|_{H^1(\Omega)}.
\end{aligned} \tag{1.22}
$$

Thus, by replacing (1.18)-(1.22) on (1.17) we obtain the following estimate,

$$
\begin{aligned}
\max_{0\le t\le T}\|e_T(t)\|_{\mathcal{H}(\Omega)} \le \frac{C}{\varepsilon^2}\Bigg\{ &\max_{T-\varepsilon\le t\le T}\left[\|\partial_t v(t)\|_{H^1(\Omega)} + \|\partial_t^2 v(t)\|_{H^1(\Omega)}\right] + \|\partial_t v\|_{L^2(T-\varepsilon,T;H^1(\Omega))} \\
&+\|\partial_t^2 v\|_{L^2(T-\varepsilon,T;H^1(\Omega))} + \|\partial_t^3 v\|_{L^2(T-\varepsilon,T;H^1(\Omega))} \\
&+\|\partial_t v(T)\|_{H^1(\Omega)} + \|\partial_t^2 v(T)\|_{H^1(\Omega)}\Bigg\}.
\end{aligned}
$$

As we can see on the right-hand side, the maximum is considered for $t \in [T-\varepsilon, T]$. Then, we can use Theorem 1.2 to estimate the above norms in terms of functions η_k and f

$$
\begin{aligned}
\max_{0\le t\le T}\|e_T(t)\|_{\mathcal{H}(\Omega)} \le \frac{C}{\varepsilon^2}\Bigg\{ &\max_{T-\varepsilon\le t\le T}\left[\eta_1(t) + \eta_2(t)\right] + \|\eta_1\|_{L^2(T-\varepsilon,T)} + \|\eta_2\|_{L^2(T-\varepsilon,T)} \\
&+\|\eta_3\|_{L^2(T-\varepsilon,T)} + \eta_1(T) + \eta_2(T)\Bigg\}\|f\|_{L^2(\Omega)}.
\end{aligned}
$$

η_k are decreasing functions and $\eta_k(t) \le \eta_{k+1}(t)$ for $t \in [0,1]$ and $\eta_{k+1}(t) \le \eta_k(t)$ for $t \in [1,\infty)$. Then,

$$
\max_{0\le t\le T}\|e_T(t)\|_{\mathcal{H}(\Omega)} \le \frac{C}{\varepsilon^2}\eta_k(T-\varepsilon)\|f\|_{L^2(\Omega)},
$$

where $k = 3$ for $T \in [0,1]$ and $k = 1$ for $T > 1$, and C is a constant depending on Ω and $c(\boldsymbol{x})$. □

We see from (1.13) that the error in approximating $f(\boldsymbol{x})$ with $\widetilde{f}(\boldsymbol{x}) := \widetilde{w}(\boldsymbol{x}, 0)$ is given by

$$\|f - \widetilde{f}\|_{H^1(\Omega)} \leq \frac{C}{\varepsilon^2}\eta(T-\varepsilon)\|f\|_{L^2(\Omega)},$$

where $\eta(t) = t^{1-n-k}$ for even n ($k = 3$ for $t \in (0,1)$, and $k = 1$ for $t > 1$) and $\eta(t) = e^{-\delta t}$ for odd n.

Theorem 1.8 recovers almost the same bound than Theorem 1.6. The difference is in the function η_k. In Hristova's result, the error function is bounded by η_2 for $T \in (0,1]$ and η_0 for $T > 1$. In our result, the error function is bounded by η_3 for $T \in (0,1]$ and η_1 for $T > 1$. This difference is due to the kind of information measured on the boundary (displacement in the first case and velocity of displacement in our case).

In practice, it is necessary to obtain explicitly the measurements $m_v(\boldsymbol{y}, t)$ over the boundary to perform the TRM method on (FORWARD PR.). This implies knowing the values of $\partial_t v(\boldsymbol{y}, t)$ on $\partial\Omega \times (0, T)$. From identity (1.8), the problem of obtaining the boundary information $m_v(\boldsymbol{y}, \cdot)$ from $m_u(\boldsymbol{y}, \cdot)$ is reduced to solve the following Volterra equation of the first kind

$$\partial_t u(\boldsymbol{y}, t) = \int_0^t \partial_t v(\boldsymbol{y}, t-\tau) g(\tau)\, d\tau,$$

for all $\boldsymbol{y} \in \partial\Omega$. In terms of operators, we have

$$\Lambda(f, g) = \Lambda_0 f * g.$$

To solve the above Volterra equation numerically, we use the Fourier transform to obtain

$$(\partial_t u_{\boldsymbol{x}})(\omega) = \mathcal{F}(\partial_t v_{\boldsymbol{x}})(\omega)\mathcal{F}(g)(\omega).$$

where $u_{\boldsymbol{x}} := u(\boldsymbol{x}, \cdot)$ and $v_{\boldsymbol{x}} := v(\boldsymbol{x}, \cdot)$. Since all functions in the convolution are defined for $t \geq 0$, the known property $\mathcal{F}(\partial_t u_{\boldsymbol{x}} * g) = \mathcal{F}(\partial_t v_{\boldsymbol{x}})\mathcal{F}(g)$, is still valid for this type of convolution (the proof is straightforward from the definition of the convolution and Fubini's Theorem). Then, we can write $\partial_t v(\boldsymbol{x}, t)$ in terms of the following inverse Fourier transform

$$\partial_t v(\boldsymbol{x}, t) = \mathcal{F}^{-1}\left(\frac{\mathcal{F}(\partial_t u_{\boldsymbol{x}})}{\mathcal{F}(g)}\right)(t),$$

for all ω such that $\mathcal{F}(g)(\omega) \neq 0$, where $\mathcal{F}^{-1}$ represents the inverse Fourier transform.

Hence, we define the operator $\mathcal{A} : L^2(0, T; H^{1/2}(\partial\Omega)) \times W^{1,\infty}(0, T) \to L^2(0, T; H^{1/2}(\partial\Omega))$ as follows

$$\mathcal{A}\,(m_u, g) = \mathcal{F}^{-1}\left(\frac{\mathcal{F}(m_u)\overline{\mathcal{F}(g)}}{|\mathcal{F}(g)|^2 + c_0}\right). \tag{1.23}$$

In the above formula, we have introduced a small regularization constant $c_0 > 0$ to avoid a possible division by zero. We estimate the velocity measurements on the boundary in (FORWARD PR.) with the velocities measured by the geophones by using the operator $\mathcal{A}$

$$m_v(\boldsymbol{x}, t) \approx \mathcal{A}(m_u, g)(\boldsymbol{x}, t).$$

We summarize the above methodology in Figure 1.1.

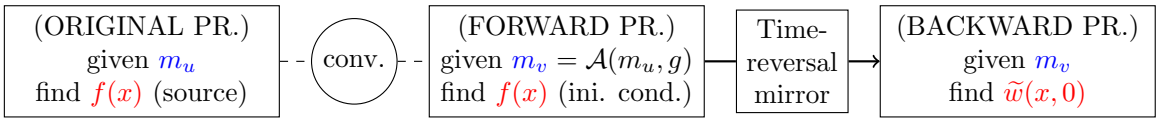

Figure 1.1: Diagram of STR method describing how to recover the source term $f(\boldsymbol{x})$.

1.5 Numerical results

In this section, we present four two-dimensional numerical experiments in different scenarios to study the STR method. The first experiment analyzes the influence of the smoothness of $f(\boldsymbol{x})$ and $g(t)$ on the reconstruction $\widetilde{f}(\boldsymbol{x})$. The second experiment studies the reconstruction behavior of $f(\boldsymbol{x})$ when the temporal source term $g(t)$ is not accurately estimated, which could be produced due to an incorrect estimation of the origin time t_0 or an improper calculation of the shape of $g(t)$. The third experiment shows the influence of constant c_0 in the reconstruction of $f(\boldsymbol{x})$. The last experiment considers a synthetic seismic event and shows the differences between the reconstruction of $f(\boldsymbol{x})$ with the classical TRM and with our STR method.

1.5.1 Numerical implementation

For these experiments, we use an explicit finite difference scheme of centered differences. We code the experiments in MATLAB considering the Courtant-Friedrichs-Lewy (CFL) condition [100] to obtain the convergence of the finite difference scheme. Also, it is important to consider an appropriate regularization constant for the STR method stability. In this case, and for all the experiments, we consider the regularization constant $c_0 = 0.01$. Finally, for implementing the Fourier transform and its inverse, we use the standard functions of MATLAB.

In the first, second, and third experiments, we consider the following parameters: a domain $\Omega = (-3\ m, 3\ m) \times (-3\ m, 3\ m)$, a total time $T = 23\ s$, and a propagation velocity $c(\boldsymbol{x}) \equiv 1\ m/s$. For the numerical discretization, we consider the step size $\Delta x = 0.1\ m$, $\Delta y = 0.1\ m$, and $\Delta t = 0.025\ s$. In addition, for these experiments we assume the geophones are located over the entire boundary of Ω. For the fourth and fifth experiments, we utilize a domain $\Omega = (-300\ m, 300\ m) \times (0\ m, 600\ m)$, where the first component represents the distance along the surface and the second one represents the depth in the Earth. In these experiments, we consider the parameters: $T = 0.5\ s$, and $c(\boldsymbol{x}) \equiv 2500\ m/s$. For the numerical discretization, we consider $\Delta x = 5\ m$, $\Delta z = 5\ m$, $\Delta t = 1.4 \times 10^{-3}\ s$. In the fourth experiment, the geophones are located on the surface and we add noise to the measurements. For the noise, we compute the standard deviation of all information recorded on the boundary, and we add the standard deviation to the *clean measurements* weighted by a factor as follow

$$m^k_{i\ noise} = m^k_{i\ clean} + factor * \mathrm{std}(m) * \mathrm{rand}^k_i,$$

where rand^k_i is a uniformly distributed random number in the interval $(-1, 1)$ for each geophone i and for all k in the time discretization. In the fifth experiment, we consider eight geophones disperse within the domain.

1.5.2 Influence of the smoothness of space- and time-term of the source on the reconstruction

This experiment consists on studying the influence of the smoothness of functions f and g on the reconstruction process. For this purpose, we consider functions $f(\boldsymbol{x})$ and $g(t)$ with different degrees of smoothness, namely, C^∞, C^0, and discontinuous, as we can see in Figures 1.2 and 1.3.

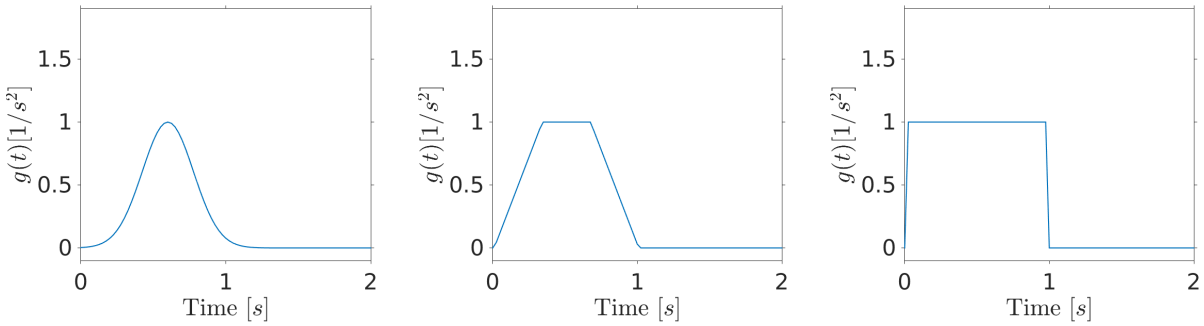

(a) $g_1(t)$ (b) $g_2(t)$ (c) $g_3(t)$

Figure 1.2: Functions selected as temporal source terms $g(t)$.

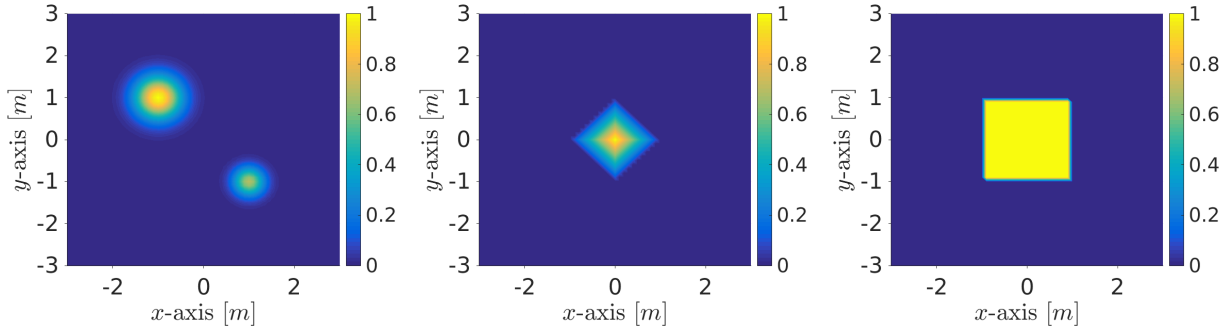

(a) $f_1(\boldsymbol{x})$ (b) $f_2(\boldsymbol{x})$ (c) $f_3(\boldsymbol{x})$

Figure 1.3: Functions selected as spatial source terms $f(\boldsymbol{x})$.

In this experiment, we simulate "tremors" with synthetic sources $f_i(\boldsymbol{x})g_j(t)$, where $i, j \in \{1, 2, 3\}$, and we use our STR methodology measuring the displacement velocity signal over the entire boundary to reconstruct the spatial source term $f_i(\boldsymbol{x})$.

In Figure 1.4, we show the results of these reconstructions. The first row (Figures 1.4a, 1.4b, and 1.4c) shows the reconstruction results of the three different spatial source terms $f_1(\boldsymbol{x})$, $f_2(\boldsymbol{x})$, and $f_3(\boldsymbol{x})$ under the assumption of tremors generated by sources $f_i(\boldsymbol{x})g_1(t)$, $i \in \{1, 2, 3\}$, respectively. The second row (Figures 1.4d, 1.4e, and 1.4f) describes the reconstruction results of the three different spatial source terms under the assumption of tremors generated by sources $f_i(\boldsymbol{x})g_2(t)$, $i \in \{1, 2, 3\}$. Similarly, the last row (Figures 1.4g, 1.4h, and 1.4i) shows the result of the spatial sources reconstruction under tremors generated by sources of type $f_i(\boldsymbol{x})g_3(t)$, $i \in \{1, 2, 3\}$.

In addition, we present the relative error in L^2-norm of these experiments in Table 1.1. From the results of this experiment, we can see that the best results in terms of the smallest

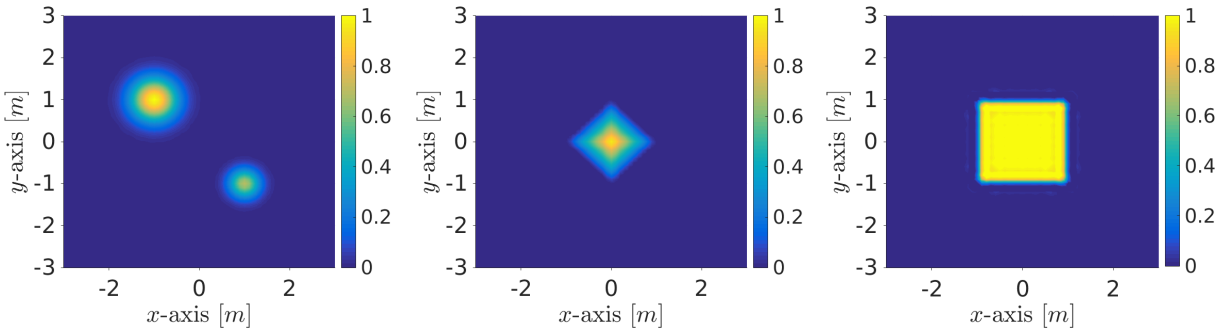

(a) $\widetilde{f}_1(\boldsymbol{x})$ using $g_1(t)$ (b) $\widetilde{f}_2(\boldsymbol{x})$ using $g_1(t)$ (c) $\widetilde{f}_3(\boldsymbol{x})$ using $g_1(t)$

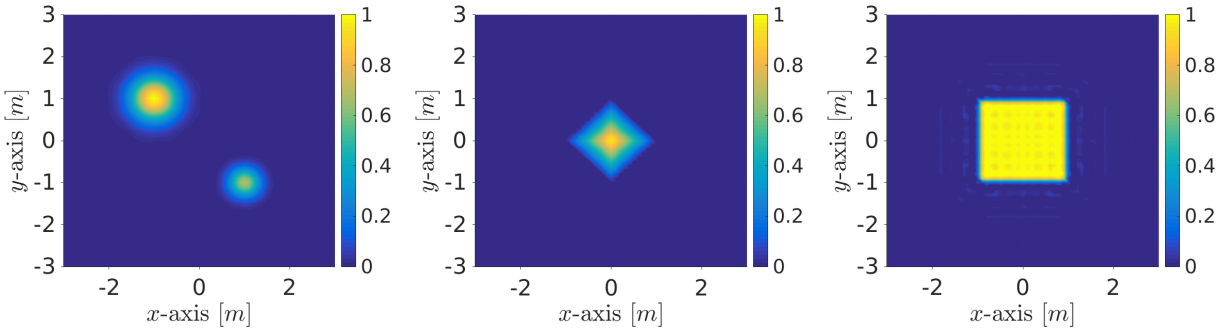

(d) $\widetilde{f}_1(\boldsymbol{x})$ using $g_2(t)$ (e) $\widetilde{f}_2(\boldsymbol{x})$ using $g_2(t)$ (f) $\widetilde{f}_3(\boldsymbol{x})$ using $g_2(t)$

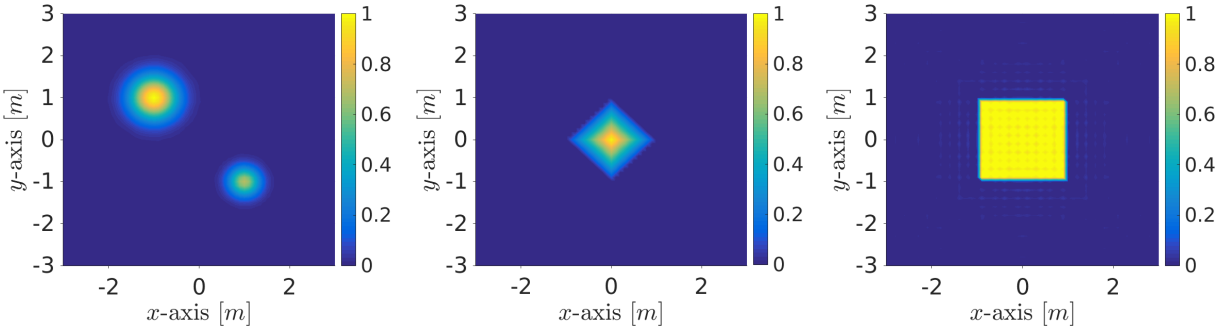

(g) $\widetilde{f}_1(\boldsymbol{x})$ using $g_3(t)$ (h) $\widetilde{f}_2(\boldsymbol{x})$ using $g_3(t)$ (i) $\widetilde{f}_3(\boldsymbol{x})$ using $g_3(t)$

Figure 1.4: Spatial source term reconstruction for the different sources $f_i(\boldsymbol{x})g_j(t)$ $i, j \in \{1, 2, 3\}$.

	$f_1(\boldsymbol{x})$	$f_2(\boldsymbol{x})$	$f_3(\boldsymbol{x})$
$g_1(t)$	0.7%	2.2%	8.7%
$g_2(t)$	1.3%	2.2%	8.2%
$g_3(t)$	0.9%	1.8%	4.1%

Table 1.1: Summary of the relative error $\frac{\|\widetilde{f}_i - f_i\|_{L^2}}{\|f_i\|_{L^2}}$ in experiment smoothness of $f(x)$ and $g(t)$.

relative error percent are obtained for a discontinuous (piecewise constant) g function. Also, we see that a change in the spatial component produce more variations in the error than a change in the temporal component. This could be due to the stability constant needed to estimate the boundary measurements $m_v(\boldsymbol{x}, t)$ by the operator in (1.23), since without this constant the method became unstable with respect to small variations of $g(t)$. Furthermore, we see from this experiment that the discontinuous spatial source $f_3(\boldsymbol{x})$ is the one that presents worst reconstruction with errors ranging from 4.1% to 8.7%.

1.5.3 Sensitivity of the reconstruction with respect to $g(t)$

In this subsection, we study the influence of employing a $g(t)$ different than the one used for generating the tremor when reconstructing the source term $f(\boldsymbol{x})$. For this purpose, we simulate synthetic "tremors" with the same three spatial source terms $f_1(\boldsymbol{x})$, $f_2(\boldsymbol{x})$, and $f_3(\boldsymbol{x})$ used in the previous experiment (see Figure 1.3), and two temporal source terms $g_a(t)$ and $g_b(t)$ (see Figure 1.5). Then, we simulate six synthetic tremors using the source combinations $f_1(\boldsymbol{x})g_a(t)$, $f_2(\boldsymbol{x})g_a(t)$, $f_3(\boldsymbol{x})g_a(t)$, $f_1(\boldsymbol{x})g_b(t)$, $f_2(\boldsymbol{x})g_b(t)$, and $f_3(\boldsymbol{x})g_b(t)$.

In order to test the robustness of our STR method, we select temporal source terms $g(t)$ different to the one used for generating the tremors, $g_a(t)$ and $g_b(t)$. We select the following function g_γ to reconstruct $f_i(\boldsymbol{x})$, for $i \in \{1, 2, 3\}$ on each case:

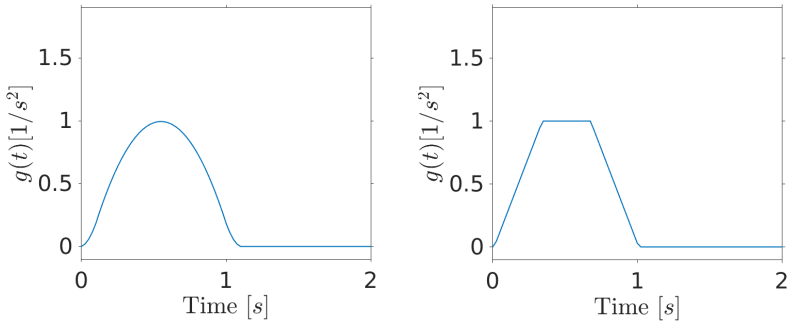

(a) $g_a(t)$ (b) $g_b(t)$

Figure 1.5: Functions selected as temporal source terms $g(t)$ to generate tremors.

$$g_\gamma(t) = \begin{cases} 1 \text{ if } t \in (0.1, \gamma) \\ 0 \text{ otherwise.} \end{cases} . \tag{1.24}$$

For this experiment, we reconstruct the spatial source term using the following set of values for γ: $\{0.6, 0.7, 0.8, 0.9, 1.0\}$. Figures 1.6 and 1.7 show the results of the reconstruction in this

	$f_1(\boldsymbol{x})g_a(t)$	$f_2(\boldsymbol{x})g_a(t)$	$f_3(\boldsymbol{x})g_a(t)$	$f_1(\boldsymbol{x})g_b(t)$	$f_2(\boldsymbol{x})g_b(t)$	$f_3(\boldsymbol{x})g_b(t)$
$\gamma = 0.6$	24.3%	29.4%	43.4%	25.4%	28.5%	43.3%
$\gamma = 0.7$	14.2%	19.4%	30.2%	10.3%	17.7%	32.1%
$\gamma = 0.8$	11.6%	12.1%	23.5%	6.3%	7.5%	18.3%
$\gamma = 0.9$	15.0%	19.5%	29.2%	21.5%	27.7%	30.9%
$\gamma = 1.0$	34.9%	29.6%	41.7%	47.0%	31.7%	47.1%

Table 1.2: Summary of the relative error $\frac{\|\widetilde{f}_i - f_i\|_{L^2}}{\|f_i\|_{L^2}}$ in experiment sensitivity with respect to $g(t)$.

experiment, and Table 1.2 summarizes the relative errors obtained when reconstructing the different tremors using $g_\gamma(t)$ for the different values of γ. In this table, the first row indicates the source employed to generate the tremor, and the first column corresponds to the γ used in $g_\gamma(t)$ to reconstruct $f_i(\boldsymbol{x})$.

As we can see in Table 1.2, the best results are obtained for $\gamma = 0.8$. This could occur because function $g_{\gamma=0.8}$ is the closest one to g_a and g_b in terms of the area contained under the curve.

1.5.4 Influence of the reconstruction with respect to c_0

We analyze the influence of constant c_0 in the reconstruction of the spatial source term. To do this, we select the three spatial source terms $f_1(\boldsymbol{x})$, $f_2(\boldsymbol{x})$, and $f_3(\boldsymbol{x})$ used in the previous experiments, and we add the MATLAB's phantom *Modified Shepp-Logan* as a fourth spatial source $f_4(\boldsymbol{x})$ (see Figure 1.9a). We also consider the three temporal source terms $g_1(t)$, $g_2(t)$, and $g_3(t)$ introduced in Subsection 1.5.2.

In the following, we study the relative error in the reconstruction of $f_i(\boldsymbol{x})$ for waves generated by the sources $f_i(\boldsymbol{x})g_j(t)$ for $i \in \{1, 2, 3, 4\}$ and $j \in \{1, 2, 3\}$, for different values of c_0.

Figure 1.8 shows the relative errors (in the L_2-norm) as a function of constant c_0 for various source combinations. For each source, we distinguish two regimes as we increase c_0. In the first part (small values of c_0), the reconstruction error diminishes as we increase c_0. Then, after attaining certain optimal value of c_0, the opposite behavior occurs. As we observe on the figures, the optimal value of c_0 is source dependent. Finding its optimal value theoretically for any source type is beyond the scope of the paper and will be further investigated in future studies.

Figure 1.9 shows reconstructions of the MATLAB's phantom for different values of c_0 and different temporal sources. Table 1.3 displays the relative errors corresponding to that figure. The boldface numbers in Table 1.3 indicate that the best errors are achieved for a "moderate" value of c_0 that is larger than 0 but small enough, as shown in Figure 1.8 for different sources. For waves generates with the source $f_4(\boldsymbol{x})g_3(t)$, the numerical simulation diverge if we try to reconstruct the spatial source term with $c_0 = 0$. Therefore, for this case we have selected a small constant $c_0 = 10^{-5}$ (Figure 1.9h), and we have obtained a

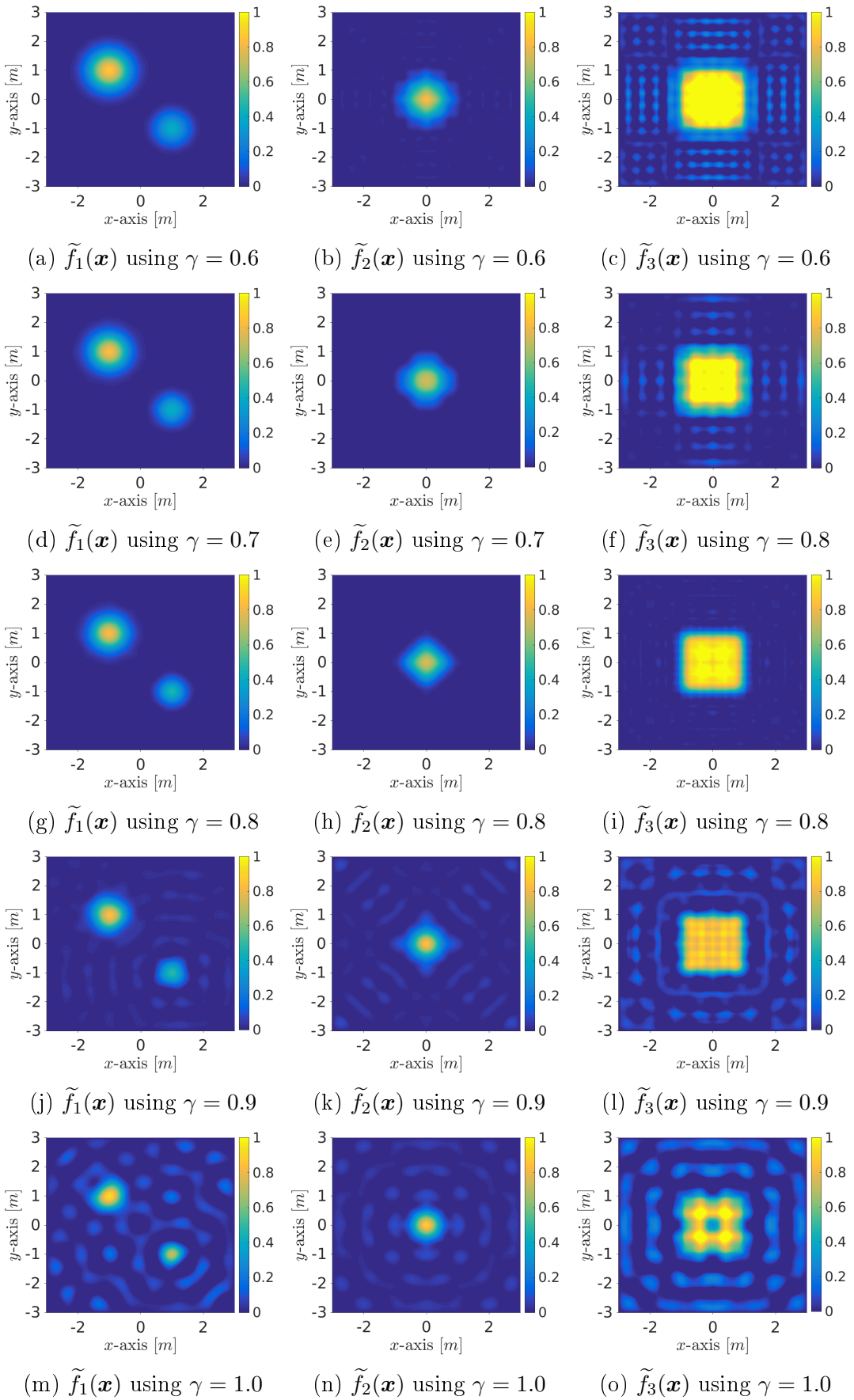

(a) $\widetilde{f}_1(\boldsymbol{x})$ using $\gamma = 0.6$ (b) $\widetilde{f}_2(\boldsymbol{x})$ using $\gamma = 0.6$ (c) $\widetilde{f}_3(\boldsymbol{x})$ using $\gamma = 0.6$

(d) $\widetilde{f}_1(\boldsymbol{x})$ using $\gamma = 0.7$ (e) $\widetilde{f}_2(\boldsymbol{x})$ using $\gamma = 0.7$ (f) $\widetilde{f}_3(\boldsymbol{x})$ using $\gamma = 0.8$

(g) $\widetilde{f}_1(\boldsymbol{x})$ using $\gamma = 0.8$ (h) $\widetilde{f}_2(\boldsymbol{x})$ using $\gamma = 0.8$ (i) $\widetilde{f}_3(\boldsymbol{x})$ using $\gamma = 0.8$

(j) $\widetilde{f}_1(\boldsymbol{x})$ using $\gamma = 0.9$ (k) $\widetilde{f}_2(\boldsymbol{x})$ using $\gamma = 0.9$ (l) $\widetilde{f}_3(\boldsymbol{x})$ using $\gamma = 0.9$

(m) $\widetilde{f}_1(\boldsymbol{x})$ using $\gamma = 1.0$ (n) $\widetilde{f}_2(\boldsymbol{x})$ using $\gamma = 1.0$ (o) $\widetilde{f}_3(\boldsymbol{x})$ using $\gamma = 1.0$

Figure 1.6: Spatial source term reconstruction using $g_\gamma(t)$ for the sources $f_i(\boldsymbol{x})g_a(t)$.

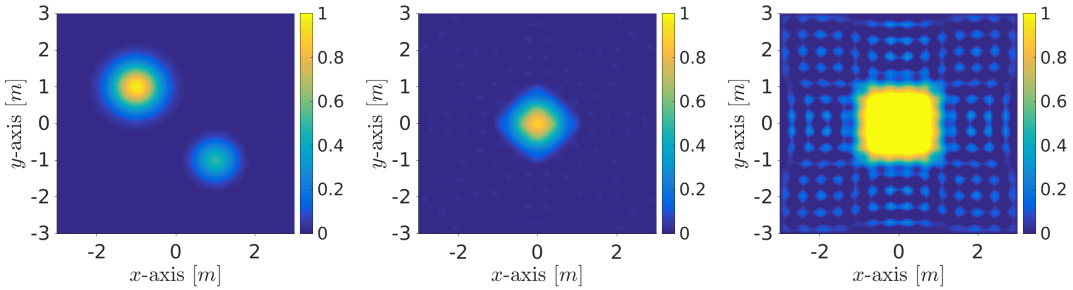

(a) $\widetilde{f}_1(\boldsymbol{x})$ using $\gamma = 0.6$ (b) $\widetilde{f}_2(\boldsymbol{x})$ using $\gamma = 0.6$ (c) $\widetilde{f}_3(\boldsymbol{x})$ using $\gamma = 0.6$

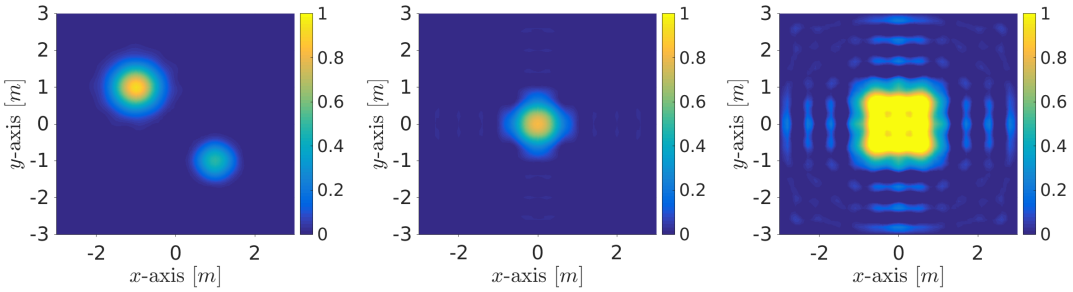

(d) $\widetilde{f}_1(\boldsymbol{x})$ using $\gamma = 0.7$ (e) $\widetilde{f}_2(\boldsymbol{x})$ using $\gamma = 0.7$ (f) $\widetilde{f}_3(\boldsymbol{x})$ using $\gamma = 0.8$

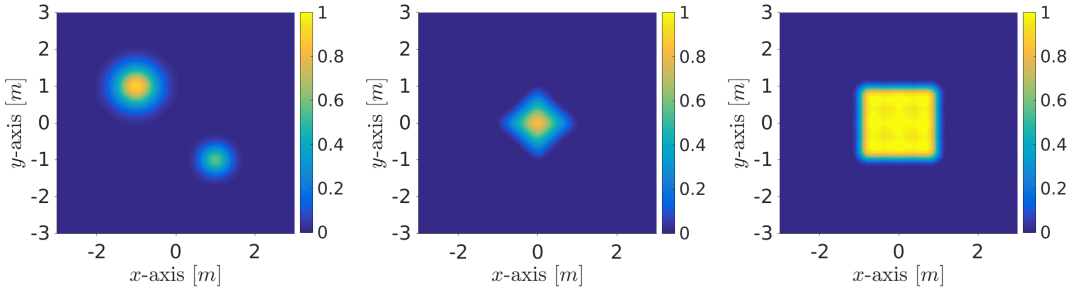

(g) $\widetilde{f}_1(\boldsymbol{x})$ using $\gamma = 0.8$ (h) $\widetilde{f}_2(\boldsymbol{x})$ using $\gamma = 0.8$ (i) $\widetilde{f}_3(\boldsymbol{x})$ using $\gamma = 0.8$

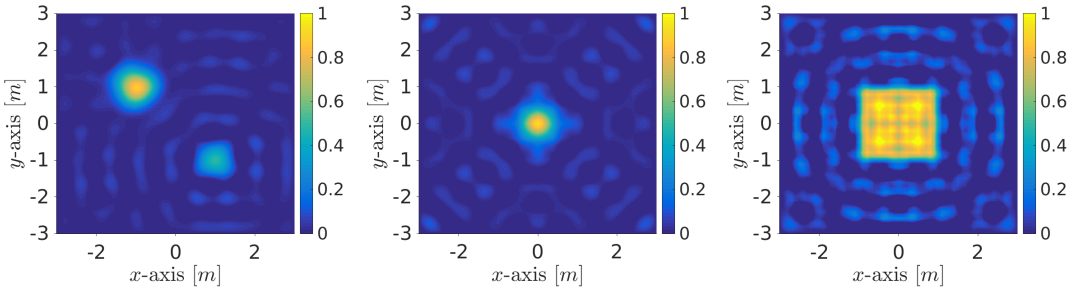

(j) $\widetilde{f}_1(\boldsymbol{x})$ using $\gamma = 0.9$ (k) $\widetilde{f}_2(\boldsymbol{x})$ using $\gamma = 0.9$ (l) $\widetilde{f}_3(\boldsymbol{x})$ using $\gamma = 0.9$

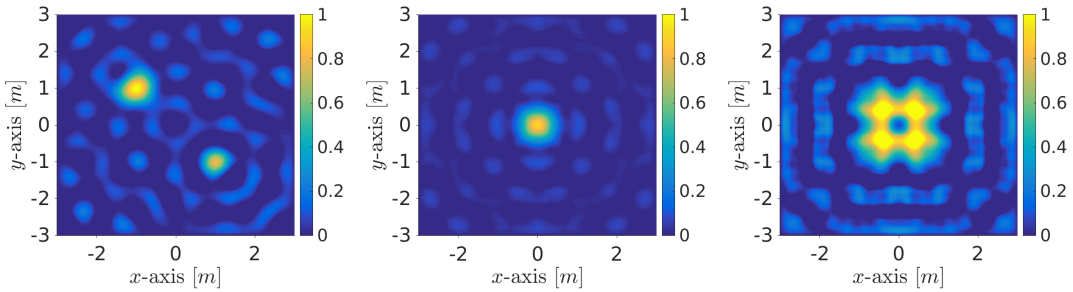

(m) $\widetilde{f}_1(\boldsymbol{x})$ using $\gamma = 1.0$ (n) $\widetilde{f}_2(\boldsymbol{x})$ using $\gamma = 1.0$ (o) $\widetilde{f}_3(\boldsymbol{x})$ using $\gamma = 1.0$

Figure 1.7: Spatial source term reconstruction using $g_\gamma(t)$ for the sources $f_i(\boldsymbol{x})g_b(t)$.

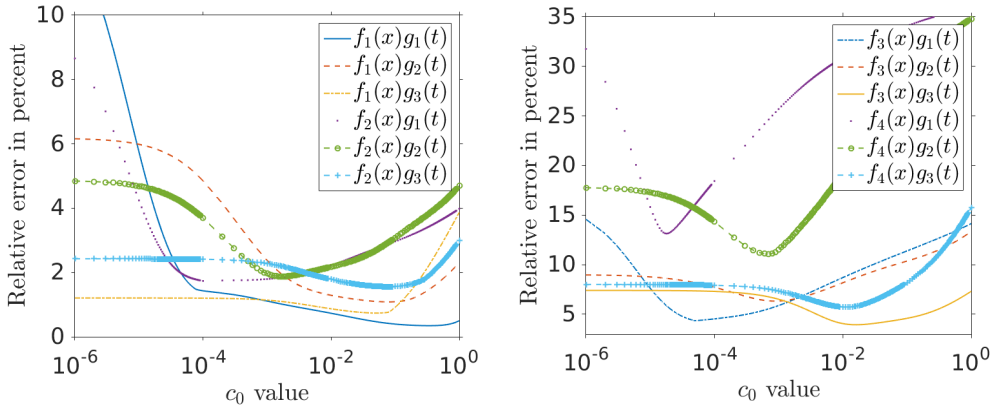

(a) c_0 analysis for $f_1(\boldsymbol{x})$ and $f_2(\boldsymbol{x})$ (b) c_0 analysis for $f_3(\boldsymbol{x})$ and $f_4(\boldsymbol{x})$

Figure 1.8: Relative error variation of the reconstruction with respect to the constant c_0.

small relative error (in comparison with the sources $f_4(\boldsymbol{x})g_1(t)$ or $f_4(\boldsymbol{x})g_2(t)$). Let us recall that g_3 is the discontinuous time-function, and this result is consistent with the observations presented in Subsection 1.5.2.

$f_4(\boldsymbol{x})g_1(t)$	35.8% (Fig. 1.9b; $c_0 = 0$)	**13.2**% (Fig. 1.9c; $c_0 = 2\times10^{-5}$)	30.9% (Fig. 1.9d; $c_0 = 0.01$)
$f_4(\boldsymbol{x})g_2(t)$	17.5% (Fig. 1.9e; $c_0 = 0$)	**11.1**% (Fig. 1.9f; $c_0 = 7\times10^{-4}$)	25.8% (Fig. 1.9g; $c_0 = 0.05$)
$f_4(\boldsymbol{x})g_3(t)$	8.0% (Fig. 1.9h; $c_0 = 10^{-5}$)	**5.7**% (Fig. 1.9i; $c_0 = 0.01$)	8.2% (Fig. 1.9j; $c_0 = 0.1$)

Table 1.3: Relative errors when reconstructing Phantom's source.

Figure 1.9 also shows that the reconstructions contain more artifacts (noise) when we consider $c_0 = 0$ than when we select a non-zero constant. At the same time, we observe that reconstructions become blurry for large values of c_0.

1.5.5 Seismicity experiments

In this subsection, we created a synthetic microseismic event to compare the classical TRM method with the proposed STR method. For this purpose, we place a synthetic source 300 m under the surface ground, as illustrated in Figure 1.10a, and we select the Ricker wavelet as the temporal source term (see Figure 1.10b). In this experiment, we consider two geophones distributions on the surface to compare both methods. In the first case, the geophones are located every 10 meters, and in the second case, they are located every 50 meters.

To add noise to the geophones measurement, we consider a factor of 0.5 in both cases.

Figures 1.11a and 1.11b (TRM and STR method respectively) describe the results of the source reconstruction for the first experiment, where the geophones are located every 10 meters; and in Figures 1.11c and 1.11d we can see the results for the experiment

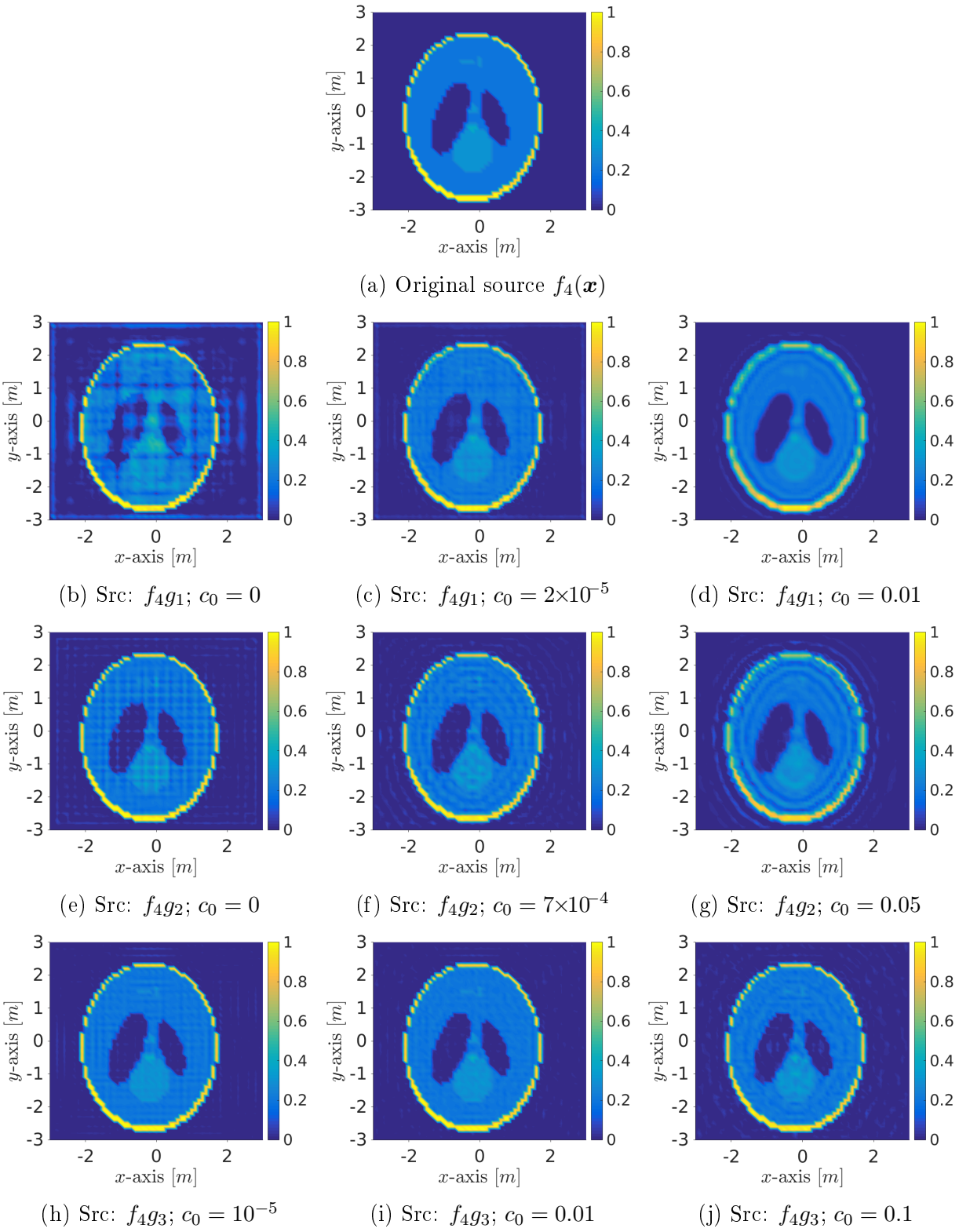

(a) Original source $f_4(\boldsymbol{x})$

(b) Src: $f_4 g_1$; $c_0 = 0$

(c) Src: $f_4 g_1$; $c_0 = 2{\times}10^{-5}$

(d) Src: $f_4 g_1$; $c_0 = 0.01$

(e) Src: $f_4 g_2$; $c_0 = 0$

(f) Src: $f_4 g_2$; $c_0 = 7{\times}10^{-4}$

(g) Src: $f_4 g_2$; $c_0 = 0.05$

(h) Src: $f_4 g_3$; $c_0 = 10^{-5}$

(i) Src: $f_4 g_3$; $c_0 = 0.01$

(j) Src: $f_4 g_3$; $c_0 = 0.1$

Figure 1.9: (a) Original function $f_4(\boldsymbol{x})$ and (b)-(j) Reconstructions $\widetilde{f}_4(\boldsymbol{x})$ for different sources and values of constant c_0.

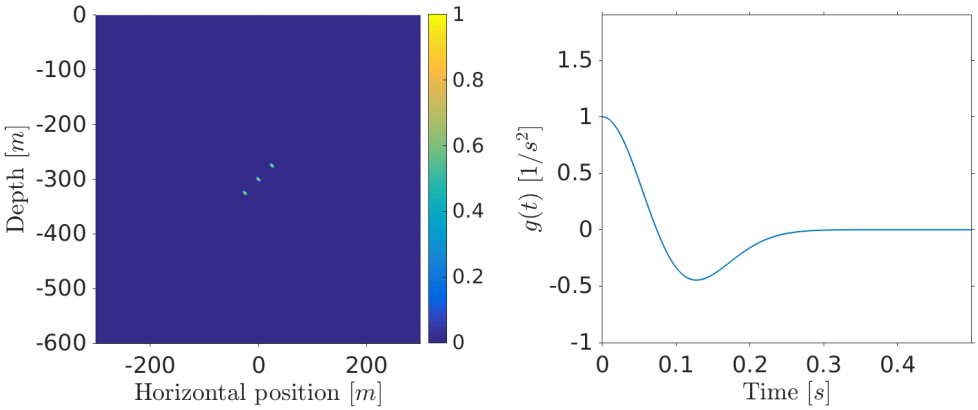

(a) Space-dependence in synthetic source

(b) Time-dependence in synthetic source

Figure 1.10: Space- and time-dependence in the synthetic seismic experiment.

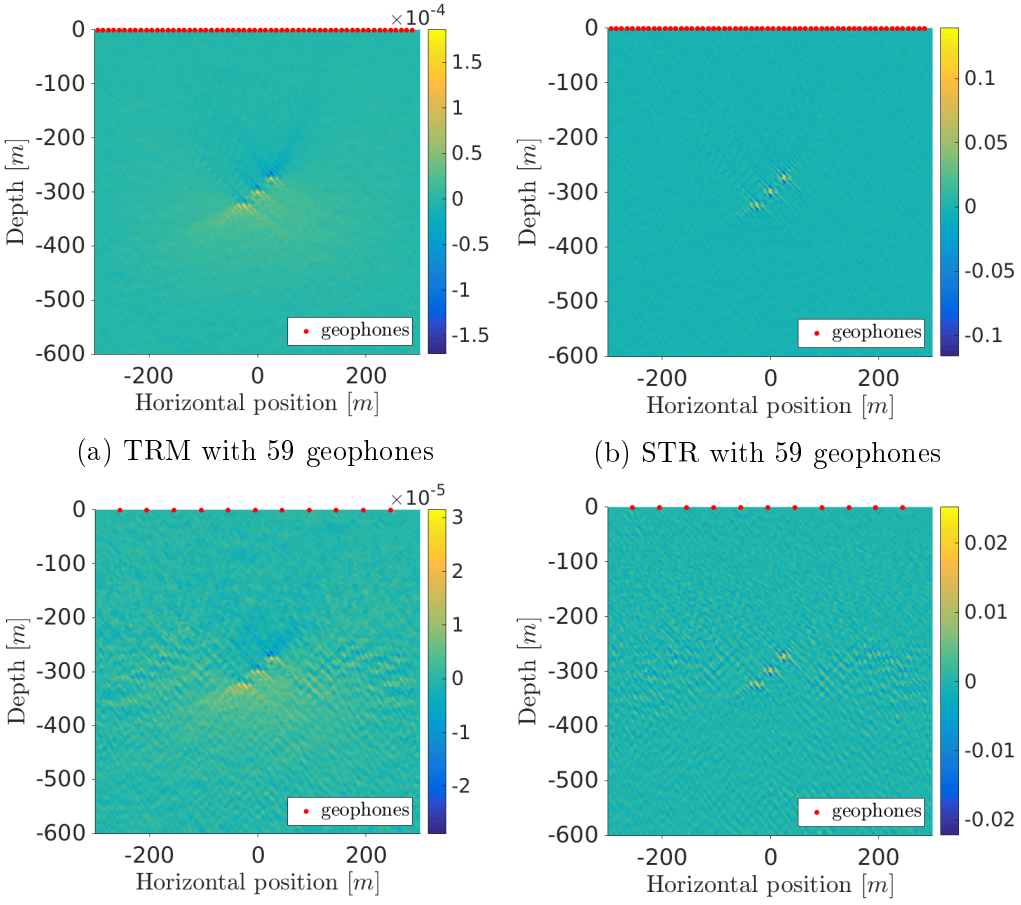

(a) TRM with 59 geophones

(b) STR with 59 geophones

(c) TRM with 11 geophones

(d) STR with 11 geophones

Figure 1.11: Spatial source term reconstruction in seismic experiments.

with the geophones distributed 50 meters apart. To study these results, we consider two aspects: the ε-support and the shape of the reconstruction. We call ε-support to $\{\boldsymbol{x} \in \Omega$, such that $|\widetilde{w}(\boldsymbol{x}, 0)| > \varepsilon\}$, and we call shape to $\{\widetilde{w}(\boldsymbol{x}, 0)$, such that $\boldsymbol{x} \in \Omega\}$. As the synthetic spatial source and the reconstructions are in different scale, it is necessary to normalize them for comparison purposes. Nonetheless, notice that the figure reconstruction scales are below the original, this is because the geophones are located only on the ground surface, and we lose information in the other directions; however, STR method is able to recover more signal information than the standard TRM method, since we consider the temporal source information on the reconstruction.

From the point of view of ε-support, it is necessary to consider a smaller threshold value to obtain a better reconstruction of the source support. As an example, with a threshold $\varepsilon = 0.1$, we obtain a relative error of 7.5% with STR method and a relative error of 13.5% with the TRM method. This means that we significantly reduce the artifacts appearing in the reconstruction. From the point if view of the shape, we also improve the reconstruction by modifying the measurements with the Duhamenl's principle to obtain more signal and increase the accuracy of the reconstruction. If we normalize the reconstructions, the relative error obtained with the STR method is 2.9% and with the classical TRM method is 4.2% for the first geophones' distribution. Then, it is clear that the STR method reduces the artifacts on the reconstruction image, and also improves the shape accuracy of the source reconstruction.

1.5.6 Mining configuration experiment

In this subsection, we recreate some limitations from a tunnel of a mine. Then, we consider a seismic experiment in homogeneous media where the geophones are located on one side of the tunnel. Assuming we have access only to the open side of the tunnel and the seism source is located on the unexplored side of the mine. We implement the STR method for the case when the geophones are dispersed within the mine tunnel. To do this, we deploy two configurations of eight geophones randomly distributed in one side of the mine.

For this experiment, the geophones are no longer part of the boundary condition for the backward problem. Instead, we consider a free boundary backward problem, where the geophones act as point sources that reverse the measurements processed with the STR method. Mathematically, this problem is known as internal measurement reconstruction.

To analyze the results, we consider threshold that eliminates the values lower than 55% of the maximum value in the reconstruction. Figure 1.12 shows the geophones configuration and the original source location (1.12a and 1.12b), it also shows the result of implementing the STR method with eight geophones located inside the computational domain (1.12c and 1.12d), and finally it displays the result of implementing the threshold to identify the higher vales in the reconstruction (1.12e and 1.12f). From this figure, we see that the STR still locates the source correctly, but it is not able to reconstruct the shape of the source. Then, we can see that the method only loses precision in the shape reconstruction when we have access to partial information of the wave.

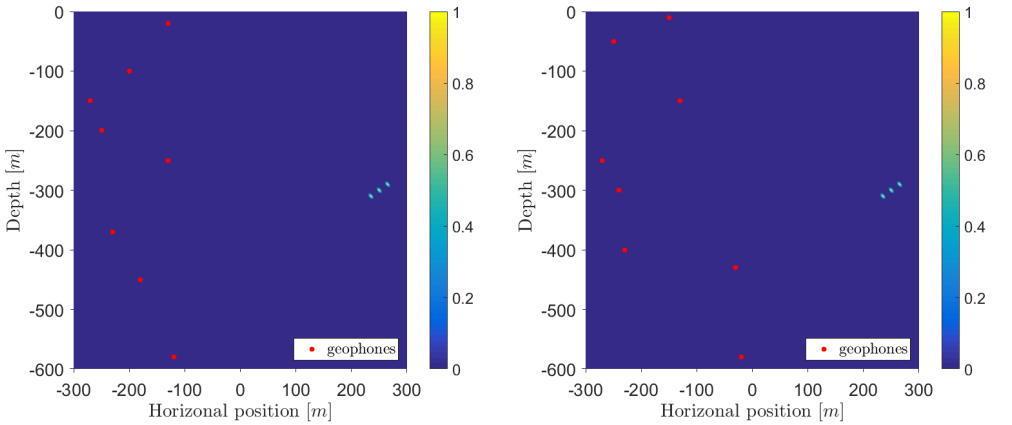

(a) Source and geoph. location, conf. 1 (b) Source and geoph. location, conf. 2

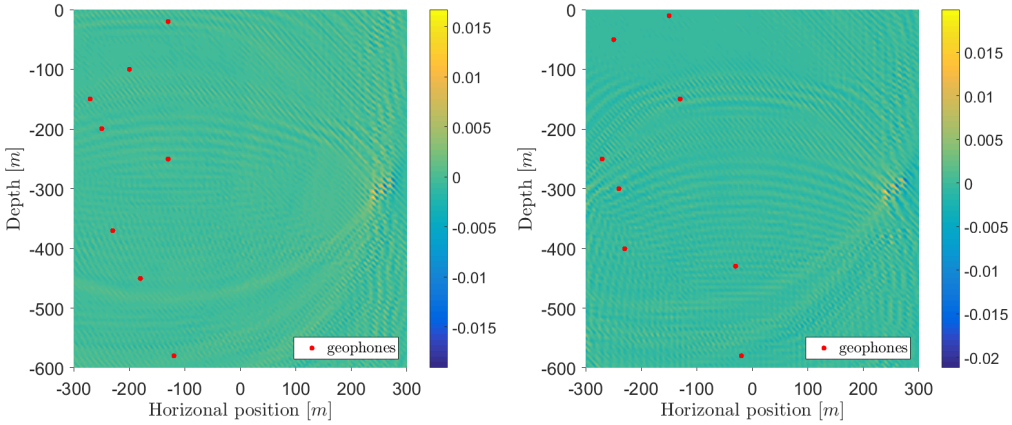

(c) STR reconstruction, conf. 1 (d) STR reconstruction, conf. 2

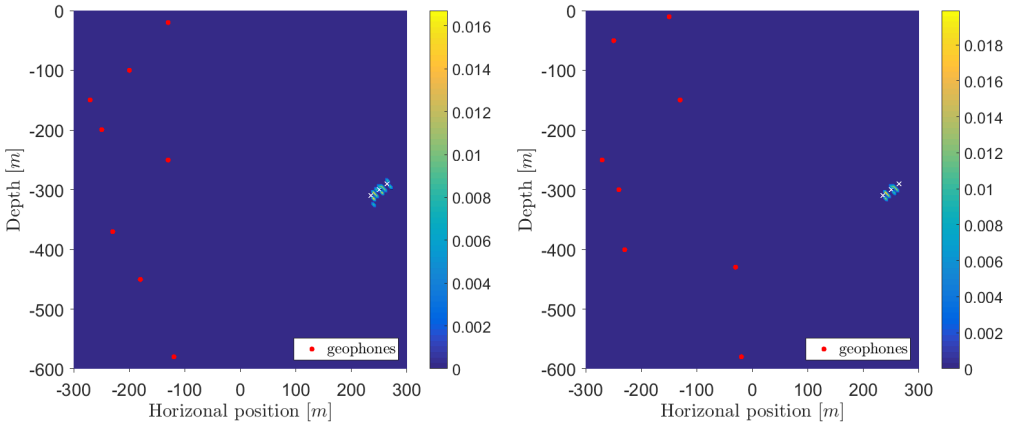

(e) Recons. with threshold, conf. 1 (f) Recons. with threshold, conf. 2

Figure 1.12: Spatial source term reconstruction in seismicity induced by mining experiments with two geophones distributions. White crosses in (e) and (f) represent the original source location.

Chapter 2

Source time reversal (STR) method for linear elasticity

We study the problem of source reconstruction for a linear elasticity problem applied to seismicity induced by mining. We assume the source is written as a variable separable function $\boldsymbol{f}(\boldsymbol{x})g(t)$. We first present a simple proof a local decay for elasticity in the case of homogeneous media. We then extend the *source time reversal* method, originally developed for acoustic waves, to an elastic system of waves. Additionally, we present a fast reconstruction implementation for large data sets. This is especially useful in the elastic case, in which the numerical cost is higher than in fluid acoustics. We complement this work with several 2D and 3D numerical experiments and an analysis of the results.

2.1 Introduction

Seismicity is described by equations of classical continuum mechanics. There are two different descriptions of motion and its mechanics: Lagrangian and Eulerian [2]. For this work, and some others seismicity applications, it is preferable to consider the Lagrangian description, which studies the displacement $\boldsymbol{u}(\boldsymbol{x}, t)$ of the particle $\boldsymbol{x}$ at time t. Since particle $\boldsymbol{x}$ is invariant in time, we obtain its velocity and acceleration by computing the first and second time derivatives of the displacement, respectively [2]. As there are no systematic differences between seismicity and mining seismicity (or induced seismicity) [50], it is valid to consider the same model for both seismic activities.

In this work, we are interested in applications to seismicity induced by mining. The understanding of seismic activity inside mines provides essential information to prevent accidents and improve the safety of miners. The main difference between seismicity and induced seismicity is the distance that the wavefronts travel from the source to the geophones, which in the case of induced seismicity is shorter than in seismicity. Due to this, it becomes relevant to take into account the time profile of the source in the case of induced seismicity. We propose a source of the form $\boldsymbol{f}(\boldsymbol{x})g(t)$, where g is a scalar-valued function with compact support. Although considering this rather general source produces some difficulties in the reconstruction, it is physically more realistic than a traditional Dirac delta source in time. The

objective is then to describe and locate the term $\boldsymbol{f}(\boldsymbol{x})$ by knowing the information provided by the geophones and $g(t)$. Geophones measure the displacement velocity by transforming the velocity of waves into voltages [59].

The problems of *source location* and *source reconstruction* have been widely studied in applied mathematics regarding their uniqueness, stability, and reconstruction. For example, V. Isakov discussed in [64] source reconstructions methods for elliptic, parabolic, and hyperbolic problems. There exist different techniques in inverse problems and control theory for solving these kinds of problems. To mention some of them, M. Yamamoto [116] in 1995 studied the problem of space-source reconstruction for the wave equation, when the source is of the form $s(\boldsymbol{x}, t) = f(\boldsymbol{x})g(t)$, using exact boundary controllability and Volterra integral equations and measuring the normal derivative on the boundary. G. Garcia et al. [48] studied in 2013 a similar problem for the heat equation and reconstructed the space-term $f(\boldsymbol{x})$ from observing the solution and its time derivative in some subdomain $\mathcal{O} \subset \Omega$, where $\Omega \subset \mathbb{R}^n$ is a nonempty open bounded domain. A. El Abadia and T. Ha-Duong [12] studied in 2000 the inverse source problem for some elliptic equations from boundary measurements. They proposed an algebraic method to carry out the identifiability and also showed theoretical results. A. El Badia et al. [13] introduced on 2000 numerical results for determining a source term in elliptic problems by using the Hilbert Uniqueness Method (HUM).

In the case of wave propagation problems (including acoustics, elasticity, and electromagnetism), time reversal exploits a fundamental symmetry of waves physics [8]. M. Fink developed the time-reversal mirror as an extension of phase conjugate mirrors [46], which consists of a receiver-emitter transducer device that first measures a signal, and then returns it in reversed chronology. Time-reversal mirror has applications in several areas. For example, detection of tumors and kidney stones in medical imaging, detection of defects in metals, and long-distance communication and mine detection in the ocean [45].

Time-reversal methods have also been applied for solving inverse source problems for acoustic and elastic waves. H. Ammari introduced in [4] the basis for time-reversal imaging in the context of small anomalies on the conductivity for Dirac delta sources in time and space. In [6], he studies the problem of source reconstruction for the thermo-viscous model considering an attenuating acoustic media. In [7], he shows a time-reversal technique for solving inverse extended source[1] problems in the acoustic case, when the source is the derivative (in distributional sense) of a Dirac delta function in time and a smooth real-valued function with smooth compact support in space. In [5], time-reversal techniques for imaging extended source detection in elastic and viscoelastic media are presented for a source given as the derivative of a Dirac delta function in time and a vector-valued function with compact support in space.

In [17], a method called *Source Time Reversal* (STR) was proposed for reconstructing the space term of a source of the form $f(\boldsymbol{x})g(t)$ for the acoustic wave equation. The work, with applications to mining seismicity, takes advantage of the information provided by a general time-source term $g(t)$ to transform the original source problem into an initial condition problem without source, where the unknown $f(\boldsymbol{x})$ now appears as an initial condition for this new problem. That work aims to time-reverse the boundary information, converting it

[1] Extended sources are those whose size is much larger than a wavelength [5].

into an initial condition of a problem without source. Via a Volterra equation, the boundary information needed to perform the time-reversal method is obtained from the boundary measurements of the original source problem.

In the present work, we extend the STR method to the case of elasticity. This extension overcomes the difficulties encountered when considering a general time-source term. To derive this extension, we first introduce a local decay result for linear elasticity in homogeneous media. We then introduce two reconstruction methods based on different regularization terms. One of the regularizations delivers a fast reconstruction method with low computational cost. This is especially useful for large data sets, as those often appearing in elasticity. Additionally, Some 2D and 3D numerical examples are considered.

The rest of the Chapter is organized as follows. Section 2.2 describes the elasticity equation under different considerations: anisotropic, isotropic, homogeneous, and inhomogeneous media. We also show some properties, behaviors, and characteristics of solutions of acoustic and elastic equations. Section 2.3 extends the STR method to an elastic system of waves. We then propose two reconstruction methods: the STR with traditional regularization and a fast STR with cut-off regularization. Section 2.4 describes two numerical implementations of the STR method, one based on the finite difference method and the other on the finite element method. In Section 2.5, we numerically analyze the STR with traditional regularization via 2D and 3D synthetic examples. Section 2.6 analyzes numerically the fast STR with cut-off regularization via more realistic 2D seismicity induced by mining examples with added noise.

2.2 Framework

In this section, we introduce some notation and review useful results of hyperbolic equations. We use bold letters to indicate vector-valued functions. Let $u : \mathbb{R}^n \to \mathbb{R}$ and $\boldsymbol{u} : \mathbb{R}^n \to \mathbb{R}^n$ be scalar-valued and vector-valued functions, respectively. Here, in the context of elastic waves $\boldsymbol{u} = (u_1, \dots, u_n)$ stands for the displacement field, and $u_i : \mathbb{R}^n \to \mathbb{R}$ with $i \in \{1, \dots, n\}$ corresponds to the i-th component of the displacement.

We denote Δu to the Laplace operator acting on a scalar field u. Then, the Laplacian of a vector field is defined as

$$\Delta \boldsymbol{u} = (\Delta u_1, \dots, \Delta u_n).$$

The curl of a vector-valued function in $\mathbb{R}^3$ is defined as

$$\operatorname{curl} \boldsymbol{u} = (\partial_{x_1}, \partial_{x_2}, \partial_{x_3}) \times (u_1, u_2, u_3) = (\partial_{x_2} u_3 - \partial_{x_3} u_2, \partial_{x_3} u_1 - \partial_{x_1} u_3, \partial_{x_1} u_2 - \partial_{x_2} u_1),$$

whereas the curl operators for a vector-valued and scalar-valued functions in $\mathbb{R}^2$ are respectively defined as

$$\operatorname{curl}_{\mathrm{v}} \boldsymbol{u} = \partial_{x_1} u_2 - \partial_{x_2} u_1 \qquad \text{and} \qquad \operatorname{curl}_{\mathrm{s}} u = (\partial_{x_2} u, -\partial_{x_1} u),$$

where we denote the curl with subscripts to differentiate both cases. Notice that $\operatorname{curl} : \mathbb{R}^3 \to \mathbb{R}^3$ in $\mathbb{R}^3$, $\operatorname{curl}_{\mathrm{v}} : \mathbb{R}^2 \to \mathbb{R}$ in $\mathbb{R}^2$, and $\operatorname{curl}_{\mathrm{s}} : \mathbb{R} \to \mathbb{R}^2$ in $\mathbb{R}^2$. Then, we have the following known properties in 3D and 2D.

Remark 2.1 *Let $\boldsymbol{u} : \mathbb{R}^3 \to \mathbb{R}^3$ be a vector-valued function and $u : \mathbb{R}^3 \to \mathbb{R}$ a scalar-valued function. Then:*

1. $\operatorname{curl} \nabla u = \mathbf{0}$.
2. $\operatorname{div} \operatorname{curl} \boldsymbol{u} = 0$.
3. $\operatorname{curl} \operatorname{curl} \boldsymbol{u} = \nabla(\operatorname{div} \boldsymbol{u}) - \Delta \boldsymbol{u}$.

Remark 2.2 *Let $\boldsymbol{u} : \mathbb{R}^2 \to \mathbb{R}^2$ be a vector-valued function and $u : \mathbb{R}^2 \to \mathbb{R}$ a scalar-valued function. Then:*

1. $\operatorname{curl}_{\mathrm{v}} \nabla u = 0$.
2. $\operatorname{div} \operatorname{curl}_{\mathrm{s}} u = 0$.
3. $\operatorname{curl}_{\mathrm{s}} \operatorname{curl}_{\mathrm{v}} \boldsymbol{u} = \nabla(\operatorname{div} \boldsymbol{u}) - \Delta \boldsymbol{u}$.
4. $\operatorname{curl}_{\mathrm{v}} \operatorname{curl}_{\mathrm{s}} u = \Delta u$.

The theory of elasticity consists of the description of stress, strain, and displacement at each point of a deformable object [53]. The general model in linear elasticity is given by the equation of motion

$$\rho \partial_t^2 \boldsymbol{u} - \nabla \cdot \underline{\underline{\sigma}}(\boldsymbol{u}) = \boldsymbol{F},$$

where $\underline{\underline{\sigma}}$ represents a second-order tensor field called *stress tensor* [37]. In the isotropic case, the stress tensor takes the particular form

$$\underline{\underline{\sigma}}(\boldsymbol{u}) = \mu \left(\nabla \boldsymbol{u} + \nabla \boldsymbol{u}^T \right) + \lambda (\nabla \cdot \boldsymbol{u}) \mathrm{Id},$$

where μ and λ are the Lamé parameters [76]. In addition, when we consider the case of homogeneous media, the tensors

$$\sigma_{ij}(\boldsymbol{u}) = \lambda \nabla \cdot \boldsymbol{u} \, \delta_{ij} + 2 \mu \, \epsilon_{ij}(\boldsymbol{u})$$

and

$$\epsilon_{ij}(\boldsymbol{u}) = \frac{1}{2} \left(\frac{\partial u_i}{\partial x_j} + \frac{\partial u_j}{\partial x_i} \right)$$

are, respectively, the classical Cauchy and stress tensors typically defined in a homogeneous and isotropic elastic media. Then, in the last case, the equation of motion is given by

$$\rho \partial_t^2 \boldsymbol{u} - \mu \Delta \boldsymbol{u} - (\mu + \lambda) \nabla (\nabla \cdot \boldsymbol{u}) = \boldsymbol{F}. \tag{2.1}$$

The solution $\boldsymbol{u}$ to linear elasticity is composed of two waves: the first one is known as a compressional wave and the second as a shear wave. These waves can be written in terms of space derivatives of solutions of acoustic problems. To do this, we consider the decomposition of the space of vector-valued square-integrable functions into a direct sum of divergence-free and curl-free spaces, called *Helmholtz decomposition* [32]. In other words, let $\boldsymbol{u} \in (L^2(\mathbb{R}^n))^n$ be a vector field. Then, there exist a vector-valued function $\boldsymbol{\psi}$ and a scalar-valued function ϕ such that

$$\boldsymbol{u} = \boldsymbol{u}_{\mathrm{div}} + \boldsymbol{u}_{\mathrm{curl}},$$

where $\boldsymbol{u}_{\text{div}} = \operatorname{curl}\boldsymbol{\psi}$ and $\boldsymbol{u}_{\text{curl}} = \nabla\phi$. Let us recall from Remark 2.1 and 2.2 that for the cases $n \in \{2, 3\}$, we obtain $\operatorname{div}\boldsymbol{u}_{\text{div}} = 0$ and $\operatorname{curl}\boldsymbol{u}_{\text{curl}} = \boldsymbol{0}$. We can find more general versions of this decomposition for different open sets in [27, 51].

In addition, it is easy to see by using Remarks 2.1 and 2.2 that problem (2.1) in 3D and 2D can be written respectively as

$$\rho\partial_t^2\boldsymbol{u} - (2\mu+\lambda)\nabla(\operatorname{div}\boldsymbol{u}) + \mu\operatorname{curl}\operatorname{curl}\boldsymbol{u} = \boldsymbol{F},$$

$$\rho\partial_t^2\boldsymbol{u} - (2\mu+\lambda)\nabla(\operatorname{div}\boldsymbol{u}) + \mu\operatorname{curl}_{\text{s}}\operatorname{curl}_{\text{v}}\boldsymbol{u} = \boldsymbol{F}.$$

In the case of homogeneous media, these expressions allow us to relate solutions of linear elasticity with acoustic solutions via the following theorem.

Theorem 2.3 (Lamé's Theorem 3D case [2]) *Let $\boldsymbol{u}$ be the solution of the following problem*

$$\begin{cases} \rho\partial_t^2\boldsymbol{u}(\boldsymbol{x},t) - L_{\mu,\lambda}\boldsymbol{u}(\boldsymbol{x},t) = \boldsymbol{F}(\boldsymbol{x},t), & \text{in } \mathbb{R}^3\times(0,T),\\ \boldsymbol{u}(\boldsymbol{x},0) = \nabla p(\boldsymbol{x}) + \operatorname{curl}\boldsymbol{q}(\boldsymbol{x}),\\ \partial_t\boldsymbol{u}(\boldsymbol{x},0) = \nabla r(\boldsymbol{x}) + \operatorname{curl}\boldsymbol{s}(\boldsymbol{x}), \end{cases}$$

where $L_{\mu,\lambda}\boldsymbol{u} = (2\mu+\lambda)\nabla(\operatorname{div}\boldsymbol{u}) - \mu\operatorname{curl}\operatorname{curl}\boldsymbol{u}$, $\boldsymbol{F} = \nabla\Phi + \operatorname{curl}\boldsymbol{\Psi}$, with

$$\operatorname{div}\boldsymbol{s} = \operatorname{div}\boldsymbol{q} = \operatorname{div}\boldsymbol{\Psi} = 0. \tag{2.2}$$

Then, there exist functions ϕ and $\boldsymbol{\psi}$ such that

$$\boldsymbol{u} = \nabla\phi + \operatorname{curl}\boldsymbol{\psi}, \tag{2.3}$$

$$\operatorname{div}\boldsymbol{\psi} = 0, \tag{2.4}$$

$$\begin{cases} \partial_t^2\phi - \dfrac{\lambda+2\mu}{\rho}\Delta\phi = \dfrac{\Phi}{\rho}, & \text{in } \mathbb{R}^3\times(0,T),\\ \phi(\boldsymbol{x},0) = p(\boldsymbol{x}),\\ \partial_t\phi(\boldsymbol{x},0) = r(\boldsymbol{x}), \end{cases} \tag{2.5}$$

$$\begin{cases} \partial_t^2\boldsymbol{\psi} - \dfrac{\mu}{\rho}\Delta\boldsymbol{\psi} = \dfrac{\boldsymbol{\Psi}}{\rho}, & \text{in } \mathbb{R}^3\times(0,T),\\ \boldsymbol{\psi}(\boldsymbol{x},0) = \boldsymbol{q}(\boldsymbol{x}),\\ \partial_t\boldsymbol{\psi}(\boldsymbol{x},0) = \boldsymbol{s}(\boldsymbol{x}), \end{cases} \tag{2.6}$$

where $\nabla\phi$ and $\operatorname{curl}\boldsymbol{\psi}$ are the P-wave and S-wave, respectively, components of $\boldsymbol{u}$.

Proof. We begin the proof by considering

$$\phi(\boldsymbol{x},t) = \frac{1}{\rho}\int_0^t (t-\tau)\left[\Phi(\boldsymbol{x},\tau) + (\lambda+2\mu)\operatorname{div}\boldsymbol{u}(\boldsymbol{x},\tau)\right]d\tau + r(\boldsymbol{x})t + p(\boldsymbol{x}), \tag{2.7}$$

and

$$\boldsymbol{\psi}(\boldsymbol{x},t) = \frac{1}{\rho}\int_0^t (t-\tau)\left[\boldsymbol{\Psi}(\boldsymbol{x},\tau) - \mu\operatorname{curl}\boldsymbol{u}(\boldsymbol{x},\tau)\right]d\tau + \boldsymbol{s}(\boldsymbol{x})t + \boldsymbol{q}(\boldsymbol{x}). \tag{2.8}$$

To prove identity (2.3), we first compute $\nabla\phi$ and $\operatorname{curl}\boldsymbol{\psi}$ from (2.7) and (2.8)

$$\begin{aligned}\nabla\phi(\boldsymbol{x},t) = \frac{1}{\rho}\int_0^t (t-\tau)\left[\nabla\Phi(\boldsymbol{x},\tau) + (\lambda+2\mu)\nabla(\operatorname{div}\boldsymbol{u})(\boldsymbol{x},\tau)\right]\,d\tau \\ +\nabla r(\boldsymbol{x})t + \nabla p(\boldsymbol{x}),\end{aligned} \tag{2.9}$$

$$\begin{aligned}\operatorname{curl}\boldsymbol{\psi}(\boldsymbol{x},t) = \frac{1}{\rho}\int_0^t (t-\tau)\left[\operatorname{curl}\boldsymbol{\Psi}(\boldsymbol{x},\tau) - \mu\operatorname{curl}\operatorname{curl}\boldsymbol{u}(\boldsymbol{x},\tau)\right]\,d\tau \\ +\operatorname{curl}\boldsymbol{s}(\boldsymbol{x})t + \operatorname{curl}\boldsymbol{q}(\boldsymbol{x}).\end{aligned} \tag{2.10}$$

Then, adding (2.9) with (2.10), we obtain

$$\begin{aligned}\nabla\phi(\boldsymbol{x},t) + \operatorname{curl}\boldsymbol{\psi}(\boldsymbol{x},t) =& \frac{1}{\rho}\int_0^t (t-\tau)\rho\partial_t^2\boldsymbol{u}(x,\tau)\,d\tau + \partial_t\boldsymbol{u}(\boldsymbol{x},0)t + \boldsymbol{u}(\boldsymbol{x},0)\\ =& t\int_0^t \partial_t^2\boldsymbol{u}(x,\tau)\,d\tau - \int_0^t \partial_t^2\boldsymbol{u}(x,\tau)\tau\,d\tau + \partial_t\boldsymbol{u}(\boldsymbol{x},0)t\\ &+\boldsymbol{u}(\boldsymbol{x},0)\\ =& \int_0^t \partial_t\boldsymbol{u}(x,\tau)\,d\tau + \boldsymbol{u}(\boldsymbol{x},0)\\ =& \boldsymbol{u}(\boldsymbol{x},t),\end{aligned}$$

for all $(\boldsymbol{x},t)\in\mathbb{R}^3\times(0,T)$, which proves (2.3). To prove the second identity, we apply the divergence operator to (2.8)

$$\operatorname{div}\boldsymbol{\psi}(\boldsymbol{x},t) = \frac{1}{\rho}\int_0^t (t-\tau)\left[\operatorname{div}\boldsymbol{\Psi}(\boldsymbol{x},\tau) + \mu\operatorname{div}\operatorname{curl}\boldsymbol{u}(\boldsymbol{x},\tau)\right]\,d\tau + \operatorname{div}\boldsymbol{s}(\boldsymbol{x})t + \operatorname{div}\boldsymbol{q}(\boldsymbol{x}).$$

Using the identities in (2.2) and Remark 2.1 yields (2.4).

To obtain the third identity, we first derive (2.7) two times with respect to t and use the expression $\operatorname{div}\boldsymbol{u} = \operatorname{div}(\nabla\phi) + \operatorname{div}\operatorname{curl}\boldsymbol{\psi} = \Delta\phi$, which gives us

$$\partial_t^2\phi(\boldsymbol{x},t) = \frac{1}{\rho}\left[\Phi(\boldsymbol{x},t) + (\lambda+2\mu)\Delta\phi(\boldsymbol{x},t)\right].$$

The initial conditions $\phi(\boldsymbol{x},0)$ and $\partial_t\phi(\boldsymbol{x},0)$ can be directly determined from evaluating (2.7) and its derivative with respect to t, which proves (2.5).

A similar procedure applies for the last identity. We derive two times (2.8) with respect to t and use the identity $\operatorname{curl}\boldsymbol{u} = \operatorname{curl}\nabla\phi + \operatorname{curl}\operatorname{curl}\boldsymbol{\psi} = \operatorname{curl}\operatorname{curl}\boldsymbol{\psi}$ to obtain

$$\begin{aligned}\partial_t^2\boldsymbol{\psi}(\boldsymbol{x},t) &= \frac{1}{\rho}\left[\boldsymbol{\Psi}(\boldsymbol{x},\tau) + \mu\operatorname{curl}\operatorname{curl}\boldsymbol{\psi}(\boldsymbol{x},\tau)\right]\\ &= \frac{1}{\rho}\left[\boldsymbol{\Psi}(\boldsymbol{x},t) - \mu(\nabla(\operatorname{div}\boldsymbol{\psi})(\boldsymbol{x},t) - \Delta\boldsymbol{\psi}(\boldsymbol{x},t))\right]\\ &= \frac{1}{\rho}\left[\boldsymbol{\Psi}(\boldsymbol{x},t) + \mu\Delta\boldsymbol{\psi}(\boldsymbol{x},t)\right].\end{aligned}$$

The initial conditions are computed directly from (2.8) and its derivative with respect to t, which proves (2.6) and completes the proof. □

Theorem 2.4 (Lamé's Theorem 2D case [2]) *Let $\boldsymbol{u}$ be the solution of the following problem*

$$\begin{cases} \rho\partial_t^2\boldsymbol{u}(\boldsymbol{x},t) - L_{\mu,\lambda}\boldsymbol{u}(\boldsymbol{x},t) = \boldsymbol{F}(\boldsymbol{x},t), & \text{in } \mathbb{R}^2\times(0,T), \\ \boldsymbol{u}(\boldsymbol{x},0) = \nabla p(\boldsymbol{x}) + \operatorname{curl}_{\mathrm{s}} q(\boldsymbol{x}), \\ \partial_t\boldsymbol{u}(\boldsymbol{x},0) = \nabla r(\boldsymbol{x}) + \operatorname{curl}_{\mathrm{s}} s(\boldsymbol{x}), \end{cases}$$

where $L_{\mu,\lambda}\boldsymbol{u} = (2\mu+\lambda)\nabla(\operatorname{div}\boldsymbol{u}) - \mu\operatorname{curl}_{\mathrm{s}}\operatorname{curl}_{\mathrm{v}}\boldsymbol{u}$, $\boldsymbol{F} = \nabla\Phi + \operatorname{curl}_{\mathrm{s}}\Psi$. Then, there exist functions ϕ and ψ such that

$$\boldsymbol{u} = \nabla\phi + \operatorname{curl}_{\mathrm{s}}\psi,$$

$$\begin{cases} \partial_t^2\phi - \dfrac{\lambda+2\mu}{\rho}\Delta\phi = \dfrac{\Phi}{\rho}, & \text{in } \mathbb{R}^2\times(0,T), \\ \phi(\boldsymbol{x},0) = p(\boldsymbol{x}), \\ \partial_t\phi(\boldsymbol{x},0) = r(\boldsymbol{x}), \end{cases}$$

$$\begin{cases} \partial_t^2\psi - \dfrac{\mu}{\rho}\Delta\psi = \dfrac{\Psi}{\rho}, & \text{in } \mathbb{R}^2\times(0,T), \\ \psi(\boldsymbol{x},0) = q(\boldsymbol{x}), \\ \partial_t\psi(\boldsymbol{x},0) = s(\boldsymbol{x}), \end{cases}$$

where $\nabla\phi$ and $\operatorname{curl}_{\mathrm{s}}\psi$ are the P-wave and S-wave components of $\boldsymbol{u}$, respectively.

Proof. Apply the same procedure as in Theorem 2.3 by considering

$$\phi(\boldsymbol{x},t) = \frac{1}{\rho}\int_0^t (t-\tau)\left[\Phi(\boldsymbol{x},\tau) + (\lambda+2\mu)\operatorname{div}\boldsymbol{u}(\boldsymbol{x},\tau)\right]\,d\tau + r(\boldsymbol{x})t + p(\boldsymbol{x}),$$

and

$$\boldsymbol{\psi}(\boldsymbol{x},t) = \frac{1}{\rho}\int_0^t (t-\tau)\left[\Psi(\boldsymbol{x},\tau) - \mu\operatorname{curl}_{\mathrm{v}}\boldsymbol{u}(\boldsymbol{x},\tau)\right]\,d\tau + s(\boldsymbol{x})t + q(\boldsymbol{x}).$$

□

To apply a time reversal process to linear elasticity, it is necessary to obtain a local energy decay type result. A classical result of B. R. Vainberg [111] establishes a decay rate of the solution and of all its derivatives for acoustic waves and large times under certain requirements on the propagation speed.

Definition 2.5 (acoustic non-trapping condition [35]) *Let $c:\mathbb{R}^n\to\mathbb{R}$ be a $C^\infty(\mathbb{R}^n)$ function. We define the Hamiltonian $H(\boldsymbol{x},\boldsymbol{\xi}) = \frac{1}{2}c^2(\boldsymbol{x})|\boldsymbol{\xi}|^2$ and the following system*

$$\begin{cases} \boldsymbol{x}_t' = \frac{\partial H}{\partial\boldsymbol{\xi}} = \boldsymbol{\xi}c^2(\boldsymbol{x}), \\ \boldsymbol{\xi}_t' = -\frac{\partial H}{\partial\boldsymbol{x}} = -\frac{1}{2}|\boldsymbol{\xi}|^2\nabla(c^2(\boldsymbol{x})), \\ \boldsymbol{x}|_{t=0} = \boldsymbol{x}_0, \\ \boldsymbol{\xi}|_{t=0} = \boldsymbol{\xi}_0, \\ H(\boldsymbol{x}_0,\boldsymbol{\xi}_0) = H_0. \end{cases} \tag{2.11}$$

Solutions of (2.11) are called bicharacteristics, and the projection of the $\boldsymbol{x}$-components into $\mathbb{R}^n$ of a bicharacteristic is called ray. We say that $c(\boldsymbol{x})$ accomplishes the non-trapping condition *if all rays go to infinity when $t \to \infty$.*

Theorem 2.6 (Local decay for acoustic solution [35]) *Let v be solution to the following problem*

$$\begin{cases} \partial_t^2 v(\boldsymbol{x},t) - c^2(\boldsymbol{x})\Delta v(\boldsymbol{x},t) = 0, & \text{in } \mathbb{R}^n \times (0,\infty), \\ v(\boldsymbol{x},0) = \varphi(\boldsymbol{x}), \\ \partial_t v(\boldsymbol{x},0) = \psi(\boldsymbol{x}), \end{cases} \tag{2.12}$$

where $c(\boldsymbol{x}) > c_1 > 0$ for all $\boldsymbol{x} \in \mathbb{R}^n$. Let us assume all the inhomogeneities of the medium and the initial conditions are confined to a bounded subset of $\Omega \subset \mathbb{R}^n$. In addition, we assume $c \in C^\infty(\mathbb{R}^n)$ accomplishes the non-trapping condition. Then, there exists $T_0 > 0$ such that the solution to problem (2.12) verifies $v \in C^\infty(\Omega \times (T_0,\infty))$ and

$$\left| \frac{\partial^{|\boldsymbol{\alpha}|} v(\boldsymbol{x},t)}{\partial t^{\alpha_0} \partial x_1^{\alpha_1} \cdots \partial x_n^{\alpha_n}} \right| \leq C\eta(t) \left(\|\varphi\|_{L^2(\Omega)} + \|\psi\|_{L^2(\Omega)} \right),$$

for all $\boldsymbol{x} \in \Omega$, for all $t \geq T_0$, and for all $\boldsymbol{\alpha} = (\alpha_0, \alpha_1, \ldots, \alpha_n) \in \mathbb{N}^{n+1}$, where $C := C(\Omega, \boldsymbol{\alpha})$. Here

$$\eta(t) = \begin{cases} t^{1-n-\alpha_0}, & \text{for even } n \\ e^{-\delta t}, & \text{for odd } n, \end{cases}$$

where δ is a constant depending on $c(\boldsymbol{x})$.

We use the local decay of acoustic wave solutions given by Theorem 2.6 to establish a local decay result for linear elasticity.

Theorem 2.7 *Let $\boldsymbol{u}$ be solution of the linear elasticity system in homogeneous media*

$$\begin{cases} \rho \boldsymbol{u}_{tt}(\boldsymbol{x},t) - L_{\mu,\lambda}\boldsymbol{u}(\boldsymbol{x},t) = \boldsymbol{0}, & \text{in } \mathbb{R}^n \times (0,T), \\ \boldsymbol{u}(\boldsymbol{x},0) = \nabla p(\boldsymbol{x}) + \operatorname{curl} \boldsymbol{q}(\boldsymbol{x}), \\ \partial_t \boldsymbol{u}(\boldsymbol{x},0) = \nabla r(\boldsymbol{x}) + \operatorname{curl} \boldsymbol{s}(\boldsymbol{x}), \end{cases} \tag{2.13}$$

where $\boldsymbol{q}$ and $\boldsymbol{s}$ are vector-valued functions for $n = 3$ and scalar-valued functions for $n = 2$. In addition, here $\operatorname{curl} \boldsymbol{q}$ and $\operatorname{curl} \boldsymbol{s}$ stand for $\operatorname{curl}_{\mathrm{s}} q$ and $\operatorname{curl}_{\mathrm{s}} s$ for $n = 2$. Let $\Omega \subset \mathbb{R}^n$ be a bounded set such that the supports of p, $\boldsymbol{q}$, r, and $\boldsymbol{s}$ are contained in Ω. Let $\sqrt{(\lambda+2\mu)/\rho}$, $\sqrt{\mu/\rho}$ belong to $C^\infty(\mathbb{R}^n)$ such that $\operatorname{supp}(c^* - \sqrt{(\lambda+2\mu)/\rho}) \cup \operatorname{supp}(c^{**} - \sqrt{\mu/\rho}) \subset \Omega$ for some constants c^* and c^{**}, $\sqrt{(\lambda+2\mu)/\rho} \geq c^\star > 0$ and $\sqrt{\mu/\rho} \geq c^{\star\star} > 0$ for some constants $c^\star$ and $c^{\star\star}$, and $\sqrt{(\lambda+2\mu)/\rho}$, $\sqrt{\mu/\rho}$ accomplish the non-trapping condition.

Then, for any $\boldsymbol{\alpha} = (\alpha, \ldots, \alpha_n)$ there exists $\widetilde{T}$ such that we have the following estimates:

In the 3D case,

$$\left| \frac{\partial^{|\boldsymbol{\alpha}|} \boldsymbol{u}(\boldsymbol{x},t)}{\partial_t^{\alpha_0} \cdots \partial_{x_3}^{\alpha_3}} \right| \leq Ce^{-\delta t} \left(\|p\|_{L^2(\Omega)} + \|r\|_{L^2(\Omega)} + \|\boldsymbol{q}\|_{(L^2(\Omega))^3} + \|\boldsymbol{s}\|_{(L^2(\Omega))^3} \right), \quad \forall\, t > \widetilde{T},$$

for all $\boldsymbol{x} \in \Omega$, *where* $C := C(\Omega, \boldsymbol{\alpha}, n)$, *and* $\delta := \delta(\mu, \lambda, \rho)$.

In the 2D case,

$$\left| \frac{\partial^{|\boldsymbol{\alpha}|} \boldsymbol{u}(\boldsymbol{x}, t)}{\partial_t^{\alpha_0} \partial_{x_1}^{\alpha_1} \partial_{x_2}^{\alpha_2}} \right| \leq C t^{1-n-\alpha_0} \left(\|p\|_{L^2(\Omega)} + \|r\|_{L^2(\Omega)} + \|q\|_{L^2(\Omega)} + \|s\|_{L^2(\Omega)} \right), \quad \forall\, t > \widetilde{T},$$

for all $\boldsymbol{x} \in \Omega$, *where* $C := C(\Omega, \boldsymbol{\alpha}, n)$.

Proof. We construct the local decay estimate for the elastic waves problem. To do this, the elastic wave is decomposed in terms of the P-wave and the S-wave, and we use the local decay result for acoustic waves. We only provide the proof for the case $n = 3$; the case $n = 2$ is analogous.

Let $\boldsymbol{u}$ be a solution to (2.13). Then, by Theorem 2.3, there exist functions ϕ and $\boldsymbol{\psi}$ such that

$$\boldsymbol{u}(\boldsymbol{x}, t) = \nabla \phi(\boldsymbol{x}, t) + \operatorname{curl} \boldsymbol{\psi}(\boldsymbol{x}, t), \tag{2.14}$$

where ϕ solves the problem

$$\begin{cases} \partial_t^2 \phi(\boldsymbol{x}, t) - \dfrac{2\mu + \lambda}{\rho} \Delta \phi(\boldsymbol{x}, t) = 0, & \text{in } \mathbb{R}^3 \times (0, \infty), \\ \phi(\boldsymbol{x}, 0) = p(\boldsymbol{x}), \\ \partial_t \phi(\boldsymbol{x}, 0) = r(\boldsymbol{x}), \end{cases}$$

and $\boldsymbol{\psi}$ solves the problem

$$\begin{cases} \partial_t^2 \boldsymbol{\psi}(\boldsymbol{x}, t) - \dfrac{\mu}{\rho} \Delta \boldsymbol{\psi}(\boldsymbol{x}, t) = \boldsymbol{0}, & \text{in } \mathbb{R}^3 \times (0, \infty), \\ \boldsymbol{\psi}(\boldsymbol{x}, 0) = \boldsymbol{q}(\boldsymbol{x}), \\ \partial_t \boldsymbol{\psi}(\boldsymbol{x}, 0) = \boldsymbol{s}(\boldsymbol{x}). \end{cases}$$

Using Theorem 2.6, we conclude that there exist T_i, $i \in \{0, 1, 2, 3\}$ such that

$$\left| \frac{\partial^{|\boldsymbol{\alpha}|} \phi(\boldsymbol{x}, t)}{\partial t^{\alpha_0} \partial x_1^{\alpha_1} \partial x_2^{\alpha_2} \partial x_3^{\alpha_3}} \right| \leq C_0 e^{-\delta_1 t} \left(\|p\|_{L^2} + \|r\|_{L^2} \right), \qquad \forall\, t \geq T_0,$$

$$\left| \frac{\partial^{|\boldsymbol{\alpha}|} \psi_i(\boldsymbol{x}, t)}{\partial t^{\alpha_0} \partial x_1^{\alpha_1} \partial x_2^{\alpha_2} \partial x_3^{\alpha_3}} \right| \leq C_i e^{-\delta_2 t} \left(\|q_i\|_{L^2(\Omega)} + \|s_i\|_{L^2(\Omega)} \right), \qquad \forall\, t \geq T_i, \quad i \in \{1, 2, 3\},$$

for all $\boldsymbol{x} \in \Omega$ and for all $\boldsymbol{\alpha} = (\alpha_0, \ldots, \alpha_3) \in \mathbb{N}^4$, where $C_k := C_k(\Omega, \boldsymbol{\alpha})$, with $k \in \{0, 1, 2, 3\}$, $\delta_1 := \delta_1(\rho, \mu, \lambda)$, and $\delta_2 := \delta_2(\rho, \mu)$.

From (2.14), we obtain the components of $\boldsymbol{u}$ in terms of ϕ and $\boldsymbol{\psi}$

$$\begin{aligned} u_1 &= \partial_{x_1} \phi + \partial_{x_2} \psi_3 - \partial_{x_3} \psi_2, \\ u_2 &= \partial_{x_2} \phi + \partial_{x_3} \psi_1 - \partial_{x_1} \psi_3, \\ u_3 &= \partial_{x_3} \phi + \partial_{x_1} \psi_2 - \partial_{x_2} \psi_1. \end{aligned}$$

Let $\boldsymbol{\alpha}_{+l} := (\alpha_i + \delta_{l,i})_{i=0,\dots,n}$, where $\delta_{l,i}$ is the Kronecker delta. Then, for all $i \in \{1,2,3\}$

$$\begin{aligned}\left|\frac{\partial^{|\boldsymbol{\alpha}|}u_i(\boldsymbol{x},t)}{\partial_t^{\alpha_0}\cdots\partial_{x_3}^{\alpha_3}}\right| \leq& \left|\frac{\partial^{|\boldsymbol{\alpha}|+1}\phi(\boldsymbol{x},t)}{\partial_{x_i}\partial_t^{\alpha_0}\cdots\partial_{x_3}^{\alpha_3}}\right| + \left|\frac{\partial^{|\boldsymbol{\alpha}|+1}\psi_j(\boldsymbol{x},t)}{\partial_{x_k}\partial_t^{\alpha_0}\cdots\partial_{x_3}^{\alpha_3}}\right| + \left|\frac{\partial^{|\boldsymbol{\alpha}|+1}\psi_k(\boldsymbol{x},t)}{\partial_{x_j}\partial_t^{\alpha_0}\cdots\partial_{x_3}^{\alpha_3}}\right| \\ \leq& \widetilde{C}_1 e^{-\delta_1 t}\left(\|p\|_{L^2(\Omega)} + \|r\|_{L^2(\Omega)}\right) + \widetilde{C}_2 e^{-\delta_2 t}\left(\|q_j\|_{L^2(\Omega)} + \|s_j\|_{L^2(\Omega)}\right) \\ &+ \widetilde{C}_3 e^{-\delta_2 t}\left(\|q_k\|_{L^2(\Omega)} + \|s_k\|_{L^2(\Omega)}\right),\end{aligned}$$

where $j \neq k$, with $j,k \in \{1,2,3\} \setminus \{i\}$, $\delta_1 := \delta_1(\mu,\lambda,\rho)$, $\delta_2 := \delta_2(\mu,\rho)$, $\widetilde{C}_1 := \widetilde{C}_1(\Omega, \boldsymbol{\alpha}_{+i})$, $\widetilde{C}_2 := \widetilde{C}_2(\Omega, \boldsymbol{\alpha}_{+j})$, and $\widetilde{C}_3 := \widetilde{C}_3(\Omega, \boldsymbol{\alpha}_{+k})$. Let us define $\delta := \min_{l\in\{1,2\}} \delta_l$. Here, we use C to denote different constants depending on Ω and $\boldsymbol{\alpha}$ (more explicitly depending on Ω, $\boldsymbol{\alpha}_{+1}$, $\boldsymbol{\alpha}_{+2}$, and $\boldsymbol{\alpha}_{+3}$). Then,

$$\begin{aligned}\left|\frac{\partial^{|\boldsymbol{\alpha}|}u_i(\boldsymbol{x},t)}{\partial_t^{\alpha_0}\cdots\partial_{x_3}^{\alpha_3}}\right| \leq& C(\Omega,\boldsymbol{\alpha}) e^{-\delta t}\left(\|p\|_{L^2(\Omega)} + \|r\|_{L^2(\Omega)} + \|q_j\|_{L^2(\Omega)} + \|s_j\|_{L^2(\Omega)}\right. \\ &\left. + \|q_k\|_{L^2(\Omega)} + \|s_k\|_{L^2(\Omega)}\right) \\ \leq& C(\Omega,\boldsymbol{\alpha}) e^{-\delta t}\left(\|p\|_{L^2(\Omega)} + \|r\|_{L^2(\Omega)} + \sum_{l=1}^{3}\left(\|q_l\|_{L^2(\Omega)} + \|s_l\|_{L^2(\Omega)}\right)\right) \\ \leq& C(\Omega,\boldsymbol{\alpha}) e^{-\delta t}\left(\|p\|_{L^2(\Omega)} + \|r\|_{L^2(\Omega)} + \sqrt{3}\left(\|\boldsymbol{q}\|_{(L^2(\Omega))^3} + \|\boldsymbol{s}\|_{(L^2(\Omega))^3}\right)\right) \\ \leq& C(\Omega,\boldsymbol{\alpha},n) e^{-\delta t}\left(\|p\|_{L^2(\Omega)} + \|r\|_{L^2(\Omega)} + \|\boldsymbol{q}\|_{(L^2(\Omega))^3} + \|\boldsymbol{s}\|_{(L^2(\Omega))^3}\right).\end{aligned}$$

Note that constant C depends on n in this last estimate. On the other hand,

$$\begin{aligned}\left|\frac{\partial^{|\boldsymbol{\alpha}|}\boldsymbol{u}(\boldsymbol{x},t)}{\partial_t^{\alpha_0}\cdots\partial_{x_3}^{\alpha_3}}\right| =& \sqrt{\left|\frac{\partial^{|\boldsymbol{\alpha}|}u_1(\boldsymbol{x},t)}{\partial_t^{\alpha_0}\cdots\partial_{x_3}^{\alpha_3}}\right|^2 + \left|\frac{\partial^{|\boldsymbol{\alpha}|}u_2(\boldsymbol{x},t)}{\partial_t^{\alpha_0}\cdots\partial_{x_3}^{\alpha_3}}\right|^2 + \left|\frac{\partial^{|\boldsymbol{\alpha}|}u_3(\boldsymbol{x},t)}{\partial_t^{\alpha_0}\cdots\partial_{x_3}^{\alpha_3}}\right|^2} \\ \leq& \left|\frac{\partial^{|\boldsymbol{\alpha}|}u_1(\boldsymbol{x},t)}{\partial_t^{\alpha_0}\cdots\partial_{x_3}^{\alpha_3}}\right| + \left|\frac{\partial^{|\boldsymbol{\alpha}|}u_2(\boldsymbol{x},t)}{\partial_t^{\alpha_0}\cdots\partial_{x_3}^{\alpha_3}}\right| + \left|\frac{\partial^{|\boldsymbol{\alpha}|}u_3(\boldsymbol{x},t)}{\partial_t^{\alpha_0}\cdots\partial_{x_3}^{\alpha_3}}\right| \\ \leq& C(\Omega,\boldsymbol{\alpha},n) e^{-\delta t}\left(\|p\|_{L^2(\Omega)} + \|r\|_{L^2(\Omega)} + \|\boldsymbol{q}\|_{(L^2(\Omega))^3} + \|\boldsymbol{s}\|_{(L^2(\Omega))^3}\right).\end{aligned}$$

Then,

$$\left|\frac{\partial^{|\boldsymbol{\alpha}|}\boldsymbol{u}(\boldsymbol{x},t)}{\partial_t^{\alpha_0}\partial_{x_1}^{\alpha_1}\partial_{x_2}^{\alpha_2}\partial_{x_3}^{\alpha_3}}\right| \leq C e^{-\delta t}\left(\|p\|_{L^2(\Omega)} + \|r\|_{L^2(\Omega)} + \|\boldsymbol{q}\|_{(L^2(\Omega))^3} + \|\boldsymbol{s}\|_{(L^2(\Omega))^3}\right),$$

for all $t > \widetilde{T}$, $\boldsymbol{x} \in \Omega$ and for all $\boldsymbol{\alpha} = (\alpha_0,\alpha_1,\alpha_2,\alpha_3) \in \mathbb{N}^4$, where $\widetilde{T} = \max\{T_0,\dots,T_3\}$.

This proves the theorem in the case $n = 3$. The same proof remains valid in the 2D case by considering $\boldsymbol{\psi}$, $\boldsymbol{q}$, and $\boldsymbol{s}$ as scalar valued functions, so we obtain

$$\left|\frac{\partial^{|\boldsymbol{\alpha}|}u_i(\boldsymbol{x},t)}{\partial_t^{\alpha_0}\partial_{x_1}^{\alpha_1}\partial_{x_2}^{\alpha_2}}\right| \leq C t^{1-n-\alpha_0}\left(\|p\|_{L^2(\Omega)} + \|q\|_{L^2(\Omega)} + \|r\|_{L^2(\Omega)} + \|s\|_{L^2(\Omega)}\right),$$

for all $t > \widetilde{T}$, $\boldsymbol{x} \in \Omega$, and for all $\boldsymbol{\alpha} = (\alpha_0,\alpha_1,\alpha_2) \in \mathbb{N}^3$, where $\widetilde{T} = \max\{T_0,T_1\}$. This completes the proof. □

2.3 Source time reversal in elasticity

STR [17] method modifies the classical Time-Reversal Mirrors (TRM) [41] for reconstructing a space-source term of the form $s(\boldsymbol{x},t) = f(\boldsymbol{x})g(t)$, where g is a real-valued function with compact support. Taking advantage of the information provided by the time-source term $g(t)$, the original source problem is related with a non-source wave problem in which the space-source term of the original problem appears as an initial condition and the boundaries information between the two problems are related by a Volterra integral equation of the first kind. Then, it is possible to apply the TRM idea over this new non-source initial condition problem by solving the integral equation to obtain its boundary information and chronologically reverse the boundary information of the non-source wave problem.

Although acoustics provide a good first approximation of compressional and shear waves, linear elasticity offers a better approximation to the ground motion. In [23], we can see the main limitations of considering the acoustic model for seismic events. Since STR method is oriented to solve problems in induced seismicity, in here we extend the original formulation for acoustic waves [17] to systems of elastic waves.

In this section, we select a model for tremors by considering compressional and shear waves propagating in an infinite medium (without boundary). Assuming our seismic events are governed by the elastic equation in an isotropic media, we use the Lagragian description [2] to define the displacement $\boldsymbol{u}(\boldsymbol{x},t)$ of the particle $\boldsymbol{x}$ at time t in an homogeneous and isotropic elastic media

$$\begin{cases} \rho\partial_t^2\boldsymbol{u}(\boldsymbol{x},t) - L_{\mu,\lambda}\boldsymbol{u}(\boldsymbol{x},t) = \boldsymbol{f}(\boldsymbol{x})g(t), & \text{in } \mathbb{R}^n \times (0,T), \\ \boldsymbol{u}(\boldsymbol{x},0) = \boldsymbol{0}, \\ \partial_t\boldsymbol{u}(\boldsymbol{x},0) = \boldsymbol{0}, \end{cases} \tag{2.15}$$

where $L_{\mu,\lambda}\boldsymbol{u} = \mu\Delta\boldsymbol{u} + (\mu+\lambda)\nabla(\nabla\cdot\boldsymbol{u})$ and $n \in \{2,3\}$.

Let us consider a bounded set $\Omega \subset \mathbb{R}^n$ such that the support of $\boldsymbol{f}(\boldsymbol{x})$ is contained in Ω, and the geophones are located on $\partial\Omega$. The boundary information will be given by the displacement velocities $\partial_t\boldsymbol{u}(\boldsymbol{y},t)$ for $\boldsymbol{y} \in \partial\Omega$ and for all $t \in (0,T)$. Then, we define the inverse problem: given the measurement displacement velocities $\{m_{\boldsymbol{u}}(\boldsymbol{y},t) := \partial_t\boldsymbol{u}(\boldsymbol{y},t) : (\boldsymbol{y},t) \in \partial\Omega \times (0,T)\}$ and the time-distribution of the source $\{g(t) : t \in (0,T)\}$, find the space-source term $\boldsymbol{f}(\boldsymbol{x})$. We introduce the operator of measurement displacement velocities as

$$\Lambda(\boldsymbol{f},g) := \partial_t\boldsymbol{u}|_{\partial\Omega\times(0,T)}.$$

Following the procedure in [17], we can define an initial condition problem

$$\begin{cases} \rho\partial_t^2\boldsymbol{v}(\boldsymbol{x},t) - L_{\mu,\lambda}\boldsymbol{v}(\boldsymbol{x},t) = \boldsymbol{0}, & \text{in } \mathbb{R}^n \times (0,T), \\ \boldsymbol{v}(\boldsymbol{x},0) = \boldsymbol{0}, \\ \partial_t\boldsymbol{v}(\boldsymbol{x},0) = \rho^{-1}\boldsymbol{f}(\boldsymbol{x}), \end{cases} \tag{2.16}$$

where the solutions to (2.15) and (2.16) are related via an integral equation by using Duhamel's principle [38]

$$\boldsymbol{u}(\boldsymbol{x},t) = \int_0^t \boldsymbol{v}(\boldsymbol{x},t-\tau)g(\tau)\,dt. \tag{2.17}$$

We are interested in obtaining the boundary measurements to problem (2.16) in order to reverse them chronologically and recover $\boldsymbol{f}(\boldsymbol{x})$. To do this, we define the operator of measurements

$$\Lambda_0 \boldsymbol{f} := \partial_t \boldsymbol{v}|_{\partial\Omega\times(0,T)}.$$

Notice that it is possible to rewrite problem (2.16) inside Ω in terms of the displacement velocity, the boundary information and its conditions at time $t = T$. Then, the solution to problem (2.18) is the restriction of $\partial_t \boldsymbol{v}(\boldsymbol{x}, t)$ in $\Omega \times (0, T]$.

$$\begin{cases} \rho\partial_t^2 \boldsymbol{w}(\boldsymbol{x},t) - L_{\mu,\lambda}\boldsymbol{w}(\boldsymbol{x},t) = \boldsymbol{0}, & \text{in } \Omega\times(0,T), \\ \boldsymbol{w}(\boldsymbol{x},T) = \partial_t \boldsymbol{v}(\boldsymbol{x},T), & \\ \partial_t \boldsymbol{w}(\boldsymbol{x},T) = \partial_t^2 \boldsymbol{v}(\boldsymbol{x},T), & \\ \boldsymbol{w}(\boldsymbol{y},t) = m_{\boldsymbol{v}}(\boldsymbol{y},t), & \text{on } \partial\Omega\times(0,T), \end{cases} \tag{2.18}$$

where $m_{\boldsymbol{v}} := \Lambda_0 \boldsymbol{f}$.

To obtain the solution to problem (2.18) at time $t = 0$ is equivalent to backpropagate the displacement velocity waves in problem (2.16). This procedure gives us an exact reconstruction of the initial velocity to problem (2.16), i.e. $\boldsymbol{w}(\boldsymbol{x}, 0) = \rho^{-1}\boldsymbol{f}(\boldsymbol{x})$. Unfortunately, the final conditions $\partial_t \boldsymbol{v}(\boldsymbol{x}, T)$ and $\partial_t^2 \boldsymbol{v}(\boldsymbol{x}, T)$ for all $\boldsymbol{x} \in \Omega$ are often unavailable in a practical setting. To overcome this problem, we notice from Theorem 2.7 that not only each component of the solution of (2.16) decays, but also its derivatives inside the bounded set Ω. Furthermore, the decay profile is polynomial in 2D and exponential in 3D. Thus, the final conditions $\partial_t \boldsymbol{v}(\boldsymbol{x}, T)$ and $\partial_t^2 \boldsymbol{v}(\boldsymbol{x}, T)$ to problem (2.18) can be approximated by zero for T large enough.

Let us assume that problem (2.16) satisfies the conditions of Theorem 2.7 and let $T-\varepsilon > \widetilde{T}$ for a fixed $\varepsilon > 0$. Then, we define the following problem

$$\begin{cases} \rho\partial_t^2 \widetilde{\boldsymbol{w}} - L_{\mu,\lambda}\widetilde{\boldsymbol{w}} = \boldsymbol{0}, & \text{in } \Omega\times(0,T), \\ \widetilde{\boldsymbol{w}}(\boldsymbol{x},T) = \boldsymbol{0}, & \\ \partial_t \widetilde{\boldsymbol{w}}(\boldsymbol{x},T) = \boldsymbol{0}, & \\ \widetilde{\boldsymbol{w}}(\boldsymbol{y},t) = m_{\boldsymbol{v}}(\boldsymbol{y},t)\phi_\varepsilon(t), & \text{on } \partial\Omega\times(0,T), \end{cases} \tag{2.19}$$

where ϕ_ε is a smooth cut-off function such that $\phi_\varepsilon(t) = 1$ for all $t \in (0, T-\varepsilon)$ and $\phi_\varepsilon = 0$ for all $t \in (T, \infty)$. By solving problem (2.19) at time $t = 0$, we obtain an approximate reconstruction of $\rho^{-1}\boldsymbol{f}(\boldsymbol{x})$. This reconstruction depends mainly on T and the dimension of the problem n.

From the physical problem (2.15), we measure the boundary information denoted by the set $\{m_{\boldsymbol{u}}(\boldsymbol{y}, t) = \partial_t \boldsymbol{u}(\boldsymbol{y}, t) : (\boldsymbol{y}, t) \in \partial\Omega \times (0, T)\}$. To solve problem (2.19), it is necessary to obtain the boundary information from the synthetic problem (2.16) given by the set $\{m_{\boldsymbol{v}}(\boldsymbol{y}, t) = \partial_t \boldsymbol{v}(\boldsymbol{y}, t) : (\boldsymbol{y}, t) \in \partial\Omega \times (0, T)\}$. Then, it only remains to obtain the measurements $m_{\boldsymbol{v}}(\boldsymbol{y}, \cdot)$ from $m_{\boldsymbol{u}}(\boldsymbol{y}, \cdot)$ for each $\boldsymbol{y} \in \partial\Omega$. From identity (2.17), this problem reduces to solve the following integral equation

$$m_{\boldsymbol{u}}(\boldsymbol{y}, t) = \int_0^t m_{\boldsymbol{v}}(\boldsymbol{y}, t-\tau) g(\tau)\, dt, \tag{2.20}$$

where $t \in (0,T)$ for all $\boldsymbol{y} \in \partial\Omega$.

Let $\mathcal{A}_0(m_{\boldsymbol{u}}, g) = m_{\boldsymbol{v}}$ be the operator that solves problem (2.20). Then, we need to solve the following problem to obtain a reconstruction to the space-source term $\boldsymbol{f}(\boldsymbol{x})$

$$\begin{cases} \rho\partial_t^2\widetilde{\boldsymbol{w}} - L_{\mu,\lambda}\widetilde{\boldsymbol{w}} = \boldsymbol{0}, & \text{in } \Omega\times(0,T), \\ \widetilde{\boldsymbol{w}}(\boldsymbol{x},T) = \boldsymbol{0}, \\ \partial_t\widetilde{\boldsymbol{w}}(\boldsymbol{x},T) = \boldsymbol{0}, \\ \widetilde{\boldsymbol{w}}(\boldsymbol{y},t) = \rho\mathcal{A}_0(m_{\boldsymbol{u}},g)(\boldsymbol{y},t)\phi_\varepsilon(t), & \text{on } \partial\Omega\times(0,T). \end{cases} \tag{2.21}$$

The Laplace transform is a standard tool to solve integral equations of the first kind when the kernel is given by a convolution. A limitation of this technique is that the inverse Laplace transform is known only for some rather simple functions and it may also be challenging to find numerically [81].

To overcome the above limitation, we propose to solve (2.20) numerically by using Fourier transform. Unfortunately, a direct resolution gives us the expression

$$\mathcal{F}^{-1}\left(\frac{\mathcal{F}(m_{\boldsymbol{u}})}{\mathcal{F}(g)}\right),$$

which may become singular for some t and it is numerically unstable. To avoid the previous stability problems, we present two regularization methods for approximating the solution to (2.20).

1. **STR with traditional regularization**. We define

$$\mathcal{A}(m_{\boldsymbol{u}}, g) := \mathcal{F}^{-1}\left(\frac{\mathcal{F}(m_{\boldsymbol{u}})\overline{\mathcal{F}(g)}}{|\mathcal{F}(g)|^2 + c_0}\right), \tag{2.22}$$

   where c_0 is a small positive regularization constant. Then, we replace the operator $\mathcal{A}_0$ with $\mathcal{A}$ in problem (2.21) to find a reconstruction of the space-source term $\boldsymbol{f}(\boldsymbol{x})$.

   With the above regularization, high frequencies appear due to the division by $F(g)$. The addition of the constant c_0 makes the deconvolution stable and avoids divisions by zero but does not eliminate high frequencies. Solving such high frequencies require the use of fine meshes in our numerical simulations. For large problems, the method may eventually become prohibitively expensive. This regularization method was considered in [17].

2. **Fast STR with cut-off regularization**. In this second regularization method, we define function Θ as

$$\Theta(\xi) = \begin{cases} \dfrac{\overline{\mathcal{F}(g)(\xi)}}{|\mathcal{F}(g)(\xi)|^2}, & \text{if } |\mathcal{F}(g)(\xi)| \geq c_1 \max\limits_{\xi} |\mathcal{F}(g)(\xi)| \\ 0, & \text{if } |\mathcal{F}(g)(\xi)| < c_1 \max\limits_{\xi} |F(g)(\xi)|, \end{cases}$$

   where $c_1 \in (0,1)$ is a constant that regulates excitations of high frequencies and avoids divisions by zero. Then, we replace the operator $\mathcal{A}$ with

$$\mathcal{F}^{-1}(\mathcal{F}(m_{\boldsymbol{u}})\Theta) \tag{2.23}$$

in problem (2.21) to find a reconstruction of the source-space term $\boldsymbol{f}(\boldsymbol{x})$. This regularization method allows the source reconstruction in coarse meshes by eliminating higher frequencies.

In summary, the STR method consists of a transformation of the boundary measurements, which are given by the displacement velocities. To transform the boundary measurements, we propose two regularization methods depending on the computational requirements. The first one reverses in time the measurements processed by operator $\mathcal{A}$ to recover the space-source term. The second regularization method eliminates high frequencies of the processed signals to be reversed in time. This second approach allows for reconstructing sources in more realistic cases when the computational requirements are larger. Figure 2.1 shows the difference in the processed signal frequencies between the two regularization methods for different regularization constants. Both procedures will give us a reconstruction of $\boldsymbol{f}(\boldsymbol{x})$ for any time-source term $g(t)$.

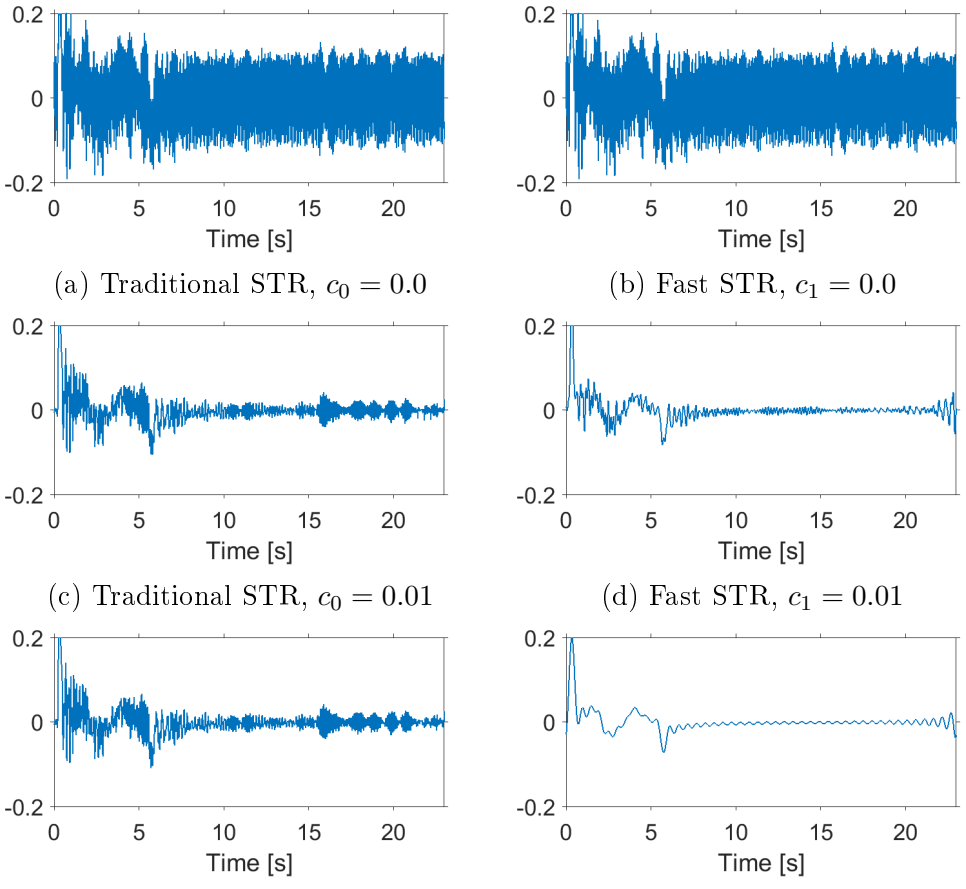

(a) Traditional STR, $c_0 = 0.0$

(b) Fast STR, $c_1 = 0.0$

(c) Traditional STR, $c_0 = 0.01$

(d) Fast STR, $c_1 = 0.01$

(e) Traditional STR, $c_0 = 0.1$

(f) Fast STR, $c_1 = 0.1$

Figure 2.1: First component of a measurement processed with both STR regularization methods for different regularization constant values.

2.4 Implementation of the STR method

We consider two simulation methods: a Finite Differences Method (FDM) and a Finite Element Method (FEM). In the absence of analytical solutions, we use both schemes to

compare our results and validate the robustness of the method.

The implementation considered for the FDM is straightforward and based on the 2D scheme presented in [69]. Additionally, in here we extend this scheme to the 3D case. For the forward problem, we consider a large enough computational domain to ensure that waves measured by the geophones are free from the effects of the computational boundary. To reverse the measurements processed by the STR method, we consider a smaller computational domain equal to Ω, where the geophones are in the computational boundary of the domain.

For the FEM, we implemented a first-order absorbing boundary condition over the domain boundary $\Gamma \subset \Omega$:

$$\rho \frac{\partial^2 \boldsymbol{u}}{\partial t^2} - \nabla \cdot \underline{\underline{\sigma}}(\boldsymbol{u}) = g(t)\,(0.5\,\nabla + 0.5\,\nabla\times)\,\delta_{\boldsymbol{x}_0}, \qquad \text{in } \Omega, \tag{2.24a}$$

$$\rho B \frac{\partial \boldsymbol{u}}{\partial t} + \underline{\underline{\sigma}}(\boldsymbol{u}) \cdot \mathbf{n} = \mathbf{0}, \qquad \text{on } \Gamma, \tag{2.24b}$$

where the external force $g(t)\,(0.5\,\nabla + 0.5\,\nabla\times)\,\delta_{\boldsymbol{x}_0}$ represents a point source in space (δ) located at $\boldsymbol{x}_0$ that generates both P- and S-waves, $g(t)$ is a source time-function based on a Ricker wavelet with peak frequency f_p (typically 10 $[Hz]$), and $\mathbf{n}$ is the exterior unit normal to the boundary Γ. Note that more point sources may be considered by simply adding similar terms to the right-hand side at different space locations. The symmetric, positive-definite matrix B appearing in the absorbing boundary condition of equation (2.24b) is defined as

$$B := \begin{pmatrix} c_P n_1^2 + c_S n_2^2 & (c_P - c_S) n_1 n_2 \\ (c_P - c_S) n_1 n_2 & c_P n_1^2 + c_S n_2^2 \end{pmatrix},$$

where n_1 and n_2 are the normal components in the first and second directions, respectively, and c_P and c_S are the compressional and the shear wave velocities, respectively, with $c_P = \sqrt{\frac{\lambda+2\mu}{\rho}}$ and $c_S = \sqrt{\frac{\mu}{\rho}}$.

The weak formulation of problem (2.24) reads as follows: $\forall t \in (0, T]$, find $\boldsymbol{u} = \boldsymbol{u}(t) \in U$ such that

$$\int_\Omega \rho \frac{\partial^2 \boldsymbol{u}}{\partial t^2} \cdot \mathbf{w} d\Omega + \int_\Omega \lambda\, \nabla \cdot \boldsymbol{u}\, \nabla \cdot \mathbf{w}\, d\Omega + \int_\Omega 2\mu \sum_{i,j=1}^{2} \epsilon_{i,j}(\boldsymbol{u}) \epsilon_{i,j}(\mathbf{w}) d\Omega$$
$$+ \int_\Gamma \rho \left(B \frac{\partial \boldsymbol{u}}{\partial t} \right) \cdot \mathbf{w} d\Gamma = \int_\Omega g(t)\,(0.5\,\nabla + 0.5\,\nabla\times)\,\delta_{\boldsymbol{x}_0} \cdot \mathbf{w}\, d\Omega,$$

for all test functions $\mathbf{w} \in W$, where the Sobolev trial space U and test space W are defined as

$$U = \{\boldsymbol{u} \in (H^1(\Omega))^2\},$$

and

$$W = \{\mathbf{w} \in (H^1(\Omega))^2 : \mathbf{w} = \mathbf{0} \text{ on } \Gamma\}.$$

We consider the Leap-frog scheme for the second-order time derivative, whereas for the first-order one we apply central differences. For the space discretization, we employ high-order hierarchical basis functions for both the finite-dimensional test and trial spaces V_h and W_h. Therefore, we obtain a numerical scheme that provides second-order accuracy in time, arbitrary accuracy in space, and that conserves the energy (see [96]) provided that a certain CFL condition is satisfied. This CFL condition imposes a constrained relationship between the magnitudes of the time step Δt and the characteristic element size h, the later selected according to f_p. For a regular mesh over a rectangular domain, this CFL condition becomes

$$\Delta t < \frac{2h}{\sqrt{\alpha\, d}},$$

where d is the dimension of the domain Ω (two in our case) and α is a constant that depends only on the space discretization method.

For the backward problem, a similar discretization holds. The only difference is that now we replace equation (2.24a) by its corresponding homogeneous problem and equation (2.24b) by a Dirichlet boundary condition on Γ using the transformed data registered by the geophones on the forward problem, as described in the previous section.

2.5 Numerical experiments of STR with traditional regularization

In this section, we employ the finite difference method. We consider a source supported in a subdomain $\Omega = (-3, 3) \times (-3, 3)$ for the 2D case, and $\Omega = (-3, 3) \times (-3, 3) \times (-3, 3)$ for the 3D case. Measurements are processed with the operator defined in (2.22). In Subsections 2.5.1, 2.5.2, and 2.5.4, we consider the regularization constant $c_0 = 0.01$ for the standard STR. Additionally, in the last experiment, we compare both STR regularization methods (traditional and fast) for data in the entire boundary and for partial boundary information.

We consider the following elastic parameters: $\rho = 1\ [Kg/m^3]$, $\mu = 1\ [Pa]$, $\lambda = 1\ [Pa]$. Thus, the speed of the P-wave is $\sqrt{2}\ [m/s]$ and that of the S-wave is $1\ [m/s]$. We generate elastic waves by considering different sources $\boldsymbol{f}(\boldsymbol{x})g(t)$. In most of these experiments, we consider three time-source terms given by

$$g_1(t) = \frac{g_s(t)}{\|g_s(t)\|},\ g_2(t) = \begin{cases} 7t, & t \in (0, 1/7) \\ 1, & t \in (1/7, 2/7) \\ 3 - 7t, & t \in (2/7, 3/7) \end{cases},\ \text{and } g_3(t) = 1\chi_{(0.01,0.4)},$$

where $g_s(t) = \exp(1 - 12^2(t - 0.2)^2)$. Figure 2.2 displays these functions.

2.5.1 Two-dimensional phantom reconstruction

The scope of this experiment is to analyze the effect of the shape of the time source on the recovered reconstruction results for 2D simulations in an ideal case. We refer to an ideal case as an experiment without noise, with geophones located at all mesh nodes along the entire $\partial\Omega$, and a final time T long enough to measure the wavefronts. To do this, we present

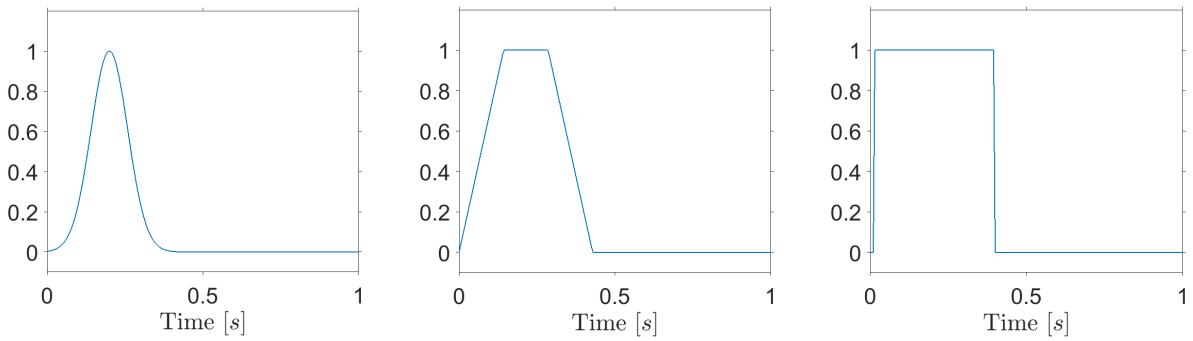

(a) $g_1(t)$ (b) $g_2(t)$ (c) $g_3(t)$

Figure 2.2: Time-source terms.

2D reconstructions of the known Shepp-Logan phantom [99] as the space-source term, see Figure 2.3a. Here, we generate the elastic waves using three different sources $\boldsymbol{f}_{\text{ph}}(\boldsymbol{x})g_i(t)$ $i \in \{1, 2, 3\}$. For this experiment, the final time T is 23 $[s]$ and the space and time steps are $h = 0.05$ $[m]$ and $dt = 0.005$ $[s]$, respectively.

Figures 2.3b, 2.3c, and 2.3d show the reconstructions of the space-source term for waves generated with sources $\boldsymbol{f}_{\text{ph}}(\boldsymbol{x})g_i(t)$, $i \in \{1, 2, 3\}$. As it occurred with the results of the experiments perfomed in [17] for acoustic waves, the discontinuous time-source term $g_3(t)$ provides better reconstructions than the other terms.

2.5.2 Three-dimensional reconstructions with complete data

Here, we show the relative error of reconstruction in L^2-norm for 3D simulations in the ideal case (without noise, with geophones located over the entire $\partial\Omega$, and with T being long enough). We simulate 3D elastic waves with a source composed by a smooth space-source term

$$\boldsymbol{f}_{\text{sm}}(\boldsymbol{x}) = \frac{\boldsymbol{f}_1(\boldsymbol{x})}{\|\boldsymbol{f}_1(\boldsymbol{x})\|} + 0.7\frac{\boldsymbol{f}_2(\boldsymbol{x})}{\|\boldsymbol{f}_2(\boldsymbol{x})\|}, \tag{2.25}$$

where $\boldsymbol{f}_1(\boldsymbol{x}) = \exp\left(1 - 2^2\left((x_1 + 0.5)^2 + (x_2 - 0.5)^2 + x_3^2\right)\right)$ and
$\boldsymbol{f}_2(\boldsymbol{x}) = \exp\left(1 - 2^2\left((x_1 - 0.5)^2 + (x_2 + 0.5)^2 + x_3^2\right)\right)$ (see Figure 2.4a). The three time-source terms are the ones considered in Section 2.5.1. The value of the parameters considered here are: $h = 0.05$ $[m]$, $dt = 0.01$ $[s]$, and $T = 7$ $[s]$. Due to local decay behavior of 3D waves (see Theorem 2.7) the final time T in the 3D case is shorter than that in the 2D one.

Figures 2.4b, 2.4c, and 2.4d show the reconstructions for the different waves generated with sources $\boldsymbol{f}_{\text{sm}}(\boldsymbol{x})g_i(t)$ for $i \in \{1, 2, 3\}$. The relative errors are lower than those observed in the 2D case for all $g_i(t)$. This is due to the faster local decay rate of 3D waves. In this case (homogeneous media and 3D waves), the Huygens' principle is valid, and we could expect to recover the space-source term exactly. The only two sources of error are the regularization constant c_0 and the numerical discretization. In the next experiment, we assess numerically the percent of error induced by the regularization constant c_0.

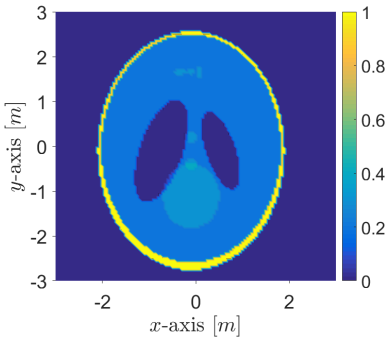

(a) Exact phantom $|\boldsymbol{f}_{\text{ph}}(\boldsymbol{x})|$

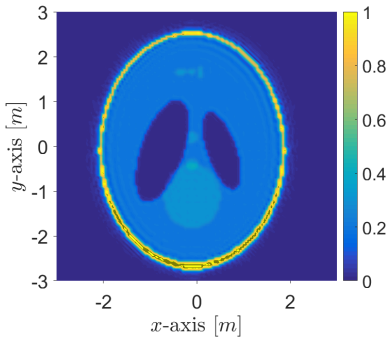

(b) Recons. with $g_1(t)$; error: 23.2%

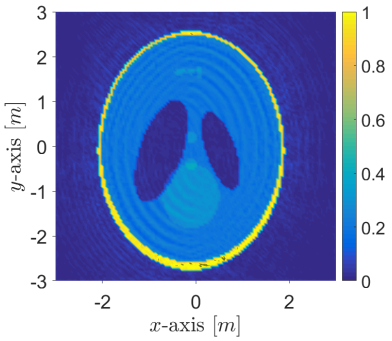

(c) Recons. with $g_2(t)$; error: 13.7%

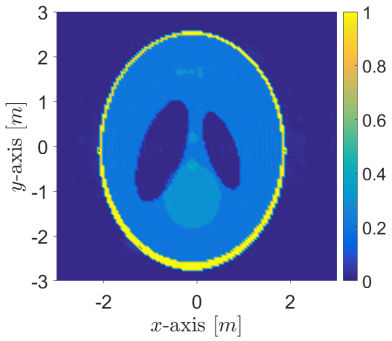

(d) Recons. with $g_3(t)$; error: 4.7%

Figure 2.3: Exact and reconstructions of $|\boldsymbol{f}_{\text{ph}}(\boldsymbol{x})|$ for waves generated with $\boldsymbol{f}_{\text{ph}}(\boldsymbol{x})g_i(t)$. Relative error in L^2-norm.

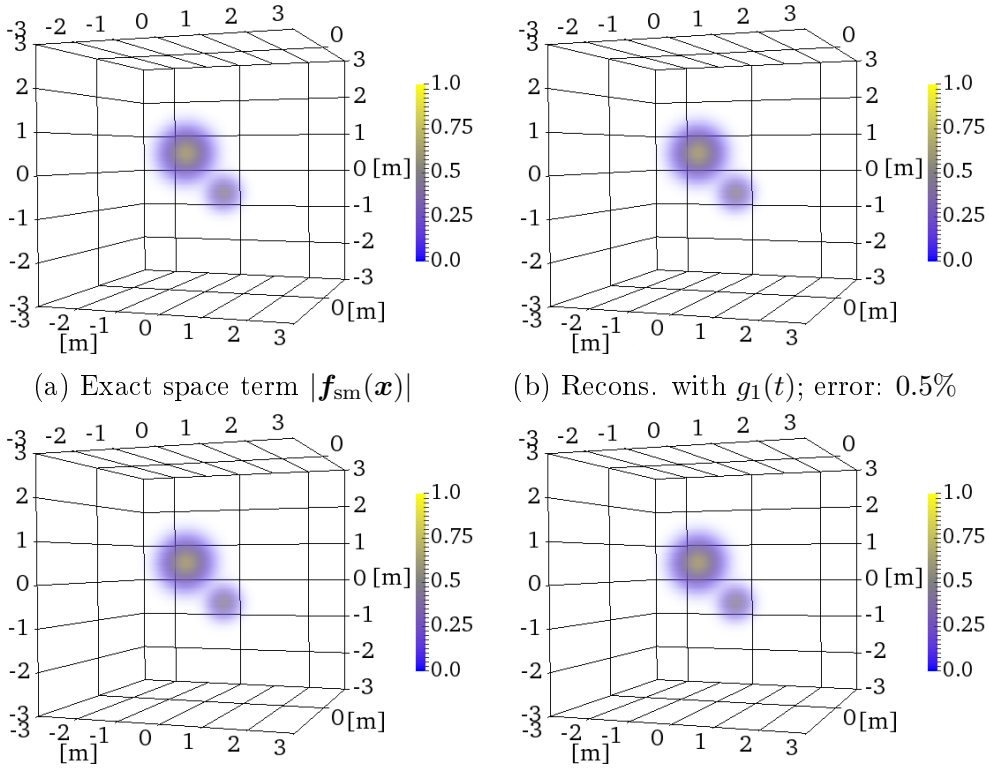

(a) Exact space term $|\boldsymbol{f}_{\mathrm{sm}}(\boldsymbol{x})|$

(b) Recons. with $g_1(t)$; error: 0.5%

(c) Recons. with $g_2(t)$; error: 0.6%

(d) Recons. with $g_3(t)$; error: 0.6%

Figure 2.4: Exact and reconstruction of $|\boldsymbol{f}_{\mathrm{sm}}(\boldsymbol{x})|$ for waves generated by $\boldsymbol{f}_{\mathrm{sm}}(\boldsymbol{x})g_i(t)$. Relative error in L^2-norm.

2.5.3 Error decay analysis

The aim of this numerical experiment is to show numerically the error induced by the regularization constant c_0. To do this, we compare the relative error decay in L^2-norm between the classical TRM method and the STR with traditional regularization for different c_0 constants in 2D and 3D cases. The parameters for the finite difference are: $h = 0.05$ $[m]$, $dt = 0.01$ $[s]$, and $T \in [3, 7]$.

To make the TRM and STR methods comparable, we consider a time-source term acting for a short period of time. Namely, $g_4(t) = 1\chi_{[0,0.1]}$. The space-source term selected in this experiment is $\boldsymbol{f}_{\text{sm}}(\boldsymbol{x})$ in (2.25) and its projection to $\mathbb{R}^2$.

For the classical time-reversal method, we consider the problem of reconstructing the initial displacement given by the following inverse problem: find $\boldsymbol{f}_{\text{sm}}(\boldsymbol{x})$ given

$$\begin{cases} \rho\partial_t^2\boldsymbol{u} - L_{\mu,\lambda}\boldsymbol{u} = \boldsymbol{0}, & \text{in } \mathbb{R}^n \times (0,T), \\ \boldsymbol{u}(\boldsymbol{x},0) = \boldsymbol{f}_{\text{sm}}(\boldsymbol{x}), \\ \partial_t\boldsymbol{u}(\boldsymbol{x},0) = \boldsymbol{0}, \end{cases} \tag{2.26}$$

knowing the measurements $m(\boldsymbol{y},t) = \boldsymbol{u}(\boldsymbol{y},t)$ for all $(\boldsymbol{y},t)$ in $\partial\Omega \times (0,T)$.

For the STR method, we consider the problem of reconstructing the source: given $g_4(t)$ for all $t \in (0,T)$ and the measurements $m(\boldsymbol{y},t) = \partial_t\boldsymbol{u}(\boldsymbol{y},t)$ for all $(\boldsymbol{y},t)$ in $\partial\Omega \times (0,T)$, find $\boldsymbol{f}_{\text{sm}}(\boldsymbol{x})$ such that

$$\begin{cases} \rho\partial_t^2\boldsymbol{u} - L_{\mu,\lambda}\boldsymbol{u} = \boldsymbol{f}_{\text{sm}}(\boldsymbol{x})g_4(t), & \text{in } \mathbb{R}^n \times (0,T), \\ \boldsymbol{u}(\boldsymbol{x},0) = \boldsymbol{0}, \\ \partial_t\boldsymbol{u}(\boldsymbol{x},0) = \boldsymbol{0}. \end{cases} \tag{2.27}$$

Problems (2.26) and (2.27) are different. However, since the time-source term g_4 acts only for a short period of time in relation with the total time T, we obtain similar wave propagations and errors for both problems, as illustrated in Figure 2.5. In this way, we can compare the intrinsic error of the TRM and the percent of error due to the STR method. Figure 2.5 also analyzes the effect of regularization constant c_0. In all cases, we observe that such constant has negligible effects on the accuracy of the resulting reconstruction.

2.5.4 Tree-dimensional reconstruction with partial data

We now analyze the case when only partial boundary data are available. To do this, we present reconstructions of the space-source term $\boldsymbol{f}_{\text{sm}(\boldsymbol{x})}$ (see (2.25)) when the measurements are obtained in a subset of the domain boundary. We consider three cases. In the first one, geophones are located on four faces of the cube $[-3,3] \times [-3,3] \times [-3,3]$; in the second one, geophones are located on two faces of the cube; and in the third case, geophones are located only along one face of the cube. The value of the finite difference discretization parameters are: $h = 0.05$ $[m]$, $dt = 0.01$ $[s]$, and $T = 7$ $[s]$.

Figure 2.6 shows the exact source and the respective reconstructions when the measurements are acquired in four, two, and one faces of the boundary domain. In the reconstructions with partial boundary information, the STR method with traditional regularization properly

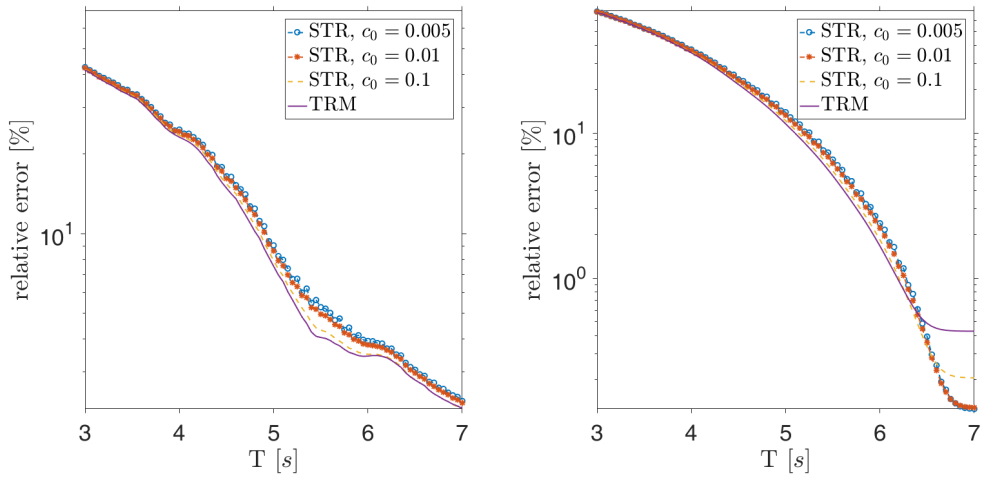

(a) 2D case (b) 3D case

Figure 2.5: Error decay comparison between TRM and STR for different values of c_0.

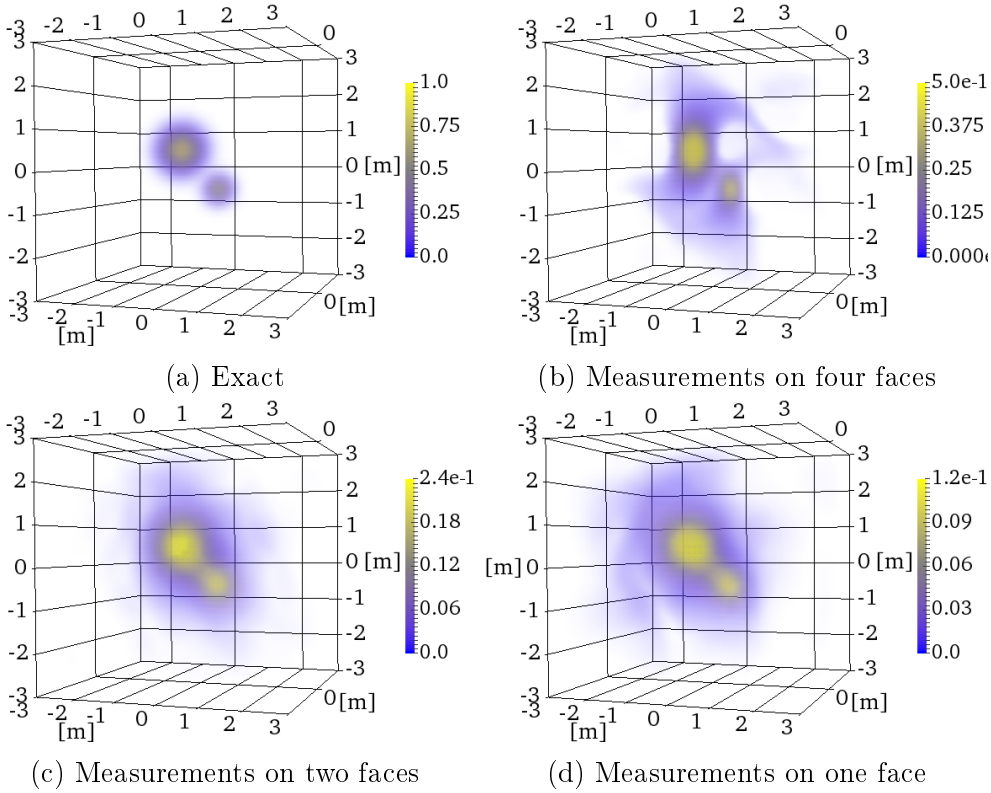

(a) Exact (b) Measurements on four faces

(c) Measurements on two faces (d) Measurements on one face

Figure 2.6: Exact and reconstruction of $|\boldsymbol{f}_{\mathrm{sm}}(\boldsymbol{x})|$ for waves generated by $\boldsymbol{f}_{\mathrm{sm}}(\boldsymbol{x})g_1(t)$.

localizes the space-source term and reconstructs it with lower resolution. The details of the reconstructed sources are related with the amount of information available in the boundary.

2.5.5 Comparison of two STR regularization methods: traditional vs fast cut-off

Here, we compare both STR regularization methods for reconstructions performed with data information on the entire boundary and with partial boundary data. To do this, we consider 2D reconstructions of the phantom $\boldsymbol{f}_{\text{ph}}(\boldsymbol{x})$ from measurements of waves generated with $\boldsymbol{f}_{\text{ph}(\boldsymbol{x})}g_3(t)$ (see Figures 2.3a and 2.2c). For each set of reconstructions the measurements are obtained on the entire boundary, on three faces, on two faces, and on one face of the boundary.

Let f_{meas} be the maximum measured frequency and f_{STR} be the maximum frequency of the signal processed with the STR method. For this comparison, we consider the regularization constant $c_1 = 0.180$, which gives us that $f_{STR} \leq f_{meas}$ for the fast STR with cut-off regularization. Additionally, we consider the case $c_1 = 0.048$, which gives us that $f_{STR} \leq 2f_{meas}$. To compare the methods, we consider the same regularization constants values for the STR with traditional regularization, but in this case the method induces higher frequencies.

Figures 2.7 and 2.8 show the reconstruction images for the different boundary information considered. The subfigures are intentionally on different scale for a better understanding of the results. The STR with traditional regularization presents a lower error percent in all cases and identifies better the edges of the phantom. Although the fast STR with cut-off regularization loses some "details" in the reconstruction when $f_{STR} \leq f_{meas}$ (and $f_{STR} \leq 2f_{meas}$), the methodology still identifies the correct location of the source and its main structure. Let us recall that low frequencies carry more global information, whereas the high frequencies contain the local information [90].

2.6 Numerical experiments of fast STR with cut-off regularization

In this section, we consider seismicity induced by mining in 2D. To more realistically do this, we pollute P- and S-waves synthetic measurements with additive Gaussian noise. To reconstruct the source, we implement the fast STR method by solving problem (2.21) and replacing operator $\mathcal{A}$ with the transformed data given by equation (2.23).

For these experiments, we generate a microseismic event considering three point sources acting simultaneously and modulated by a Ricker wavelet on time. These sources are located at points $(170, -135)$, $(0, -10)$, and $(140, 160)$, where the units are now in meters. Geophones are distributed ten meters away along the boundary of the set $\Omega = (-300, 300) \times (-300, 300)$. Besides, we incorporate additive Gaussian noise to the measurements obtained at the geophones as follows: let $m^k_{i\,clean}$ the measurement by the geophone i at time k under ideal conditions (i.e., with no uncertainty). Then the measurement with noise is computed by

$$m^k_{i\,noise} = m^k_{i\,clean} + \mathcal{N}\left(0, \sigma^2\right)^k_i,$$

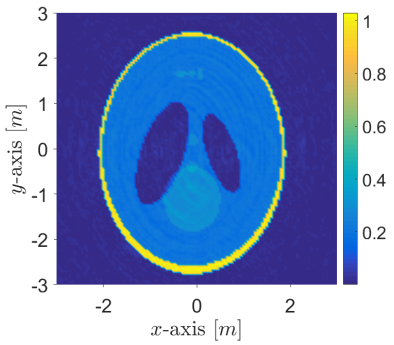

(a) 4 faces; $c_0 = 0.180$; error 7.8%

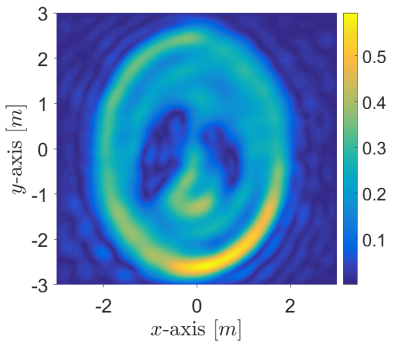

(b) 4 faces; $c_1 = 0.180$; error 64.9%

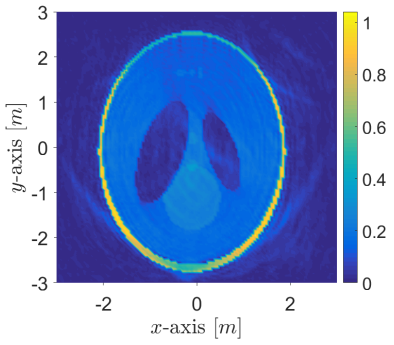

(c) 3 faces; $c_0 = 0.180$; error 31.7%

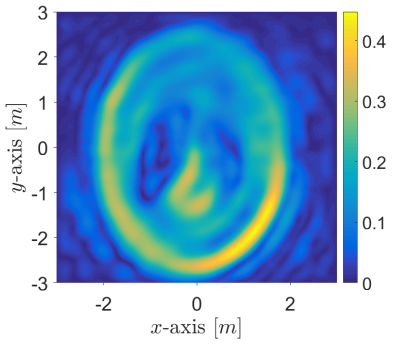

(d) 3 faces; $c_1 = 0.180$; error 68.8%

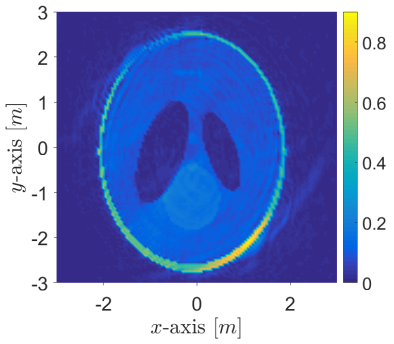

(e) 2 faces; $c_0 = 0.180$; error 50.9%

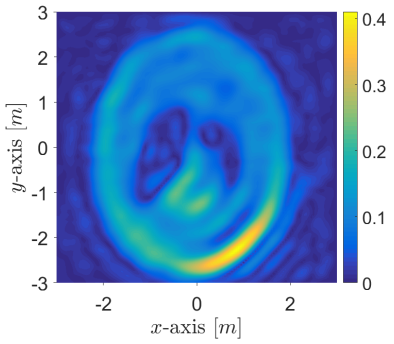

(f) 2 faces; $c_1 = 0.180$; error 74.7%

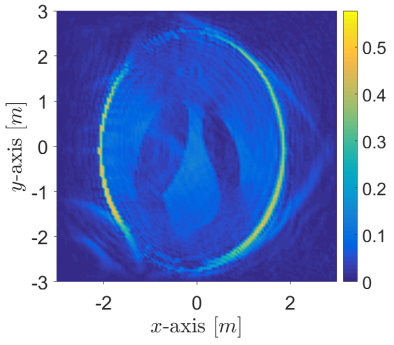

(g) 1 face; $c_0 = 0.180$; error 76.5%

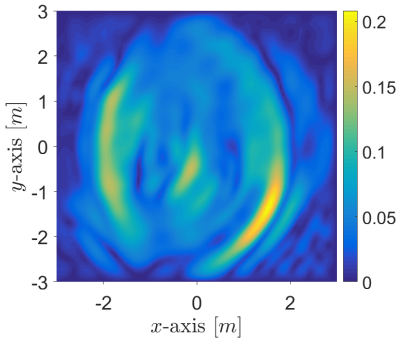

(h) 1 face; $c_1 = 0.180$; error 87.1%

Figure 2.7: Comparison of STR with traditional regularization ($c_0 = 0.180$) and fast reconstructions with cut-off regularization ($c_1 = 0.180$). Reconstruction of $|\boldsymbol{f}_{\text{ph}}(\boldsymbol{x})|$ with partial data for waves generated with $\boldsymbol{f}_{\text{ph}}(\boldsymbol{x})g_3(t)$. Relative error in L^2-norm.

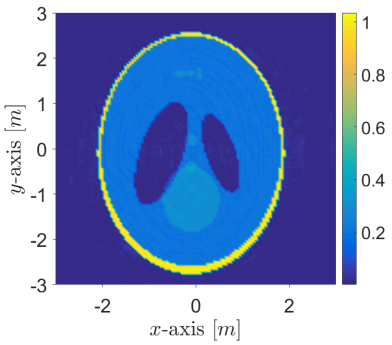

(a) 4 faces; $c_0 = 0.048$; error 5.6%

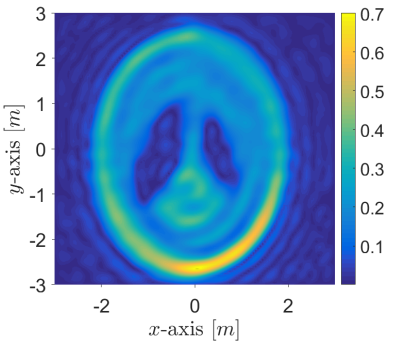

(b) 4 faces; $c_1 = 0.048$; error 61.6%

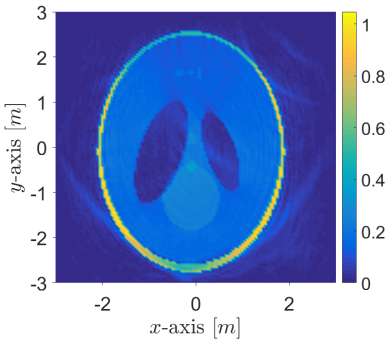

(c) 3 faces; $c_0 = 0.048$; error 31.1%

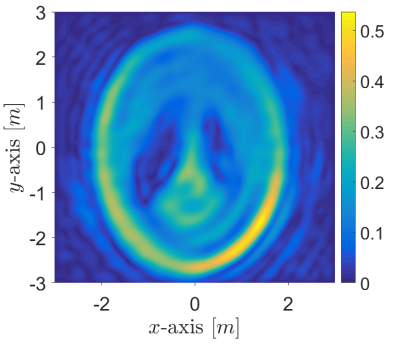

(d) 3 faces; $c_1 = 0.048$; error 65.9%

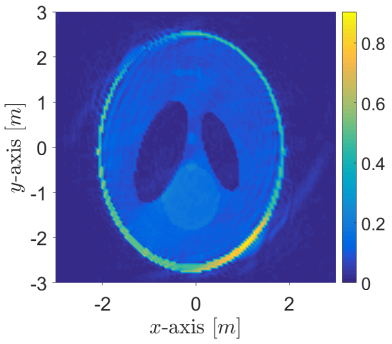

(e) 2 faces; $c_0 = 0.048$; error 50.5%

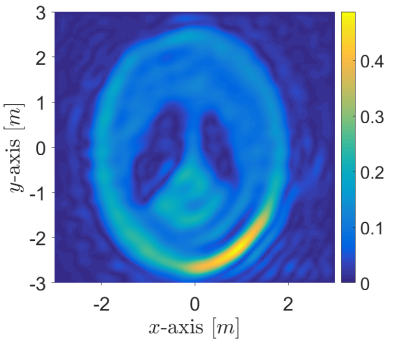

(f) 2 faces; $c_1 = 0.048$; error 72.5%

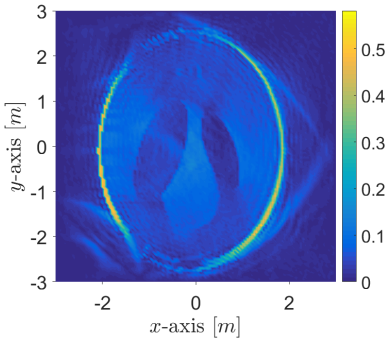

(g) 1 face; $c_0 = 0.048$; error 76.4%

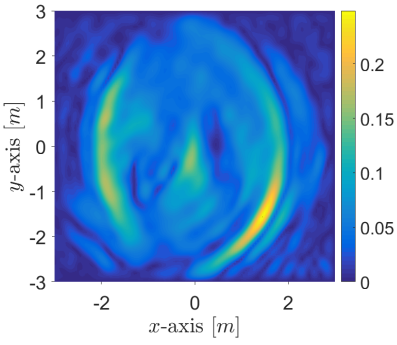

(h) 1 face; $c_1 = 0.048$; error 86.2%

Figure 2.8: Comparison of STR with traditional regularization ($c_0 = 0.048$) and fast reconstructions with cut-off regularization ($c_1 = 0.048$). Reconstruction of $|\boldsymbol{f}_{\text{ph}}(\boldsymbol{x})|$ with partial data for waves generated with $\boldsymbol{f}_{\text{ph}}(\boldsymbol{x})g_3(t)$. Relative error in L^2-norm.

where $\mathcal{N}(0, \sigma^2)_i$ is a Gaussian distribution associated to the i-th geophone, with zero mean and variance

$$\sigma^2 = \frac{P(m_{iclean})}{\text{SNR}}.$$

Here, $P(m_{iclean})$ is the power of the discrete signal m_{iclean} and SNR is the signal-to-noise ratio which allow us to control the percentage of the noise with respect to the signal, in the statistical sense. We consider $\rho = 2500\ [Kg/m^3]$, $\mu = 9.6334225\times10^9\ [Pa]$, $\lambda = 9.633155\times10^9$ $[Pa]$. Thus, $v_p = \sqrt{(2\mu+\lambda)/\rho} = 3400\ [m/s]$ and $v_s = \sqrt{\mu/\rho} = 1963\ [m/s]$, so $v_p/v_s \approx \sqrt{3}$. The case $v_p/v_s = \sqrt{3}$ is considered close to the real conditions for much of the Earth [50].

In addition, we set the cut-off constant $c_1 = 0.01$ to compute the fast STR method. For the computational mesh, we select $h = 10\ [m]$ and $dt = 0.001\ [s]$.

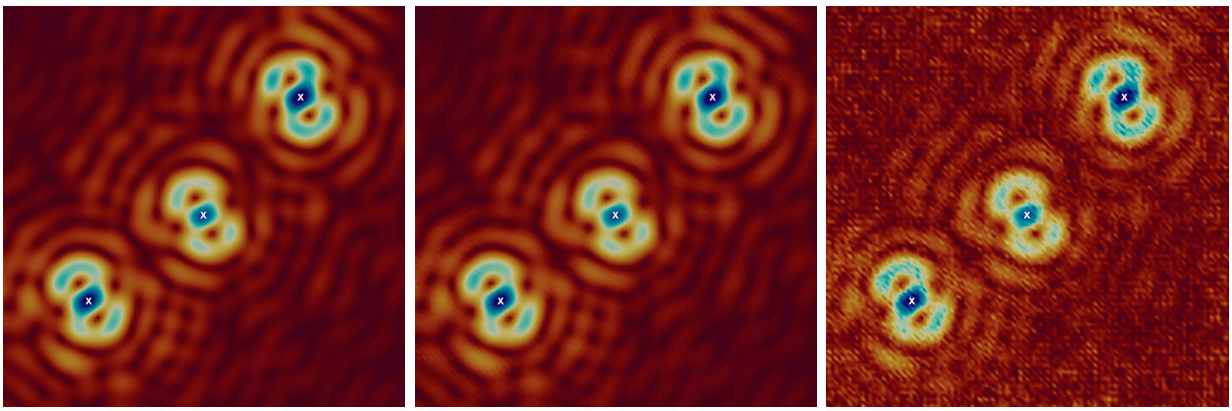

(a) without noise (b) noise: 10% (c) noise: 30%

Figure 2.9: Source reconstruction of seismicity induced by mining experiment from measurements with different percent of additive noise. The white crosses represent the exact position of the original point source.

Figure 2.9 shows the results of the source reconstructions where the measurements are acquired in presence of additive noise. In all cases, we observe superior reconstruction results.

Chapter 3

Source detection in elastic waves for sources with temporal component of Dirac type

Here, we consider the problem of source reconstruction in seismicity induced by mining. We are interested in sources of the form $\boldsymbol{s}(\boldsymbol{x},t) = \sum_{j=1}^{J} g_j(t)\boldsymbol{f}_j(\boldsymbol{x})$, where $g_j(t) = g(t-t_j)$ is a shift in t_j of a function g with compact support and J is the number (finite) of seismic events close in time. In this chapter, we study the problem when $g(t) = \delta(t)$, where δ represents the Dirac delta function. In other words, this means that each $\boldsymbol{f}_j(\boldsymbol{x})$ acts at the time t_j. To do this, we adapt a strategy for identifying discrete-in-time sources in acoustic waves equations to linear elasticity systems. Besides, we present a reconstruction algorithm and numerical experiments for acoustic and elastic cases.

3.1 Introduction

Seismicity induced by mining is usually divided into two types. The first one directly associated with mining operations, i.e., the formation of fractures at stope faces. The second type is associated with major geological discontinuities. This often occurs at some distance of the mine face. Usually, seisms associated with the first type are lower in magnitude than the second one. Additionally, seisms associated with the first class occur with more frequency than those associated with the second class, because of this the acknowledgement of seisms of the first class is superior. In fact, in the first case it is possible to associate a dependence function with the mining activity and the excavation ratio, while the second type presents a more erratic behavior [50].

In exploration geophysics, the elastic waves are commonly approximated by acoustic waves, for example, in migration techniques [23]. Regarding the computational cost and the required memory, 2D acoustic forward models gain up to two orders of magnitude with respect to elastic forward models [83]. This approximation is valid for isotropic homogeneous media or small heterogeneous media (concerning the wavelength). However, for large heterogeneities, the approximation introduces errors in the amplitude and the phase of the waves

[23], which makes necessary to consider the full elastic model.

A source composed by Dirac delta functions both in time and space is accepted in seismic studies to synthesize a realistic source displacement in terms of the displacement produced by the simplest source $\boldsymbol{\delta}(\boldsymbol{x}-\boldsymbol{x}_0)\delta(t-t_0)$ [2]. Additionally, to consider a time-source term as a Dirac delta function or a Heaviside function is commonly employed in theory of seismic disturbances [50]. Here, discrete-in-time sources consist of a sum of variable separable functions where the time-source term is a Dirac delta function and the space-source term is a compact support function, with the form $\sum_{j=1}^{J}\boldsymbol{f}_j(\boldsymbol{x})\delta(t-t_j)$. This kind of source models velocity changes in short slip [30].

To model the ground motion with the Lagrangian description [2], we consider a linear elasticity equation in isotropic and homogeneous media. Let $\boldsymbol{u}$ be the solution of the following problem

$$\begin{cases} \rho\partial_t^2\boldsymbol{u}(\boldsymbol{x},t) - L_{\mu,\lambda}\boldsymbol{u}(\boldsymbol{x},t) = \displaystyle\sum_{j=i}^{J}\boldsymbol{f}_j(\boldsymbol{x})\delta(t-t_j), \quad \text{in } \mathbb{R}^n\times(0,\infty), \\ \boldsymbol{u}(\boldsymbol{x},0) = \boldsymbol{0}, \\ \partial_t\boldsymbol{u}(\boldsymbol{x},0) = \boldsymbol{0}, \end{cases} \tag{3.1}$$

where $\boldsymbol{u}(\boldsymbol{x},t)$ represents the displacement of the point $\boldsymbol{x}$ at time t, and the operator $L_{\mu,\lambda}$ is given by $\mu\Delta\boldsymbol{u}+(\mu+\lambda)\nabla(\nabla\cdot\boldsymbol{u})$. Let us also consider a bounded set $\Omega\subset\mathbb{R}^n$ such that the support of $\boldsymbol{f}_j$ is contained in Ω for all j. Then, the inverse problem is defined by: find $\{\boldsymbol{f}_j(\boldsymbol{x}),t_j\}_{j=1}^{J}$ by knowing the displacement $\{\boldsymbol{u}(\boldsymbol{y},t):(\boldsymbol{y},t)\in\partial\Omega\times(0,T)\}$.

In this work, we propose an extension and an implementation of the discrete-in-time source reconstruction method for acoustic waves presented in [31] to linear elasticity. It is based on an invariance in time of the acoustic waves. M. Fink in [46] studied this property on waves and proposed a method called *time-reversal mirror* that allows recovering the initial pressure for acoustic waves. This invariance is also present in elastic and electromagnetic waves. Then, it is possible to implement the time-reversal mirror idea to different types of waves, for example, acoustics waves [14, 40, 42, 61], electromagnetic waves [79], elastic waves [91, 63], and Rouge waves [25].

The rest of this chapter is organized as follows. Section 3.2 introduces the classical time-reversal mirror from the P. Stefanov and G. Uhlmann point of view. Their approach considers a compatibility condition as an initial condition in the backward problem. In Section 3.3, we reproduce the discrete-in-time source reconstruction method proposed by M. de Hoop in [31] for acoustic waves. Section 3.4 is intended to extend the discrete-in-time source reconstruction to linear elastic systems of waves. Section 3.5 describes the methodology implementation for elastic waves problems. Sections 3.6 and 3.7 present some numerical examples of the source reconstruction for the 2D acoustic case, and for 2D and 3D elastic cases.

3.2 Time reversal

The time-reversal mirror strategy was developed by M. Fink et al. in the late 80's to focus an ultrasonic wave through an inhomogeneous medium [46]. Also, they realized the first physical experiment of the time-reversal mirror. C. Bardos and M. Fink in [14] presented a

mathematical formulation of the time-reversal mirror for the acoustic equation with Dirichlet and impedance boundary conditions. Later in 2012, P. Stefanov and G. Uhlmann in [103] proposed a time-reversal method to recover the first initial condition from ultrasound measurements, by considering a compatibility condition. After that, P. Stefanov and G. Uhlmann in [104] presented an extension of the previous work that recovers both initial conditions.

We explain briefly the approach in [104]. Let u be the solution of the forward problem

$$\begin{cases} \partial_t^2 u - c^2 \Delta u, = 0 & \text{in } \mathbb{R}^n \times (0,T), \\ u(\boldsymbol{x},0) = \phi(\boldsymbol{x}), \\ \partial_t u(\boldsymbol{x},0) = \psi(\boldsymbol{x}), \end{cases} \tag{3.2}$$

where ϕ and ψ are compactly supported in a bounded set Ω. In addition, we say that $c \in C^\infty(\mathbb{R}^n)$ accomplishes the non-trapping condition if the projection into the $\boldsymbol{x}$-components in $\mathbb{R}^n$ (rays) of the solution to the following system

$$\begin{cases} \boldsymbol{x}_t' = \frac{\partial H}{\partial \boldsymbol{\xi}} = \boldsymbol{\xi} c^2(\boldsymbol{x}), \\ \boldsymbol{\xi}_t' = -\frac{\partial H}{\partial \boldsymbol{x}} = -\frac{1}{2}|\boldsymbol{\xi}|^2 \nabla(c^2(\boldsymbol{x})), \\ \boldsymbol{x}|_{t=0} = \boldsymbol{x}_0, \\ \boldsymbol{\xi}|_{t=0} = \boldsymbol{\xi}_0, \\ H(\boldsymbol{x}_0, \boldsymbol{\xi}_0) = H_0, \end{cases}$$

where $H(\boldsymbol{x}, \boldsymbol{\xi}) = \frac{1}{2} c^2(\boldsymbol{x}) |\boldsymbol{\xi}|^2$ represents the Hamiltonian system, it goes to infinity when $t \to \infty$ (see, e.g., [35]).

Then, the inverse problem is defined by: find the unknown initial conditions (ϕ, ψ) given $\{m(\boldsymbol{y},t) := u(\boldsymbol{y},t) : (\boldsymbol{y},t) \in \partial\Omega \times (0,T)\}$. Then, let us define mathematically the operator $\Lambda(\phi,\psi) := u|_{\partial\Omega \times (0,T)}$, which give us the boundary measurements.

We define the space $\mathbf{H}(\Omega) := H_D(\Omega) \oplus L^2(\Omega)$, where $H_D(\Omega)$ is the completion of $C_0^\infty(\Omega)$ under the norm

$$\|u\|_{H_D(\Omega)} = \int_\Omega |\nabla u(\boldsymbol{x})|^2 \, dx.$$

Let us define the backward problem

$$\begin{cases} \partial_t^2 v - c^2 \Delta v = 0, & \text{in } \Omega \times (0,T), \\ v(\boldsymbol{x},T) = E m(\cdot,T)(\boldsymbol{x}), \\ \partial_t v(\boldsymbol{x},T) = 0, \\ v(\boldsymbol{y},t) = m(\boldsymbol{y},t), & \text{on } \partial\Omega \times (0,T), \end{cases} \tag{3.3}$$

where E represents the harmonic extension operator that solves

$$\begin{cases} c^2 \Delta \theta = 0, & \text{in } \Omega, \\ \theta = m(\cdot,T), & \text{on } \partial\Omega. \end{cases}$$

The main result in [104] is the following reconstruction theorem, which gives us a theoretical path to reconstruct the initial conditions.

Theorem 3.1 (Reconstruction [104]) *Let $c(\boldsymbol{x})$ accomplish the non-trapping condition, and let $T > T(\Omega)$. Then $\boldsymbol{A}\Lambda = \boldsymbol{I} - \boldsymbol{K}$, where $\boldsymbol{K}$ is compact in $\mathbf{H}(\Omega)$, and $\|\boldsymbol{K}\|_{\mathbf{H}(\Omega)} < 1$. In particular, $\boldsymbol{I} - \boldsymbol{K}$ is reversible on $\mathbf{H}(\Omega)$, and Λ has an explicit left inverse of the form*

$$(\phi, \psi) = \sum_{m=0}^{\infty} \boldsymbol{K}^m \boldsymbol{A} m, \tag{3.4}$$

where $m := \Lambda(\phi, \psi)$ is the boundary information and $\boldsymbol{A}m := (v(\cdot, 0), \partial_t v(\cdot, 0))$ is a pseudo-inverse operator.

3.3 Detection of discrete-in-time sources for acoustics

M. de Hoop in [31] presents a time-reversal method to recover the source position and the times t_j when the source is a finite sum of variable separable functions, where the time-source terms are Dirac delta functions of the form $\delta(t-t_j)$. In this section, we show its main results.

Let us consider the following acoustic wave equation

$$\begin{cases} \partial_t^2 u(\boldsymbol{x}, t) - \nabla \cdot \left(c^2(\boldsymbol{x}) \nabla u(\boldsymbol{x}, t)\right) = \displaystyle\sum_{j=i}^{J} f_j(\boldsymbol{x}) \delta(t - t_j), \quad \text{in } \mathbb{R}^n \times (0, \infty), \\ u(\boldsymbol{x}, 0) = 0, \\ \partial_t u(\boldsymbol{x}, 0) = 0, \end{cases} \tag{3.5}$$

for $n \in \{2, 3\}$, where $0 < t_j < t_0$ for all $j \in \{1, \ldots, J\}$, $f_j(\boldsymbol{x}) = \widetilde{f}_j(\boldsymbol{x}) \chi_{S_j}(\boldsymbol{x})$, and $c \in C^\infty(\mathbb{R}^n)$. Here $\widetilde{f}_j$ is a positive function and S_j is a connected set, for all $j \in \{1, \ldots, J\}$. In addition, we assume that there exits $\Omega \subset \mathbb{R}^n$ bounded such that $S_j \subset \Omega$ for all $j \in \{1, \ldots, J\}$.

Let us define the inverse problem: find the set $\{t_j, f_j(\boldsymbol{x})\}_{j=1}^J$ given $\{m(\boldsymbol{y}, t) := u(\boldsymbol{y}, t) : (\boldsymbol{y}, t) \in \partial\Omega \times (0, T)\}$ such that u solves (3.5).

To solve the inverse problem, we need to ensure that all rays left the domain after certain finite time T_Ω. Then, we assume that $c(\boldsymbol{x})$ accomplishes the non-trapping condition. In addition, to employ a time-reversal method, it is necessary to consider Duhamel's principle [38]. This principle establishes a relation via a convolution between the solution of a problem with an external source and the solution of an initial condition problem. Let us define the following problems

$$\begin{cases} \partial_t^2 u(\boldsymbol{x}, t) - \nabla \cdot (c(\boldsymbol{x})^2 \nabla u(\boldsymbol{x}, t)) = F(\boldsymbol{x}, t), \quad \text{in } \mathbb{R}^n \times (0, \infty), \\ u(\boldsymbol{x}, 0) = 0, \\ \partial_t u(\boldsymbol{x}, 0) = 0, \end{cases} \tag{3.6}$$

and we define the family of functions $\{v(\cdot, \cdot; s)\}_{s \in (0, \infty)}$ to be solution of

$$\begin{cases} \partial_t^2 v(\boldsymbol{x}, t; s) - \nabla \cdot (c(\boldsymbol{x})^2 \nabla v(\boldsymbol{x}, t; s)) = 0, \qquad \text{in } \mathbb{R}^n \times (s, \infty), \\ u(\boldsymbol{x}, s; s) = 0, \\ \partial_t u(\boldsymbol{x}, s; s) = F(\boldsymbol{x}, s). \end{cases}$$

Then, Duhamel's principle asserts that

$$u(\boldsymbol{x},t)=\int_0^t v(\boldsymbol{x},t;s)\,ds,$$

is solution to problem (3.6). Furthermore, when the source is a variable separable function and the time-source term has the form of a Dirac delta function, we obtain a direct relation between the solutions of both problems. Indeed, let us consider the following problems

$$\begin{cases}\partial_t^2 u(\boldsymbol{x},t)-\nabla\cdot(c(\boldsymbol{x})^2\nabla u(\boldsymbol{x},t))=f(\boldsymbol{x})\delta(t-t_0), & \text{in } \mathbb{R}^n\times(0,T),\\ u(\boldsymbol{x},0)=0,\\ \partial_t u(\boldsymbol{x},0)=0,\end{cases}\tag{3.7}$$

$$\begin{cases}\partial_t^2 v(\boldsymbol{x},t)-\nabla\cdot(c(\boldsymbol{x})^2\nabla v(\boldsymbol{x},t))=0, & \text{in } \mathbb{R}^n\times(t_0,T),\\ v(\boldsymbol{x},t_0)=0,\\ \partial_t v(\boldsymbol{x},t_0)=f(\boldsymbol{x}),\end{cases}\tag{3.8}$$

where the solutions to problems (3.7) and (3.8), respectively u and v, are related by $u(\boldsymbol{x},t)=v(\boldsymbol{x},t)$ for all $t\geq t_0$. Then, we can extend the problem (3.8) to the entire interval $(0,T)$ by defining

$$\begin{cases}\partial_t^2 w_0(\boldsymbol{x},t)-\nabla\cdot(c(\boldsymbol{x})^2\nabla w_0(\boldsymbol{x},t))=0, & \text{in } \mathbb{R}^n\times(0,T),\\ w_0(\boldsymbol{x},t_0)=0,\\ \partial_t w_0(\boldsymbol{x},t_0)=f(\boldsymbol{x}).\end{cases}$$

Here, $w_0(\boldsymbol{x},t)$ is odd with respect to t_0 in the interval $(0,2t_0)$. Then, we obtain that $u(\boldsymbol{x},t)=w_0(\boldsymbol{x},t)\chi_{\{t\geq t_0\}}(t)$.

Proposition 3.2 (Uniqueness [31]) *Let $\Omega\subset\mathbb{R}^n$ be a bounded set such that $w_0(\cdot,t)$ and $\partial_t w_0(\cdot,t)$ are compactly supported in Ω for all $t_0\leq t\leq 2t_0$ and $T>T(\Omega)$. Then, w_0 is uniquely determined by $u|_{\partial\Omega\times(0,T)}$. In addition, $\partial_t w_0(\boldsymbol{x},t_0)=f(\boldsymbol{x})$ can be recovered with Theorem 3.1.*

To solve the inverse problem defined above, it is possible to rewrite problem (3.5) in terms of J initial value problems by considering Duhamel's principle as in the previous paragraph

$$\begin{cases}\partial_t^2 w_j-\nabla\cdot(c^2\nabla w_j)=0, & \text{in } \mathbb{R}^n\times(0,\infty),\\ w_j(\boldsymbol{x},t_j)=0,\\ \partial_t w_j(\boldsymbol{x},t_j)=f_j(\boldsymbol{x}),\end{cases}\tag{3.9}$$

where each w_j is an odd function in time with respect to t_j in the interval $(0,2t_j)$. By superposition we obtain that

$$u(\boldsymbol{x},t)=\sum_{j=1}^{J} w_j(\boldsymbol{x},t)\chi_{\{t\geq t_j\}}(t).$$

As we do not know the times t_j where each $w_j(\boldsymbol{x},t)$ start acting, we consider the following function in the reconstruction process

$$\widetilde{u}(\boldsymbol{x},t)=\sum_{j=1}^{J} w_j(\boldsymbol{x},t),$$

where $\widetilde{u}$ solves inside Ω and for a given T the problem

$$\begin{cases} \partial_t^2 \widetilde{u} - c^2 \Delta \widetilde{u} = 0, & \text{in } \Omega \times (0,T), \\ \widetilde{u}(\boldsymbol{x}, T) = u(\boldsymbol{x}, T), & \\ \partial_t \widetilde{u}(\boldsymbol{x}, T) = \partial_t u(\boldsymbol{x}, T), & \\ \widetilde{u}(\boldsymbol{y}, t) = m(\boldsymbol{y}, t) & \text{on } \partial\Omega \times (0,T). \end{cases}$$

Here, we consider the time-reversal approach (3.3) of P. Stefanov and G. Uhlmann to reverse in time the measurements and obtain a reconstruction of $f_j(\boldsymbol{x})$ at t_j.

Theorem 3.3 (Uniqueness [31]) *Suppose that there exists t^* such that $0 < t_j < t^* < T$ and $\operatorname{dist}(S_j, \partial\Omega) > t^*$ for all $j \in \{1, \dots, J\}$, and $T > T_\Omega$. Then the boundary information $u(\boldsymbol{y}, t)$ for all $(\boldsymbol{y}, t) \in \partial\Omega \times (0,T)$ uniquely determines $\widetilde{u}$, and $\widetilde{u}$ can be recovered by a Neumann series as in Theorem 3.1.*

The key of this methodology is to notice that, when we reverse the time measurements performed over a bounded set Ω in problem (3.9), the support of the wave focuses toward S_j for $t > t_j$, collapses at $t = t_j$, and then expands again for $t < t_j$. Then, w_j vanishes at t_j but $\partial_t w_j$ does not vanish, for all $j \in \{1, \dots, J\}$. This fact is employed to find $\{t_j, f_j(\boldsymbol{x})\}_{j=1}^J$.

3.4 Extension to linear elasticity

Time-reversal mirror has been studied on elastic problems for different problems, see for example [10, 56, 91, 92]. In the context of seismicity induced by mining, the natural extension of the acoustic model is to consider linear elasticity. In [23], we can see a discussion about the validity of acoustic waves to model seismic phenomena in homogeneous and heterogeneous media and its limitation. Then, we extend the method presented in the previous section to linear elasticity problems.

Let us recall the inverse problem: find the set $\{t_j, \boldsymbol{f}_j(\boldsymbol{x})\}_{j=1}^J$ given $\{\boldsymbol{m}(\boldsymbol{y}, t) := \boldsymbol{u}(\boldsymbol{y}, t) : (\boldsymbol{y}, t) \in \partial\Omega \times (0,T)\}$ such that $\boldsymbol{u}$ solves (3.1).

First, we check Duhamel's principle for systems of elastic waves.

Proposition 3.4 *We define the following system of elastic waves*

$$\begin{cases} \rho \partial_t^2 \boldsymbol{u} - L_{\mu,\lambda} \boldsymbol{u} = \boldsymbol{F}(\boldsymbol{x}, t), & \text{in } \mathbb{R}^n \times (0, \infty), \\ \boldsymbol{u}(\boldsymbol{x}, 0) = \boldsymbol{0}, & \\ \partial_t \boldsymbol{u}(\boldsymbol{x}, 0) = \boldsymbol{0}, & \end{cases} \tag{3.10}$$

Let us define the family of functions $\{\boldsymbol{v}(\cdot, \cdot, s)\}_{s \in (0,T)}$, such that

$$\begin{cases} \rho \partial_t^2 \boldsymbol{v} - L_{\mu,\lambda} \boldsymbol{v} = \boldsymbol{0}, & \text{in } \mathbb{R}^n \times (0, \infty), \\ \boldsymbol{v}(\boldsymbol{x}, s; s) = \boldsymbol{0}, & \\ \partial_t \boldsymbol{v}(\boldsymbol{x}, s; s) = \dfrac{1}{\rho} \boldsymbol{F}(\boldsymbol{x}, s), & \end{cases}$$

Then,

$$\boldsymbol{u}(\boldsymbol{x},t) = \int_0^t \boldsymbol{v}(\boldsymbol{x},t;s)\,ds \tag{3.11}$$

solves problem (3.10).

Proof. Let $\boldsymbol{u}$ be as in (3.11), then

$$\begin{aligned}
\rho\partial_t^2\boldsymbol{u}(\boldsymbol{x},t) &= \rho\partial_t^2\int_0^t \boldsymbol{v}(\boldsymbol{x},t;s)\,ds \\
&= \rho\partial_t\left[\boldsymbol{v}(\boldsymbol{x},t;t) + \int_0^t \partial_t\boldsymbol{v}(\boldsymbol{x},t;s)\,ds\right] \\
&= \rho\left[\partial_t\boldsymbol{v}(\boldsymbol{x},t;t) + \int_0^t \partial_t^2\boldsymbol{v}(\boldsymbol{x},t;s)\,ds\right] \\
&= \boldsymbol{F}(\boldsymbol{x},t) + \int_0^t \rho\partial_t^2\boldsymbol{v}(\boldsymbol{x},t;s)\,ds.
\end{aligned}$$

Additionally, we compute

$$\begin{aligned}
L_{\mu,\lambda}\boldsymbol{u}(\boldsymbol{x},t) &= L_{\mu,\lambda}\int_0^t \boldsymbol{v}(\boldsymbol{x},t;s)\,ds \\
&= \mu\Delta\int_0^t \boldsymbol{v}(\boldsymbol{x},t;s)\,ds + (\mu+\lambda)\nabla\left(\nabla\cdot\int_0^t \boldsymbol{v}(\boldsymbol{x},t;s)\,ds\right) \\
&= \int_0^t \mu\Delta\boldsymbol{v}(\boldsymbol{x},t;s)\,ds + \int_0^t (\mu+\lambda)\nabla\left(\nabla\cdot\boldsymbol{v}(\boldsymbol{x},t;s)\,ds\right) \\
&= \int_0^t L_{\mu,\lambda}\boldsymbol{v}(\boldsymbol{x},t;s)\,ds.
\end{aligned}$$

Then, $\rho\partial_t^2\boldsymbol{u} - L_{\mu,\lambda}\boldsymbol{u} = \boldsymbol{F}$. And the initial conditions are obtained from direct evaluation of $\boldsymbol{u}(\boldsymbol{x},0)$ and $\partial_t\boldsymbol{u}(\boldsymbol{x},0)$, which completes the proof. □

By Duhamel's principle, we known that there exist J systems of elastic wave equations

$$\begin{cases}
\partial_t^2\boldsymbol{w}_j - L_{\mu,\lambda}\boldsymbol{w}_j = \boldsymbol{0}, & \text{in } \mathbb{R}^n\times(0,\infty), \\
\boldsymbol{w}_j(\boldsymbol{x},t_j) = \boldsymbol{0}, \\
\partial_t\boldsymbol{w}_j(\boldsymbol{x},t_j) = \boldsymbol{f}_j(\boldsymbol{x}),
\end{cases} \tag{3.12}$$

where $j\in\{1,\dots,J\}$ and the solution to problem (3.1) can be written in terms of each solution to problem 3.12

$$\boldsymbol{u}(\boldsymbol{x},t) = \sum_{j=1}^{J}\boldsymbol{w}_j(\boldsymbol{x},t)\chi_{\{t\geq t_j\}}(t).$$

As in the previous section, we do not known the times t_j. Then, to reverse on time the boundary information to problem 3.1 is equivalent to reversing the boundary information to the following function

$$\widetilde{\boldsymbol{u}}(\boldsymbol{x},t) = \sum_{j=1}^{J}\boldsymbol{w}_j(\boldsymbol{x},t),$$

when exists t^* with $t^* > t_j$ for all $j \in \{1, \ldots, J\}$ such that each $\boldsymbol{w}_j(\boldsymbol{x}, \cdot)$ and $\partial_t \boldsymbol{w}_j(\boldsymbol{x}, \cdot)$ are compactly supported inside Ω for all $t < t^*$.

To do this, we backpropagate the boundary measurements using time-reversal mirror with a compatibility condition. The compatibility condition, similar to the one proposed in [103], is described by operator E_e that solves

$$\begin{cases} L_{\mu,\lambda}\boldsymbol{\theta} = \mathbf{0}, & \text{in } \Omega, \\ \boldsymbol{\theta} = \boldsymbol{m}(\cdot, T), & \text{on } \partial\Omega. \end{cases}$$

Then, we consider the backward problem

$$\begin{cases} \partial_t^2 \widetilde{\boldsymbol{v}} - L_{\mu,\lambda}\widetilde{\boldsymbol{v}} = \mathbf{0}, & \text{in } \Omega \times (0, \infty), \\ \widetilde{\boldsymbol{v}}(\boldsymbol{x}, T) = E_e \boldsymbol{m}(\cdot, T)(\boldsymbol{x}), & \\ \partial_t \widetilde{\boldsymbol{v}}(\boldsymbol{x}, T) = \mathbf{0}, & \\ \widetilde{\boldsymbol{v}}(\boldsymbol{y}, t) = \boldsymbol{m}(\boldsymbol{y}, t), & \text{on } \partial\Omega \times (0, T). \end{cases}$$

Here we look for the times and places inside Ω where the displacement is zero and the displacement velocity is different from zero. When both previous conditions accomplish simultaneously indicates the instant of time when a source acts. Also, the displacement velocity, in a neighborhood where both conditions are accomplished, give us the shape of the source.

3.5 Implementation

In this section, we detail the implementation employed in the source reconstructions. To do this, we present a pseudocode with the primary steps necessary to identify the times when the discrete-in-time sources act and reconstruct the source shape.

We intend to identify the times t_j and the sources shape $\boldsymbol{f}(\boldsymbol{x})$ of the external source in the model (3.1). As demonstrated in the previous section, the displacement should be zero at the instant right before the source collapses into its original location when we reverse in time the boundary information in the backward problem. We use a Finite Difference Method (FDM) to solve the partial differential equation with boundary data. Numerically, it is difficult to obtain a value equals to zero. In practice, we look for the points $\boldsymbol{x}$ in the solutions such that the displacement magnitude is lower than a threshold and simultaneously the velocity magnitude is higher than a second threshold. Both thresholds will be determined by the boundary measurements and the size of the domain. We identify the time and the points in the domain when the two previous conditions are accomplished simultaneously. Finally, the source will be given by the displacement velocity in a neighborhood of point $\boldsymbol{x}$. Algorithm 1 shows in detail the described procedure.

3.6 Numerical results with acoustic examples

In this section, we present the results of discrete-in-time source reconstruction for an acoustic model, such that the source is written as a finite sum of variable separable functions, where the

Algorithm 1 2D source and time detection

function SOURCEDETECTION(boundaryData, $\widetilde{\boldsymbol{v}}_1$, $\widetilde{\boldsymbol{v}}_0$, thld_1, thld_2, r)
  times $\leftarrow$ List() ▷ initial conditions $\widetilde{\boldsymbol{v}}_1$ and $\widetilde{\boldsymbol{v}}_0$
  locations $\leftarrow$ List()
  shapes $\leftarrow$ List()
  for t from T to 0 **do**
    $\widetilde{\boldsymbol{v}}_2 \leftarrow$ SolveFDM(boundaryData, $\widetilde{\boldsymbol{v}}_1$, $\widetilde{\boldsymbol{v}}_0$)
    dis $\leftarrow$ MagnitudeDisplacement($\widetilde{\boldsymbol{v}}_2$)
    vel $\leftarrow$ MagnitudeVelocity($\widetilde{\boldsymbol{v}}_2$, $\widetilde{\boldsymbol{v}}_1$)
    if (dis $<$ thld_1) & (vel $>$ thld_2) **then**
      center $\leftarrow$ find point such that (dis $<$ thld_1) & (vel $>$ thld_2)
      neighborhood $\leftarrow$ B_r(center) ▷ $B_r(c)$ Ball of radius r centered in c
      times.Append(t)
      locations.Append(center)
      shapes.Append(vel·neighborhood)
    end if
    $\widetilde{\boldsymbol{v}}_0 \leftarrow \widetilde{\boldsymbol{v}}_1$ ▷ update initial conditions
    $\widetilde{\boldsymbol{v}}_1 \leftarrow \widetilde{\boldsymbol{v}}_2$
  end for
  return [times, locations, shapes]
end function

time-source terms are given by Dirac delta functions. To locate and reconstruct the source, we employ the algorithm described in Section 3.5, considering that in the acoustic case the displacement and displacement velocity are scalar functions. To simulate the forward and backward problems, we employ an explicit finite difference method with a space-step of 0.05 $[m]$ and a time-step of 0.01 $[s]$, with a total simulation time of 15 seconds. In the forward and backward problems, we propagate the waves, originated by the source and the boundary data respectively, with a second-order central difference scheme in space and a forward difference scheme in time. Additionally, in the forward problem, we consider a computational domain larger than the subset Ω where the measurements are performed such that the waves are free from the computational boundary influence. In the backward problem, we consider a computational domain with the same size as the set Ω where the measurements are performed. For computing the Dirac delta function, we consider the approximating function

$$\delta_\alpha(t - t_0) = \frac{1}{|\alpha|\sqrt{\pi}} e^{-((t-t_0)/\alpha)^2}, \tag{3.13}$$

with $\alpha = 0.005$.

For these experiments, we consider two source configurations. The first one with two sources acting at times 0.2 $[s]$ and 0.5 $[s]$ (see Figure 3.1a). The second configuration with three sources acting at times 0.1 $[s]$, 0.3 $[s]$, and 0.5 $[s]$ (see Figure 3.1b). For the space-source term, we define the following functions $\eta_1(x, y) = \exp(1 - 4^2((x + 1)^2 + (y - 1)^2))$, $\eta_2(x, y) = \exp(1 - 3^2((x-1)^2 + (y+1)^2))$, and $\xi_{x_0,y_0}(x, y) = 1_{\chi_{\{|x-x_0|<0.2\}}} 1_{\chi_{\{|y-y_0|<0.2\}}}$. Then, the space-source terms are given by

$$f_{1,1}(x, y) = 1.0\frac{\eta_1(x, y)}{\max \eta_1(x, y)}, \quad f_{1,2}(x, y) = 0.7\frac{\eta_2(x, y)}{\max \eta_2(x, y)}.$$

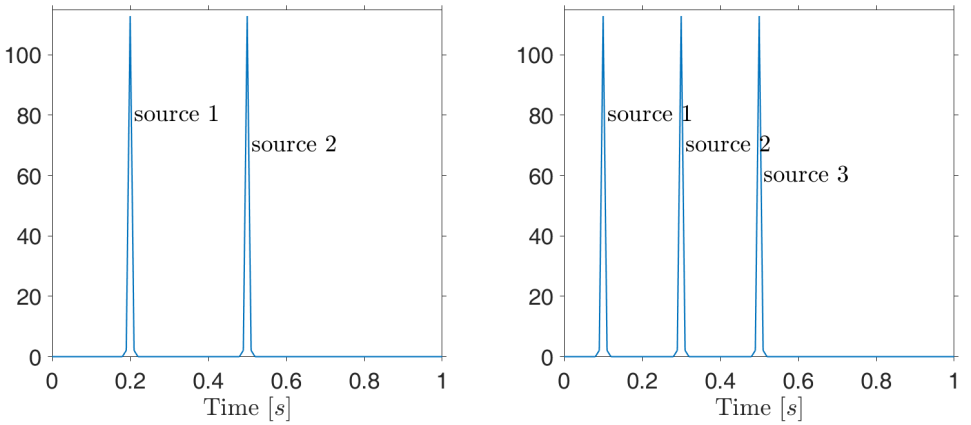

(a) Conf. 1, $\delta_a(t-t_j)$ for $j=\{1,2\}$ (b) Conf. 2, $\delta_a(t-t_j)$ for $j=\{1,2,3\}$

Figure 3.1: Time-source term configurations.

and

$$f_{2,1}(x,y)=\xi_{1,1}(x,y),\quad f_{2,2}(x,y)=\xi_{0,0}(x,y),\quad f_{2,3}(x,y)=\xi_{-1,1}(x,y).$$

Then, the first source is given by

$$F_1(x,y,t)=f_{1,1}(x,y)\delta_\alpha(t-0.2)+f_{1,2}(x,y)\delta_\alpha(t-0.5), \tag{3.14}$$

and the second source is given by

$$F_2(x,y,t)=f_{2,1}(x,y)\delta_\alpha(t-0.1)+f_{2,2}(x,y)\delta_\alpha(t-0.3)+f_{2,3}(x,y)\delta_\alpha(t-0.5). \tag{3.15}$$

Figure 3.2 shows the space-source terms for each configuration.

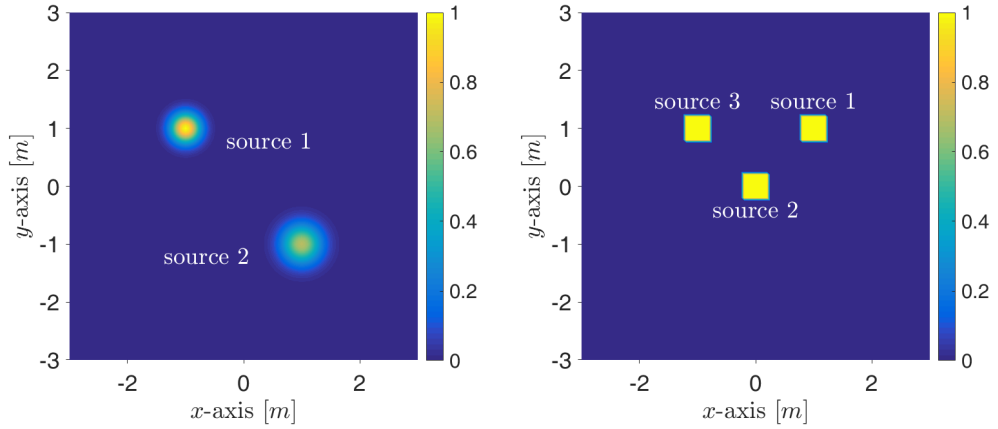

(a) Conf. 1, $f_{1,j}(\boldsymbol{x})$ for $j=\{1,2\}$ (b) Conf. 2, $f_{2,j}(\boldsymbol{x})$ for $j=\{1,2,3\}$

Figure 3.2: Space-source term configurations.

3.6.1 Reconstruction of two sources with smooth space term

In this subsection, we present the results of discrete-in-time source reconstruction for the first configuration given by the source term (3.14), composed of two smooth space-source terms

$f_{1,1}(x, y)$ and $f_{1,2}(x, y)$ acting at times 0.2 $[s]$ and 0.5 $[s]$, respectively. For this experiment, we employ the boundary data given by the displacement of the forward problem to generate synthetic measurements. Additionally, we set the displacement threshold at 0.001 (thld_1) and the displacement velocity in 0.8 (thld_2). The cut-off radius r to define the maximum length of the source is defined as 0.7.

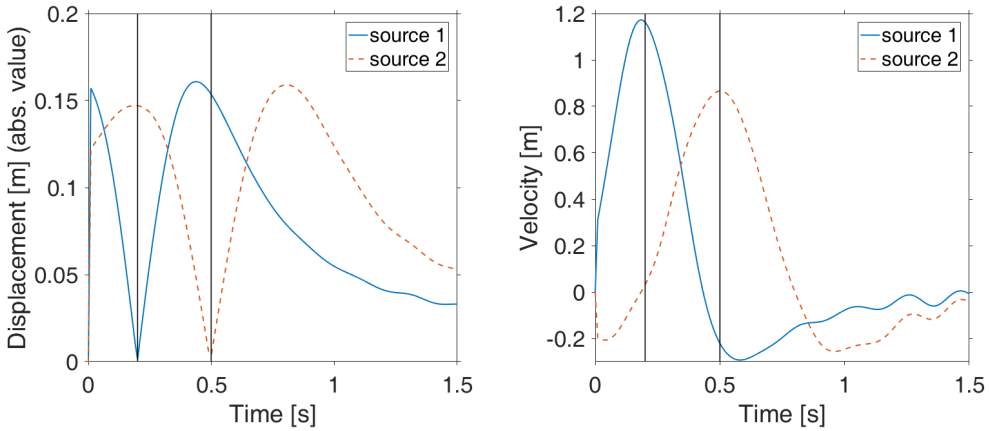

(a) Displacement through time at points $(-1, 1)$ and $(1, -1)$

(b) Displacement velocity through time at points $(-1, 1)$ and $(1, -1)$

Figure 3.3: Displacement and displacement velocity behavior at center of space-source terms given by the backward problem, first conf. Vertical black lines represent the exact acting time.

Figure 3.3 shows the displacement and displacement velocity behavior given by the backward problem at the points where the center of both sources were originally located. Here, we can see from the first subfigure that the displacement decays to zero at the times when the source term starts in the forward problem. In turn, the second subfigure shows the velocity behavior at the same points. Here, we see that the velocity takes high values at the acting times for the forward problem in relation to the remaining times.

Table 3.1 shows the source times detected by the method. In this case, we identify the two sources correctly. Figure 3.4 describes the results of the shape reconstructions of the two different space-source terms. The caption of each subfigure shows the correspondence of the space and time source terms.

Time	Source number
0.20	source 1
0.50	source 2

Table 3.1: Source identification at different times for acoustic case, first conf.

In this experiment, both source terms are located correctly in time and space. Also, the shape of each term is correctly reconstructed.

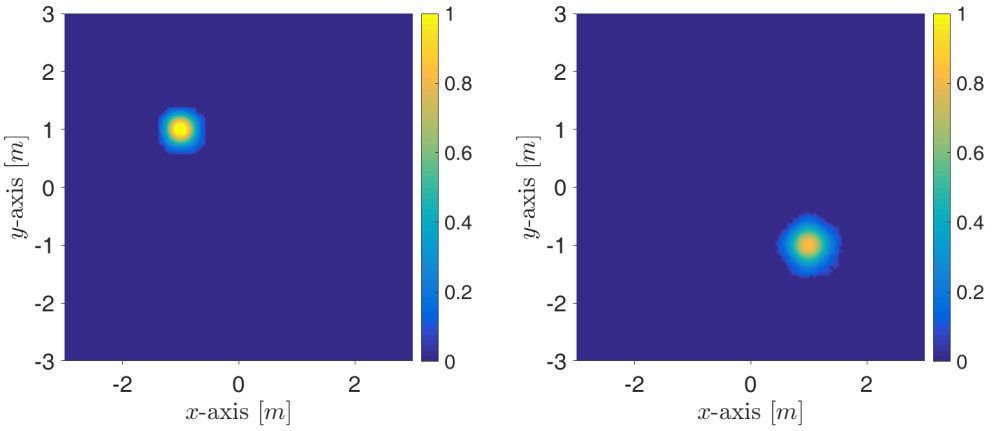

(a) Reconstruction at $t = 0.20$ (b) Reconstruction at $t = 0.50$

Figure 3.4: Space-term reconstruction for the different times, first conf.

3.6.2 Reconstruction of three sources with discontinuous space term

In this subsection, we present the results of the discrete-in-time source reconstruction for the second configuration. Here, the source is given by the identity (3.15), which is composed of three discontinuous space-source terms $f_{2,1}(x, y)$, $f_{2,2}(x, y)$, and $f_{2,3}(x, y)$ acting at times 0.1 $[s]$, 0.3 $[s]$, and 0.5 $[s]$, respectively. As in the previous experiment, the boundary data is obtained from the displacement measured in the forward problem. We set the thresholds: $\text{thld}_1 = 0.0011$ and $\text{thld}_2 = 1.0$. Additionally, the cut-off radius r to define the maximum length of the source is selected as 0.7.

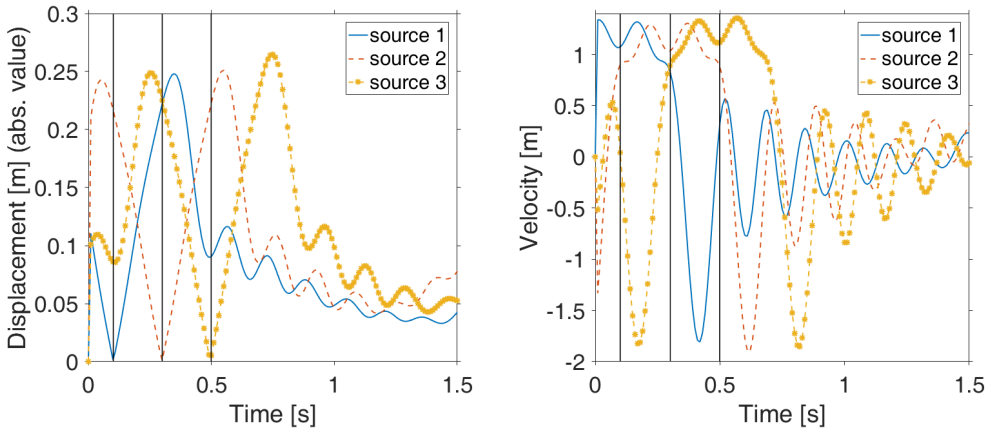

(a) Displacement through time at points $(1, 1)$, $(0, 0)$, and $(-1, 1)$ (b) Displacement velocity through time at points $(1, 1)$, $(0, 0)$, and $(-1, 1)$

Figure 3.5: Displacement and displacement velocity behavior at center of space-source terms given by the backward problem, second conf. Vertical black lines represent the exact acting time.

Figure 3.5 shows the displacement and displacement velocity behavior for the solution of the backward problem given by the reversed measurements as boundary data. Here, we can see that the displacement, at the points where the source terms are located in the

forward problem, takes the minimum values at the times when each source term starts. The displacement velocity takes high values in a neighborhood of the acting source time with respect to the values far from the acting time. Let notice that in this case the value of the velocity at the correct reconstruction time is given by what it seems a *local minimum*.

Table 3.2 shows the results of the times detected by the methodology. In this case, the methodology identifies the three time sources correctly but also detects the time 0.39 as a source start time. In Figure 3.6, we see the results of the shape reconstructions for the three space-source terms $f_{2,1}(x, y)$, $f_{2,2}(x, y)$, and $f_{2,3}(x, y)$. Here, we can see the correct shape reconstruction of the three sources a the right start times. This figure also shows that the extra time detection corresponds to a repeated identification of source 3. This can not be avoided by changing the thresholds since the displacement value at point $(-1, 1)$ at time 0.39 is lower than that at time 0.4.

Time	Source number
0.20	source 1
0.30	source 2
0.39	source 3
0.40	source 3

Table 3.2: Source identification at different times for acoustic case, second conf.

This experiment presents a correct shape reconstruction of the three source terms, and it shows the correct localization in time and space of the three source terms, but also identifies an extra time as a source start time, when in fact is the next time step in the computational discretization of a source start time.

3.7 Numerical results with elastic examples

In this section, we present some numerical discrete-in-time source reconstructions for elastic problems in 2D and 3D domains. Here, we present two configuration examples in 2D case and also two configuration examples in the 3D case. On each example, the first step is to generate synthetic boundary measurements given by a determined source configuration. Then in the second step, we reverse the boundary measurements with the backward problem, where the methodology is implemented to identify the source terms. To locate and reconstruct the source terms, we employ the algorithm described in Section 3.5. To implement the forward and backward problems in the 2D and 3D cases, we consider an explicit finite difference method with a space-step of 0.05 $[m]$ and a time-step of 0.001 $[s]$. The total time of simulation is 15 seconds for the 2D case and 7 seconds for the 3D case.

We consider the finite difference scheme given by [69] for the forward and backward problems. For the forward problem, we define a computational domain that contains subset Ω where we perform the measurement, and large enough such that the waves are free from the computational boundary influence. For the backward problem, we consider a computational domain equal to subset Ω, where the boundary conditions are given by the measurements.

Here, we employ the expression (3.13) to approximate the Dirac delta function with $\alpha =$

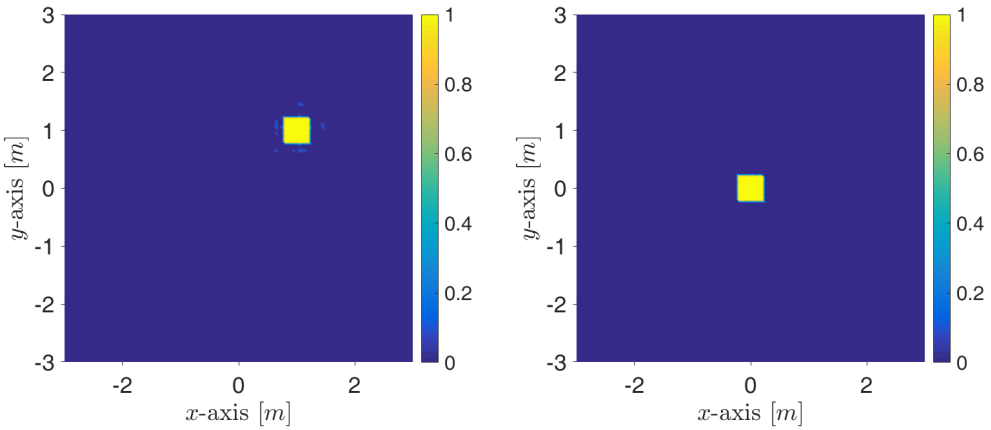

(a) Reconstruction at $t = 0.20$

(b) Reconstruction at $t = 0.30$

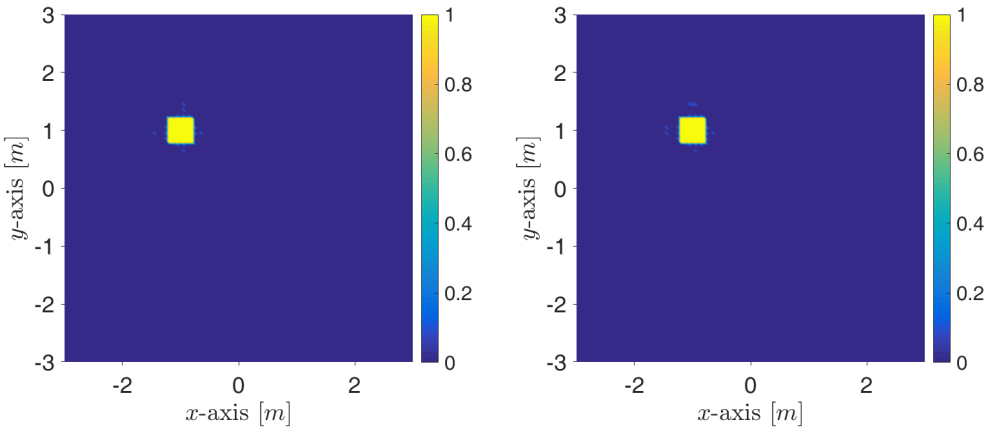

(c) Reconstruction at $t = 0.39$

(d) Reconstruction at $t = 0.40$

Figure 3.6: Space-term reconstruction for the different times, second conf.

0.005, and we consider the same distribution on time for the source acting times than in the previous section (see Figure 3.1). For the 2D case, on each component of the space-source terms, we consider the expressions $F_1(x, y, t)$ (3.14) and $F_2(x, y, t)$ (3.15). In the 3D case, we generalize the functions η_1, η_2, and ξ_{x_0,y_0} as

$$\eta_1(x, y, z) = \exp(1 - 4^2((x + 1)^2 + (y - 1)^2 + (z - 0)^2)),$$

$$\eta_2(x, y, z) = \exp(1 - 3^2((x - 1)^2 + (y + 1)^2 + (z - 0)^2)),$$

and

$$\xi_{x_0,y_0,z_0}(x, y, z) = 1\chi_{\{|x-x_0|<0.2\}}1\chi_{\{|y-y_0|<0.2\}}1\chi_{\{|z-z_0|<0.2\}},$$

Then, we construct $F_1(x, y, z, t)$ and $F_2(x, y, z, t)$ as in the previous section for each component.

$$F_1(x, y, z, t) = f_{1,1}(x, y, z)\delta_\alpha(t - 0.2) + f_{1,2}(x, y, z)\delta_\alpha(t - 0.5), \tag{3.16}$$

where

$$f_{1,1}(x, y, z) = 1.0\frac{\eta_1(x, y, z)}{\max \eta_1(x, y, z)}, \quad f_{1,2}(x, y, z) = 0.7\frac{\eta_2(x, y, z)}{\max \eta_2(x, y, z)},$$

and

$$F_2(x, y, t) = f_{2,1}(x, y)\delta_\alpha(t - 0.1) + f_{2,2}(x, y)\delta_\alpha(t - 0.3) + f_{2,3}(x, y)\delta_\alpha(t - 0.5). \tag{3.17}$$

Figures 3.7a and 3.8a show the magnitude of the space-source terms for the first and second configuration in the 2D case, respectively. Figures 3.9a and 3.10a shows the space-source terms for the first and second configuration in the 3D case, respectively.

3.7.1 2D reconstruction of two sources with smooth space term

In this subsection, we present the results of discrete-in-time source reconstruction for a source composed in each component by the function (3.14). Then, the space-source term $(f_{1,1}(x, y), f_{1,1}(x, y))$ acts at time 0.2 $[s]$ and $(f_{1,2}(x, y), f_{1,2}(x, y))$ acts at time 0.5 $[s]$. With this configuration, the forward problem generates the boundary information necessary for implementing the source detection methodology. Then, we define the thresholds as $\text{thld}_1 = 0.004$ and $\text{thld}_2 = 1.1$. The cut-off radius r is selected as 0.6.

Time	Source number
0.20	source 1
0.50	source 2

Table 3.3: Source identification at different times for 2D elastic case, first conf.

Table 3.3 displays the times detected as a start source times. Figure 3.7 shows the magnitude of the original space-source terms (3.7a) and its reconstructions (3.7c and 3.7b) in correspondence with the times given by Table 3.3. For this experiment, the methodology recovers the shape of each source terms at the correct time and location.

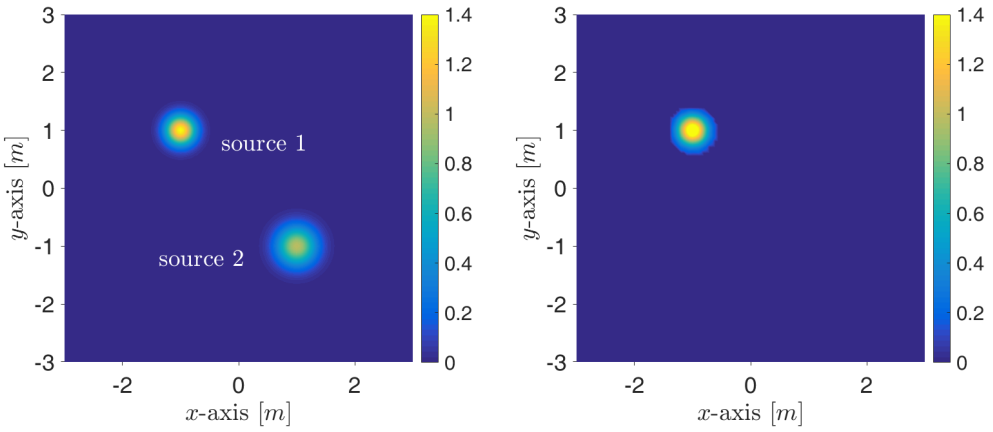

(a) Original source location

(b) Reconstruction at $t = 0.20$

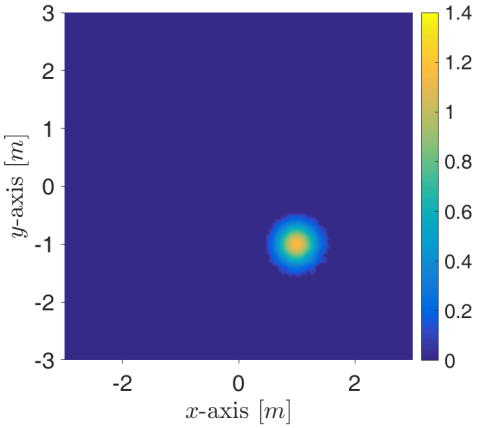

(c) Reconstruction at $t = 0.50$

Figure 3.7: Original and recons. of the space-source terms for 2D elastic case, first conf.

3.7.2 2D reconstruction of three sources with discontinuous space term

In this subsection, we show the results of discrete-in-time source reconstruction for a source composed in each component by the function (3.15). This means that $(f_{2,1}(x,y), f_{2,1}(x,y))$ starts at 0.1 $[s]$, $(f_{2,2}(x,y), f_{2,2}(x,y))$ starts at 0.3 $[s]$, and $(f_{2,3}(x,y), f_{2,3}(x,y))$ starts at 0.5 $[s]$. After generating the boundary data with the forward problem, we set the thresholds in 0.007 for the displacement magnitude and 1.4 for the displacement velocity magnitude. The cut-off radius is given by $r = 0.7$.

Time	Source number
0.10	source 1
0.30	source 2
0.50	source 3

Table 3.4: Source identification at different times for 2D elastic case, second conf.

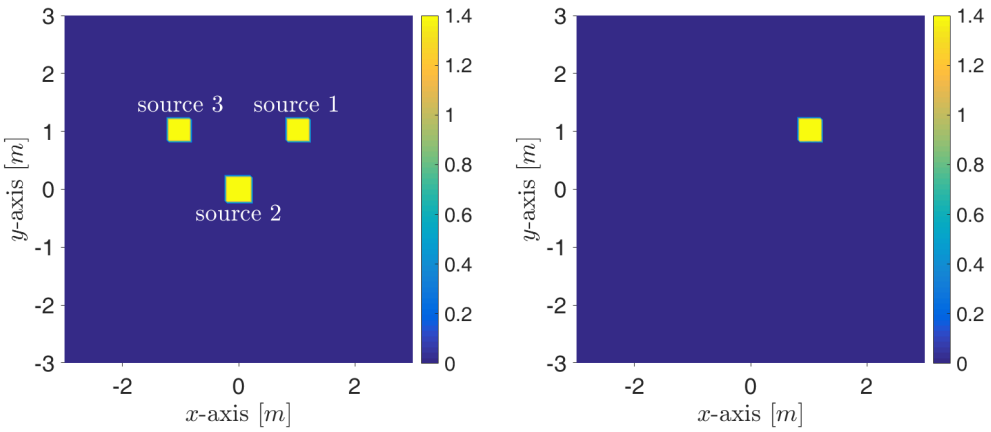

(a) Original source location

(b) $t = 0.10$

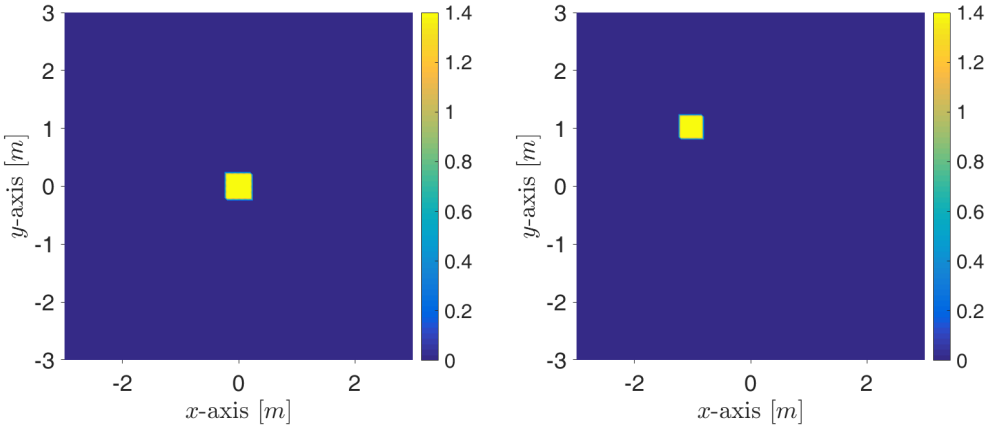

(c) $t = 0.30$

(d) $t = 0.50$

Figure 3.8: Original and recons. of the space-source terms for 2D elastic case, second conf.

Table 3.4 displays the detected times. Figure 3.8 shows the original position and the shape of the source terms (3.8a) and also the reconstructed terms on each time detected

(3.8b, 3.8c, and 3.8d). In this experiment, the three source terms are correctly identified and reconstructed with the selected threshold values.

3.7.3 3D reconstruction of two sources with smooth space term

This subsection shows the results of the discrete-in-time source reconstruction for the first configuration given by the source term $(F_1(x,y,z,t), F_1(x,y,z,t), F_1(x,y,z,t))$, where each component is given by (3.16). The space-source term $(f_{1,1}(x,y,z), f_{1,1}(x,y,z), f_{1,1}(x,y,z))$ acts at the time 0.2 $[s]$ and $(f_{1,2}(x,y,z), f_{1,2}(x,y,z), f_{1,2}(x,y,z))$ acts at the time 0.5 $[s]$. For this experiment, we consider the threshold values 5×10^{-5} and 1.4 for the displacement magnitude and displacement velocity magnitude, respectively. We also consider the radius r in 0.6.

Time	Source number
0.20	source 1
0.50	source 2

Table 3.5: Source identification at different times for 3D elastic case, first conf.

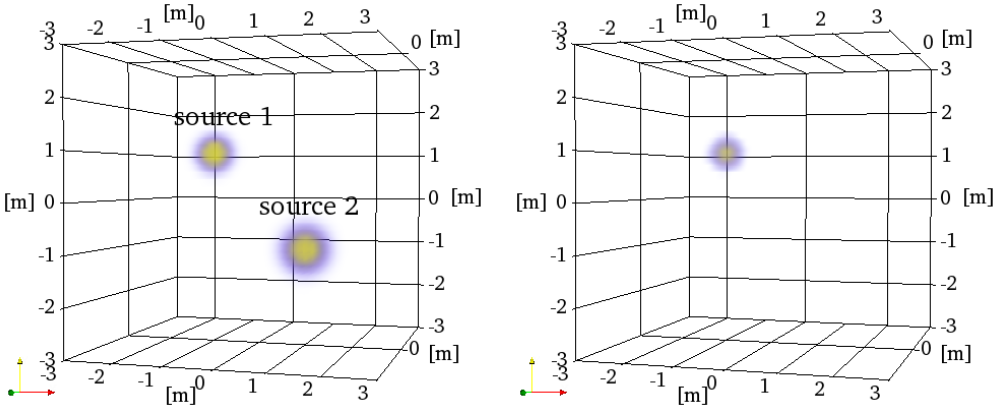

(a) Original source location

(b) Reconstruction at $t = 0.20$

(c) Reconstruction at $t = 0.50$

Figure 3.9: Original and recons. of the space-source terms for 3D elastic case, first conf.

Table 3.5 shows the times detected by the methodology. Figure 3.9 shows the magnitude

of the original space-source terms and its reconstructions at the times given by Table 3.5. This experiment recover properly the location and the shape of the source.

3.7.4 3D reconstruction of three sources with discontinuous space term

In this last subsection, we present the results for the second configuration given by the source $(F_2(x,y,z,t), F_2(x,y,z,t), F_2(x,y,z,t))$, where each component is given by (3.17). This source is composed of three discontinuous space-source terms $(f_{2,1}(x,y,z), f_{2,1}(x,y,z), f_{2,1}(x,y,z))$, $(f_{2,2}(x,y), f_{2,2}(x,y), f_{2,2}(x,y))$, and $(f_{2,3}(x,y), f_{2,3}(x,y), f_{2,3}(x,y))$ acting at the times 0.1 $[s]$, 0.3 $[s]$, and 0.5 $[s]$, respectively. We set the thresholds in $\text{thld}_1 = 0.002$ and $\text{thld}_2 = 2.0$. Additionally, the cut-off radius r to define the maximum length of the source is 0.6.

Time	Source number
0.10	source 1
0.30	source 2
0.50	source 3

Table 3.6: Source identification at different times for 3D elastic case, second conf.

Table 3.6 displays the times detected by the methodology. Figure 3.10 presents the original source terms and the shape reconstructions for the detected times. Here, we can see the correct location in time and space and the correct shape reconstruction of these three discontinuous sources.

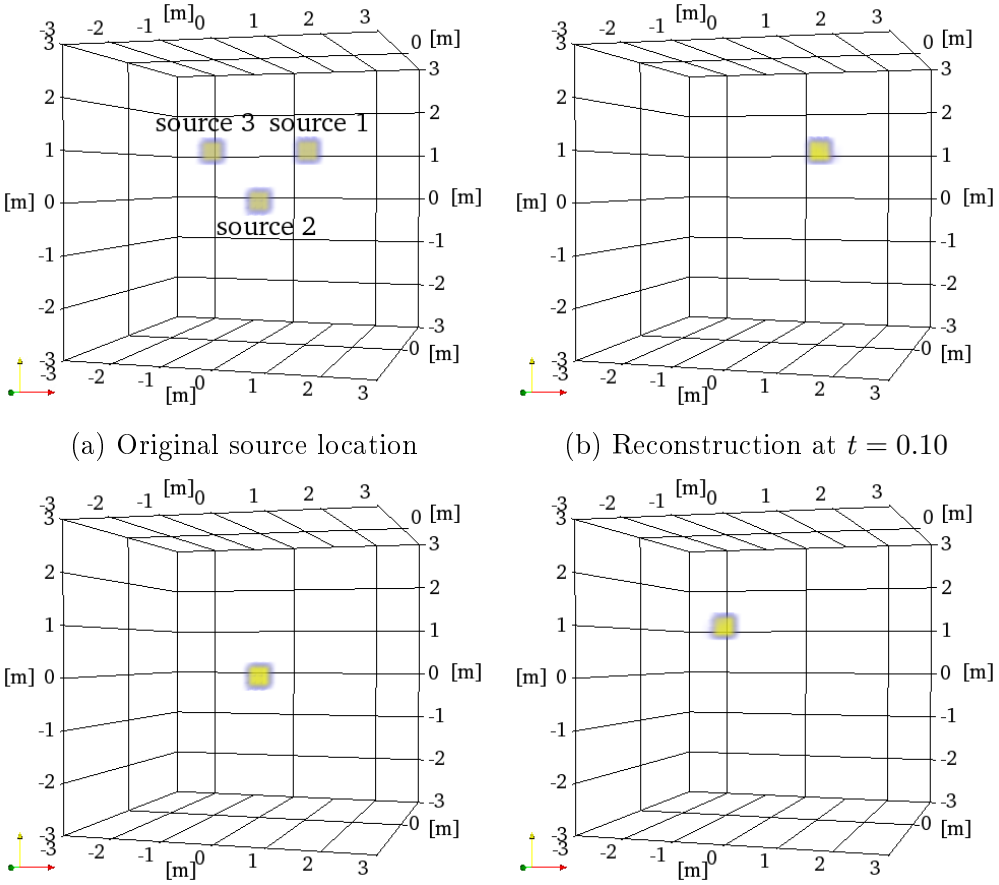

(a) Original source location

(b) Reconstruction at $t = 0.10$

(c) Reconstruction at $t = 0.30$

(d) Reconstruction at $t = 0.50$

Figure 3.10: Original and recons. of the space-source terms for 3D elastic case, second conf.

Main achievements

To study the problem of reconstruction and location of a source in seismicity induced by mining is common to consider the source as a variable separable function where each term is a Dirac delta function. The Time-Reversal Mirror (TRM) method enables to reconstruct a variable separable source with a more general compact support function in space and a Dirac delta function in time. The main achievement of this dissertation is to develop a method capable of reconstructing the space-source term in an even more general variable separable source, where each term can be considered as a compact support function (in space and time). While developing the method, we achieved the following research accomplishments:

- To develop the source time reversal method for acoustic problems.
- To estimate the source reconstruction error in the acoustic case.
- To find a local decay result for elastic waves.
- To extend the source time reversal method for systems of elastic waves.
- To develop two regularization methods for the source time reversal method.
- To implement 2D and 3D codes employing finite difference methods for acoustic and elastic waves.
- To implement several numerical experiments to test the properties of the method.
- To validate the fast source time reversal with cut-off regularization with a finite element method.
- To extend the reconstruction of discrete-in-time sources for linear elasticity.
- To develop an algorithm for elastic waves.

We thus increased the number of tools available in seismicity from a rigorous mathematical point of view for a better comprehension of the seismicity induced by mining in underground mining. This has a positive impact on the safety of miners inside mines.

The works included in this dissertation have been exposed in several occasions:

- MINIWORKSHOP Control y Problemas Inversos de EDP 2018, 18-19 January, Valparaíso, Chile.
- PRIMA 2017 third congress, 14-18 August, Oaxaca, Mexico (co-author).
- X Congress GAFEVOL 2016: "Evolution Equations and Functional Analysis", 23-25 November, Santiago, Chile.
- PICOF 2016, 1-3 June, Autrans, France (co-author).

Additionally, we have published the Chapter 1 under the same name "A source time reversal method for seismicity induced by mining" on the journal *Inverse Problems and Imaging*. We have submitted the Chapter 2 in a first-quartile journal. Chapter 3, at the moment of finishing this dissertation, will soon become the third paper stemming from this dissertation.

I also generated an international network composed of researchers at Universidad del País Vasco (UPV/EHU), where I spent 10 months during my dissertation, the Basque Center for Applied Mathematics (BCAM), Instituto de Matemática (IMA) at Universidad Catolica de Valparaíso, and the Center for Mathematical Modeling (CMM) at Universidad de Chile. Additionally, I worked as a part-time teacher at Departamento de Matemática y Ciencia de la Computación (DMCC) at Universidad de Santiago de Chile.

Conclusion

Chapter 1 describes a novel source reconstruction method called Source Time Reversal (STR) based on a Time-Reversal Mirror (TRM) method, which is able to properly recover the spatial source dependence in microseismic events. The methodology reconstruct the spatial source term, regardless of the source time duration. This characteristic is the principal difference with classical time-reversal methods, since traditional methods lose precision when the temporal source term is different from a Dirac delta function.

We obtain an error estimate in the wave equation for the TRM method in the case when the boundary measurements are the wave displacement velocities over the entire boundary. This estimate depends on the domain, the propagation velocity map, and the initial displacement velocity. In terms of our original problem, this estimate depends on the domain where the measurements are acquired, the propagation velocity map, and the source. The error decays with T exponentially for odd dimensions and polynomially for even dimensions.

Our proposed method properly reconstructs continuous (exhibiting a relative error below 3%) and discontinuous (relative error below 9%) spatial sources when the velocity information is available over the entire boundary. In the case with partial boundary information, the reconstruction also exhibits good results, although the reconstructed scale is significantly smaller than in the original source. Nonetheless, the relative error remains below 3% when the reconstruction is normalized. In addition, we compare the STR method with the classical approach of TRM method, and we show quantitatively the advantages of our methodology, reducing the error by approximately a factor of two in the considered examples.

In Chapter 2, we have developed a space-source term reconstruction method in linear elasticity for sources of the form $\boldsymbol{f}(\boldsymbol{x})g(t)$. The proposed method is based on the STR methodology introduced in Chapter 1 for acoustic waves. Additionally, we describe two regularization methods: a traditional one, and a fast cut-off regularization.

The STR method has its basis on a property that allows waves to be reversed in time and the Duhamel's principle to define an auxiliary problem with final conditions. Additionally, the STR method requires a non-trapping condition to ensure the wavefronts measurements and a local decay result to approximate by zero the final conditions of the auxiliary problem given by the Duhamel's principle. A Volterra integral equation of the first kind with a convolution kernel gives the relation between the boundary measurements of the physical and the auxiliary problems. To reverse in time the boundary information in the auxiliary problem, it is necessary to solve the Volterra equation. Here, we have developed the two regularization methods mentioned above to solve such Volterra equation.

We have performed numerical experiments in 2D and 3D to test the reconstruction method with both regularization approaches. The STR method with traditional regularization considers a regularization constant c_0 to avoid divisions by zero. This methodology works well with partial data but excites some high frequencies that require a fine mesh in time to backpropagate them. The fast STR method with cut-off regularization introduces a cut-off constant c_1 as a low-pass filter to avoid the higher frequencies in the processed measurements. The fast method works well under noise measurements and with coarser meshes but presents some reconstruction limitations in the case with partial data. Additionally, 3D simulations exhibit a better local decay rate, which is traduced into better source reconstructions at shorter times.

In Chapter 3, we have extended the discrete-in-time source reconstruction from acoustic to elastic waves. Here the source has a from of a finite sum of variable separable functions, where each time-source term is a Dirac delta function. Under this assumption, it is possible to relate the solution of the original source problem with the solutions of a set of synthetic problems without source, where cardinalilty of the set is the number of different Dirac delta functions that compose the source. The original and synthetic solutions to problems are related by the Duhamel's principle. A difference with the previous chapters, the integral relation given by Duhamel's principle is easily solvable for this case.

Then, we present and implementation algorithm for locating and reconstructing each component of the source. The algorithm is based in the fact that reversing the boundary information from the original source problem, it is possible to detect the times when each source term starts by analyzing the displacement and the displacement velocity of the backward problem. Finally, we show some numerical source reconstructions for 2D acoustic waves and for 2D and 3D elastic waves.

The path forward could be divided into two parts: The STR method and discrete-in-time source reconstruction. In the STR method, we shall extend the methodology to heterogeneous elastic materials. Heterogeneous media allows a more accurate description of the ground and a better representation of the different layers that compose the Earth. Since the TRM method is suitable also for heterogeneous media (see [91]), the STR methodology should also be applicable provided that the media accomplishes a non-trapping condition. We also plan to study a theoretical estimate of the reconstruction error in the elastic case. Additionally, we may look for another way to solve the deconvolution problem, different from both regularization methods proposed. In the discrete-in-time source reconstruction, we can summarize the future work as follows

- To study a criteria to exclude the repeated localization of a source with small times difference.
- To analyze a relation between the threshold and the available information, e.g., the boundary forward data and the length of the domain.
- To find a uniqueness result for the inverse problem in elasticity.
- To implement the proposed method for heterogeneous elastic media with a non-trapping condition.

Bibliography

[1] M. Agranovsky and P. Kuchment. Time reversal in attenuating acoustic media. *Inverse Problems*, 23:2089–2102, 2007.

[2] K. Aki and P. G. Richars. *Quantitative seismology.* University Science Books, 2nd edition, 2002.

[3] A. Alessandrini. Stable determination of conductivity by boundary measurements. *Applicable Analysis*, 27:153–172, 1988.

[4] H. Ammari. *An introduction to mathematics of emerging biomedical imaging.* Springer, 2008.

[5] H. Ammari, E. Bretin, J. Garnier, H. Kang, H. Lee, and A. Wahab. *Mathematical methods in elasticity imaging.* Princeton University Press, 2015.

[6] H. Ammari, E. Bretin, J. Garnier, and A. Wahab. Time reversal in attenuating acoustic media. *Contemporary Mathematics*, 548:151–163, 2011.

[7] H. Ammari, J. Garnier, W. Jing, H. Kang, M. Lim, K. Sølna, and H. Wang. *Mathematical and statistical methods for multistatic imaging.* Springer, 2013.

[8] H. Ammari(Ed.). *Mathematical modeling in biomedical imaging I: Electrical and ultrasound tomographies, anomaly detection, and brain imaging.* Springer, Berlin, 2009.

[9] B. E. Anderson, M. Griffa, C. Larmat, T. J. Ulrich, and P. A. Johnson. Time reversal. *Physics Today*, 4:5–13, 2008.

[10] B. E. Anderson, M. Griffa, T. J. Ulrich, and P. A. Johnson. Time reversal reconstruction of finite sized sources in elastic media. *The Journal of the Acoustical Society of America*, 130:EL219–EL225, 2011.

[11] R. C. Aster, B. Borchers, and C. H. Thurber. *Parameter estimation and inverse problems.* Academic Press, Boston, 2nd edition, 2013.

[12] A. El Badia and T. Ha-Duong. An inverse source problem in potential analysis. *Inverse Problems*, 16:651–663, 2000.

[13] A. El Badia, T. Ha-Duong, and F. Moutazaim. Numerical solution for the identification

of source terms from boundary measurements. *Inverse Problems in Engineering*, 8:345–364, 2000.

[14] C. Bardos and M. Fink. Mathematical foundations of the time reversal mirror. *Asymptotic Analysis*, 29:157–182, 2002.

[15] M. Bertero and P. Boccacci. *Introduction to inverse problems in imaging*. Institute of Physics Publishing, Bristol, 1998.

[16] A. Bobet and H. H. Einstein. Tunnel reinforcement with rockbolts. *Tunnelling and Underground Space Technology*, 26:100–123, 2011.

[17] R. I. Brevis, J. H. Ortega, and D. Pardo. A source time reversal method for seismicity induced by mining. *Inverse Problems and Imaging*, 11:25–45, 2017.

[18] R. I. Brevis, A. Rodríguez-Rozas, J. H. Ortega, and D. Pardo. Source time reversal (STR) method for linear elasticity. *Manuscript submitted for publication*, 2017.

[19] H. Brezis. *Functional analysis, Sobolev spaces and partial differential equations*. Springer, New York, 2010.

[20] P. Burgholzer and G. J. Matt. Exact and approximative imaging methods for photoacoustic tomography using an arbitrary detection surface. *Physical Review E*, 75:046706, 2007.

[21] A. P. Calderón. On an inverse boundary value problem. In *Seminar on Numerical Analysis and its Applications to Continuum Physics (Rio de Janeiro, 1980)*, pages 65–73, 1980.

[22] A. P. Calderón. On an inverse boundary value problem. *Computational and Applied Mathematics*, 25:133–138, 2006.

[23] P. Cance and Y. Capdeville. Validity of the acoustic approximation for elastic waves in heterogeneous media. *Geophysics*, 80:T161–T173, 2015.

[24] N. W. Carlson, W. R. Babbitt, T. W. Mossberg, L. J. Rothberg, and A. G. Yodh. Storage and time reversal of light pulses using photon echoes. *Optics Letters*, 8:483–485, 1983.

[25] A. Chabchoub and M. Fink. Time-reversal generation of rogue waves. *Physical Review Letters*, 112:124101, 2014.

[26] H. Chen, H. Qi, R. Long, and M. Zhang. Research on 10-year tendency of China coal mine accidents and the characteristics of human factors. *Safety Science*, 50:745–750, 2012.

[27] A. Chorin and J. E. Marsden. *A mathematical introduction to fluid mechanics*. Springer, New York, 3rd edition, 1993.

[28] D. Colton and R. Kress. *Inverse acoustic and electromagnetic scattering theory.* Springer, New York, 3rd edition, 2013.

[29] Z. Dai-Ying and N. Bai-Sheng. Statistical analysis of China's coal mine particularly serious accidents. *Procedia engineering*, 26:2213–2221, 2011.

[30] M. V. de Hoop, L. Oksanen, and J. Tittelfitz. Uniqueness for a seismic inverse source problem modeling a subsonic rupture. *Communications in Partial Differential Equations*, 41:1895–1917, 2016.

[31] M. V. de Hoop and J. Tittelfitz. An inverse source problem for a variable speed wave equation with discrete-in-time sources. *Inverse Problems*, 31:075007, 2015.

[32] E. Deriaz and V. Perrier. Orthogonal helmholtz decomposition in arbitrary dimension using divergence-free and curl-free wavelets. *Applied and Computational Harmonic Analysis*, 26:249–269, 2009.

[33] C. Draeger and M. Fink. One-channel time reversal of elastic waves in a chaotic 2D-silicon cavity. *Physical Review Letters*, 79:407–410, 1997.

[34] F. Du, N. Hu, Y. Xie, and G. Li. An undersea mining microseism source location algorithm considering wave velocity probability distribution. *Mathematical Problems in Engineering*, 2014:7 pages, 2014.

[35] Y. V. Egorov and M. A. Shubin. *Foundations of the classical theory of partial differential equations.* Springer-Verlag, Berlin, 1998.

[36] H. W. Engl, M. Hanke, and A. Neubauer. *Regularization of inverse problems.* Kluwer Academic Publishers, 1996.

[37] M. R. Eslami, R. B. Hetnarski, J. Ignaczak, N. Noda, N. Sumi, and Y. Tanigawa. *Theory of elasticity and thermal stresses.* Springer, Dordrecht, 2013.

[38] L. Evans. *Partial differential equations.* American Mathematical Society, Providence, 2nd edition, 2010.

[39] A. Fahimifar and M. Ranjbarnia. Analytical approach for the design of active grouted rockbolts in tunnel stability based on convergence-confinement method. *Tunnelling and Underground Space Technology*, 24:363–375, 2009.

[40] M. Fink. Time reversal of ultrasonic fields. I. Basic principles. *IEEE Transactions on Ultrasonics, Ferroelectrics, and Frequency Control*, 39:555–566, 1992.

[41] M. Fink. Time-reversal mirrors. *Journal of Physics D: Applied Physics*, 26:1333–1350, 1993.

[42] M. Fink. Time reversed acoustics. *Physics Today*, 50:34–40, 1997.

[43] M. Fink. Time-reversal waves and super resolution. *Journal of Physics: Conference*

Series, 124:012004, 2008.

[44] M. Fink. Time reversal mirrors. In *2013 Transducers and Eurosensors XXVII: The 17th International Conference on Solid-State Sensors, Actuators and Microsystems, TRANSDUCERS and EUROSENSORS 2013*, pages 788–789, 2013.

[45] M. Fink, D. Cassereau, A. Derode, C. Prada, P. Roux, M. Tanter, J.-L. Thomas, and F. Wu. Time-reversed acoustics. *Reports on Progress in Physics*, 63:1933–1995, 2000.

[46] M. Fink, C. Prada, F. Wu, and D. Cassereau. Self focusing in inhomogeneous media with time reversal acoustic mirrors. *Proceedings., IEEE Ultrasonics Symposium*, 2:681–686, 1989.

[47] J.-P. Fouque, J. Garnier G. Papanicolaou, and K. Sølna. *Wave Propagation and time reversal in randomly layered media*. Springer, New York, 2007.

[48] G. C. Garcia, A. Osses, and M. Tapia. A heat source reconstruction formula from single internal measurements using a family of null controls. *Journal of Inverse and Ill-posed Problems*, 21:755–779, 2013.

[49] L. Geiger. Probability method for the determination of earthquake epicenters from the arrival time only (translated from Geiger's 1910 German article). *Bulletin of St. Louis University*, 8:56–71, 1912.

[50] S. J. Gibowicz and A. Kijko. *An introduction to mining seismology*. Academic Press, 1994.

[51] V. Girault and P. A. Raviart. *Finite element methods for Navier-Stokes Equations*. Springer, Berlin, 1986.

[52] V. B. Glasko. *Inverse problems of mathematical physics*. American Institute of Physics, New York, 1984.

[53] P. L. Gould. *Introduction to linear elasticity*. Springer, New York, 2013.

[54] D. J. Gross. The role of symmetry in fundamental physics. *Proceedings of the National Academy of Sciences of the United States of America*, 93:14256–14259, 1996.

[55] B. Haberman and D. Tataru. Uniqueness in Calderón's problem with Lipschitz conductivities. *Duke Mathematical Journal*, 162:497–516, 2013.

[56] C. Heaton, B. E. Anderson, and S. M. Young. Time reversal focusing of elastic waves in plates for an educational demonstration. *The Journal of the Acoustical Society of America*, 141:1084–1092, 2017.

[57] L. Henderson. Can the second law be compatible with time reversal invariant dynamics? *Studies in History and Philosophy of Science Part B: Studies in History and Philosophy of Modern Physics*, 47:90–98, 2014.

[58] E. Hoek, P. K. Kaiser, and W. F. Bawden. *Support of underground exacavations in hard rock*. CRC Press, 2000.

[59] M. S. Hons, R. R. Stewart, D. C. Lawton, M. B. Bertram, and G. Hauer. Field data comparisons of mems accelerometers and analog geophones. *The Leading Edge*, 27:896–903, 2008.

[60] Y. Hristova. Time reversal in thermoacoustic tomography—an error estimate. *Inverse Problems*, 25:055008, 2009.

[61] Y. Hristova, P. Kuchment, and L. Nguyen. Reconstruction and time reversal in thermoacoustic tomography in acoustically homogeneous and inhomogeneous media. *Inverse Problems*, 24:055006, 2008.

[62] O. Y. Imanuvilov, G. Uhlmann, and M. Yamamoto. The calderón problem with partial data in two dimensions. *Journal of the American Mathematical Society*, 23:655–691, 2010.

[63] R. K. Ing, M. Fink, and O. Casula. Self-focusing Rayleigh wave using a time reversal mirror. *Applied Physics Letters*, 68:161–163, 1996.

[64] V. Isakov. *Inverse source problems*. American Mathematical Society, Providence, 1990.

[65] V. Isakov. *Inverse problems for partial differential equations*. Springer, 2nd edition, 2006.

[66] J. Joy. Occupational safety risk management in Australian mining. *Occupational medicine*, 54:311–315, 2004.

[67] Lassi Päivärinta K. Astala. Calderón's inverse conductivity problem in the plane. *Annals of Mathematics*, 163:265–299, 2006.

[68] J. B. Keller. Inverse problems. *The American Mathematical Monthly*, 83:107–118, 1976.

[69] K. R. Kelly, R. W. Ward, S. Treitel, and R. M. Alford. Synthetic seismograms: a finite-difference approach. *Geophysics*, 41:2–27, 1976.

[70] C. E. Kenig, J. Sjöstrand, and G. Uhlmann. The Calderón problem with partial data. *Annals of Mathematics*, 165:567–591, 2007.

[71] A. Kirsch. *An introduction to the mathematical theory of inverse problems*. Springer, New York, 2011.

[72] C. Kisslinger. A review of theories of mechanisms of induced seismicity. *Engineering Geology*, 10:85–98, 1976.

[73] L. A. Kunyansky. A series solution and a fast algorithm for the inversion of the spherical mean radon transform. *Inverse Problems*, 23:S11–S20, 2007.

[74] W. A. Kuperman, W. S. Hodgkiss, H. C. Song, T. Akal, C. Ferla, and D. R. Jackson.

Phase conjugation in the ocean: Experimental demonstration of an acoustic time-reversal mirror. *The Journal of the Acoustical Society of America*, 103:25–40, 1998.

[75] P. Kyritsi, G. Papanicolaou, P. Eggers, and A. Oprea. Time reversal techniques for wireless communications. In *Vehicular technology conference, 2004. VTC2004-Fall. 2004 IEEE 60th*, volume 1, pages 47–51, 2004.

[76] G. Lamé. *Leçons sur la théorie mathématique de l'elasticité des corps solides*. Gauthier-Villars, 1852.

[77] C. Larmat, J.-P. Montagner, M. Fink, Y. Capdeville, A. Tourin, and E. Clévédé. Time-reversal imaging of seismic sources and application to the great sumatra earthquake. *Geophysical Research Letters*, 33:L19312, 2006.

[78] P. D. Lax and R. S. Phillips. *Scattering theory*. Academic Press, Boston, 2nd edition, 1989.

[79] G. Lerosey, J. de Rosny, A. Tourin, A. Derode, G. Montaldo, , and M. Fink. Time reversal of electromagnetic waves. *Physical Review Letters*, 92:193904, 2004.

[80] C. C. Li. Principles of rockbolting design. *Journal of Rock Mechanics and Geotechnical Engineering*, 9:396–414, 2017.

[81] P. Linz. *Analytical and numerical methods for Volterra equations*. Society for Industrial and Applied Mathematics, Philadelphia, 1985.

[82] S. Mallick and K. Mukherjee. An empirical study for mines safety management through analysis on potential for accident reduction. *Omega*, 24:539–550, 1996.

[83] S. Marelli, H. Maurer, and E. Manukyan. Validity of the acoustic approximation in full-waveform seismic crosshole tomography. *Geophysics*, 77:R129–R139, 2012.

[84] M. Matsu'ura. Bayesian estimation of hypocenter with origin time eliminated. *Journal of Physics of the Earth*, 32:469–483, 1984.

[85] A. Nachman. Reconstructions from boundary measurements. *Annals of Mathematics*, 128:531–576, 1988.

[86] A. Nachman. Global uniqueness for a two-dimensional inverse boundary value problem. *Annals of Mathematics*, 143:71–96, 1996.

[87] A. Nachman and B. Street. Reconstruction in the Calderón problem with partial data. *Communications in Partial Differential Equations*, 35:375–390, 2010.

[88] F. Natterer. *The mathematics of computerized tomography*. Society for Industrial and Applied Mathematics, 2001.

[89] H. T. Nguyen, J. B. Andersen, G. F. Pedersen, P. Kyritsi, and P. Eggers. Time reversal in wireless communications: A measurement-based investigation. *IEEE Transactions*

on Wireless Communications, 5:2242–2252, 2006.

[90] M. Nixon and A. Aguado. *Feature extraction and image processing*. Academic Press, 2nd edition, 2008.

[91] P. D. Norville and W. R. Scott Jr. Time-reversal focusing of elastic surface waves. *The Journal of the Acoustical Society of America*, 118:735–744, 2005.

[92] P. D. Norville and W. R. Scott Jr. Time-reversal focusing of elastic surface waves with an asymmetric surface layer. *The Journal of the Acoustical Society of America*, 122:EL95–EL100, 2007.

[93] A. Parvulescu and C. S. Clay. Reproducibility of signal transmissions in the ocean. *The Radio and Electronic Engineer*, 29:223–228, 1965.

[94] A. Przadka, S. Feat, and P. Petitjeans. Time reversal of water waves. *Physical Review Letters*, 109:064501, 2012.

[95] N. Ricker. The form and laws of propagation of seismic wavelets. *Geophysics*, 18:10–40, 1953.

[96] A. Rodríguez-Rozas and J. Diaz. Non-conforming curved finite element schemes for time-dependent elastic–acoustic coupled problems. *Journal of Computational Physics*, 305:44–62, 2016.

[97] M. Salo. *Calderón problem. Lecture notes*. Department of Mathematics and Statistics. University of Helsinki, Spring 2008.

[98] L. Sanmiquel, J. M. Rossell, and C. Vintró. Study of spanish mining accidents using data mining techniques. *Safety Science*, 75:49–55, 2015.

[99] L. A. Sheep and B. F. Logan. The Fourier reconstruction of a head section. *IEEE Transactions on Nuclear Science*, 21:21–43, 1974.

[100] G. D. Smith. *Numerical solution of partial differential equations: Finite difference methods*. The Clarendon Press, Oxford University Press, New York, 3rd edition, 1985.

[101] H. C. Song, W. A. Kuperman, W. S. Hodgkiss, T. Akal, and C. Ferla. Iterative time reversal in the ocean. *The Journal of the Acoustical Society of America*, 105:3176–3184, 1999.

[102] W. Spence. Relative epicenter determination using P-wave arrival-time differences. *Bulletin of the Seismological Society of America*, 70:171–183, 1980.

[103] P. Stefanov and G. Uhlmann. Multi-wave methods via ultrasound. *Inverse Problems and Applications, Inside Out II, MSRI Publications*, 60:271–323, 2012.

[104] P. Stefanov and G. Uhlmann. Instability of the linearized problem in multiwave tomography of recovery both the source and the speed. *Inverse Problems and Imaging*,

7:1367–1377, 2013.

[105] K. Sundermeyer. *Symmetries in fundamental physics*. Springer, Heidelberg, 2nd edition, 2014.

[106] J. Sylvester and G. Uhlmann. A global uniqueness theorem for an inverse boundary value problem. *Annals of Mathematics*, 125:153–169, 1987.

[107] A. Tarantola. *Inverse problem theory and methods for model parameter estimation*. Society for Industrial and Applied Mathematics, New York, 2005.

[108] J. Tittelfitz. Thermoacoustic tomography in elastic media. *Inverse Problems*, 28:055004, 2012.

[109] G. Uhlmann. Developments in inverse problems since Calderón's foundational paper. In *Harmonic Analysis and Partial Differential Equations in honor of Alberto P. Calderon*, pages 295–345, 1999.

[110] G. Uhlmann. Electrical impedance tomography and Calderón's problem. *Inverse Problems*, 25:123011, 2009.

[111] B. R. Vainberg. On the short wave asymptotic behaviour of solutions of stationary problems and the asymptotic behaviour as $t \to \infty$ of solutions of non-stationary problems. *Russian Mathematical Surveys*, 30:1–58, 1975.

[112] F. Wu, J. L. Thomas, and M. Fink. Time reversal of ultrasonic fields. II. Experimental results. *IEEE Transactions on Ultrasonics, Ferroelectrics, and Frequency Control*, 39:567–578, 1992.

[113] L. Wu, Z. Jiang, W. Cheng, X. Zuo, D. Lv, and Y. Yao. Major accident analysis and prevention of coal mines in China from the year of 1949 to 2009. *Mining Science and Technology (China)*, 21:693–699, 2011.

[114] M. Xu and L. V. Wang. Time reversal and its application to tomography with diffracting sources. *Physical Review Letters*, 92:033902, 2005.

[115] M. Xu and L. V. Wang. Universal back-projection algorithm for photoacoustic computed tomography. *Physical Review E*, 71:016706, 2005.

[116] M. Yamamoto. Stability, reconstruction formula and regularization for an inverse source hyperbolic problem by a control method. *Inverse Problems*, 11:481–496, 1995.

[117] M. F. Yanik and S. Fan. Time reversal of light with linear optics and modulators. *Physical Review Letters*, 93:173903, 2004.

[118] A. Yariv. Phase conjugate optics and real-time holography. *IEEE Journal of Quantum Electronics*, 14:650–660, 1978.

[119] B. Y. Zel'Dovich, N. F. Pilipetsky, and V. V. Shkunov. *Principles of phase conjugation*.

Springer-Verlag, Berlin, 1985.